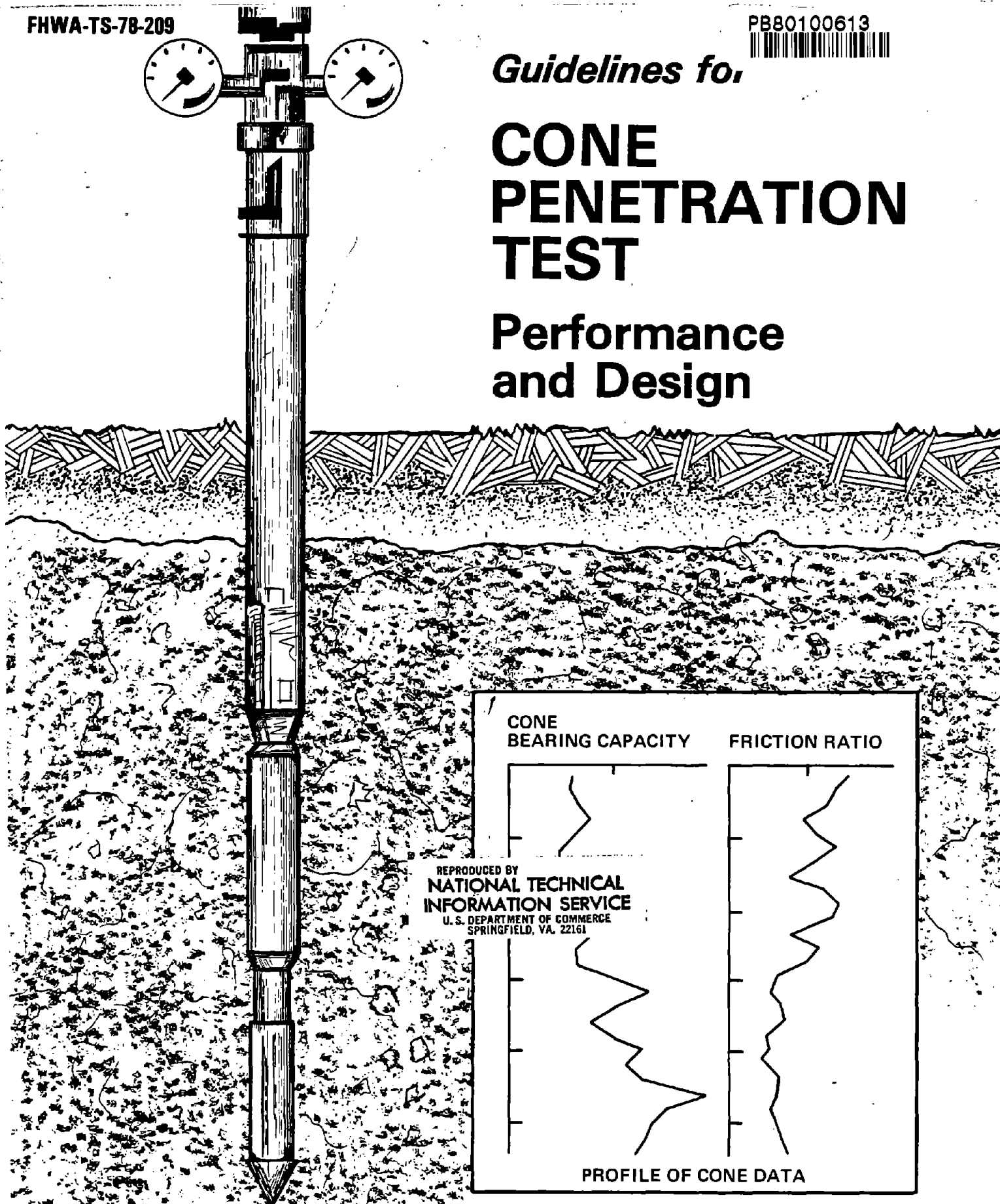




Guidelines for

# CONE PENETRATION TEST

## Performance and Design



REPRODUCED BY  
NATIONAL TECHNICAL  
INFORMATION SERVICE  
U.S. DEPARTMENT OF COMMERCE  
SPRINGFIELD, VA. 22161

PROFILE OF CONE DATA

**U.S. DEPARTMENT OF TRANSPORTATION**

FEDERAL HIGHWAY ADMINISTRATION  
OFFICES OF RESEARCH AND DEVELOPMENT  
IMPLEMENTATION DIV. WASH., D.C. 20590

Y 1978



## NOTICE

This document is disseminated under the sponsorship of the Department of Transportation in the interest of information exchange. The United States Government assumes no liability for its contents or use.

The contents of this report reflect the views of Dr. John H. Schmertmann, who is responsible for the facts and the accuracy of the data presented herein. The contents do not necessarily reflect the official views or policy of the Department of Transportation. This report does not constitute a standard, specification, or regulation.

The United States Government does not endorse products or manufacturers. Trade or manufacturers' names appear herein only because they are considered essential to the object of this document.

1. Report No. FHWA-TS-78-209	2. Government Accession No.	3. Recipient's Catalog No. PB80-100613
4. Title and Subtitle Guidelines for Cone Penetration Test (Performance and Design)	5. Report Date July 1978	6. Performing Organization Code
	7. Author(s) John H. Schmertmann	8. Performing Organization Report No. FHWA-TS-78-209
9. Performing Organization Name and Address 226 N.W. 14th Place Gainesville, Florida 32605	10. Work Unit No.	11. Contract or Grant No. 6-3-0054
	12. Sponsoring Agency Name and Address* U. S. Department of Transportation Federal Highway Administration (HDV-22) Washington, D.C. 20590	13. Type of Report and Period Covered Final Report
15. Supplementary Notes FHWA Contract Manager: Chien-Tan Chang (HDV-22)		
16. Abstract This manual presents procedures and guidelines applicable to the use of the cone penetration test. Dr. Schmertmann prepared this manual in February 1977 and made minor additions in May 1978. It represents his interpretation of the state-of-the-art in Dutch static cone testing as of February 1977. Its contents should provide assistance and uniformity to engineers concerned with the interpretation of the data obtained from such testing. Only geotechnical engineers familiar with the fundamentals of soil mechanics and foundation engineering should use this manual.  The manual includes:  1. Introduction and review of the general principals concerning cone penetrometer testing.  2. Individual design chapters which address topics such as: pile design, shear strength estimation, settlement calculation and compaction control.  3. Appendices which present previously published, pertinent information on cone penetrometer testing.		
17. Key Words Cone Penetration, Foundation, Dutch Cone, Soil Mechanics	18. Distribution Statement No restrictions	
19. Security Classif. (of this report) Unclassified	20. Security Classif. (of this page) Unclassified	21. No. of Pages   22. Price PCA08 A01



## NOTICE

THIS DOCUMENT HAS BEEN REPRODUCED FROM THE BEST COPY FURNISHED US BY THE SPONSORING AGENCY. ALTHOUGH IT IS RECOGNIZED THAT CERTAIN PORTIONS ARE ILLEGIBLE, IT IS BEING RELEASED IN THE INTEREST OF MAKING AVAILABLE AS MUCH INFORMATION AS POSSIBLE.



## PREFACE

The quasi-static Dutch cone penetration test has a development history of over 40 years. Many engineers throughout the world have found this test a useful and economical tool for site investigation and geotechnical design. The modern advances of using trucks with up to 20 ton thrust capacity, and the inventions of the friction-cone and electrical cone tips have made this test even more attractive technically without sacrifice of economy. Dr. Schmertmann re-introduced this test into the USA in 1965. Since then its use and acceptance has spread steadily, as has equipment availability and suppliers, and the ASTM now has a tentative standard for this test.

This manual was prepared under contract with the Federal Highway Administration by Dr. John Schmertmann, Professor of Civil Engineering at the University of Florida, in conjunction with a 43 minute video tape program on AN INTRODUCTION TO THE DUTCH CONE PENETRATION TEST. The FHWA contract managers were Messrs. Larry Wolf and Chien-Tan Chang.

This manual presents procedures and guidelines applicable to the use of the cone penetration test. Dr. Schmertmann prepared this manual in February, 1977, and made minor additions in May, 1978. It represents his interpretation of the state-of-the-art in Dutch static cone testing as of February, 1977. Its contents should provide assistance and uniformity to engineers concerned with the interpretation of the data obtained from such testing. Only geotechnical engineers familiar with the fundamentals of soil mechanics and foundation engineering should use this manual.

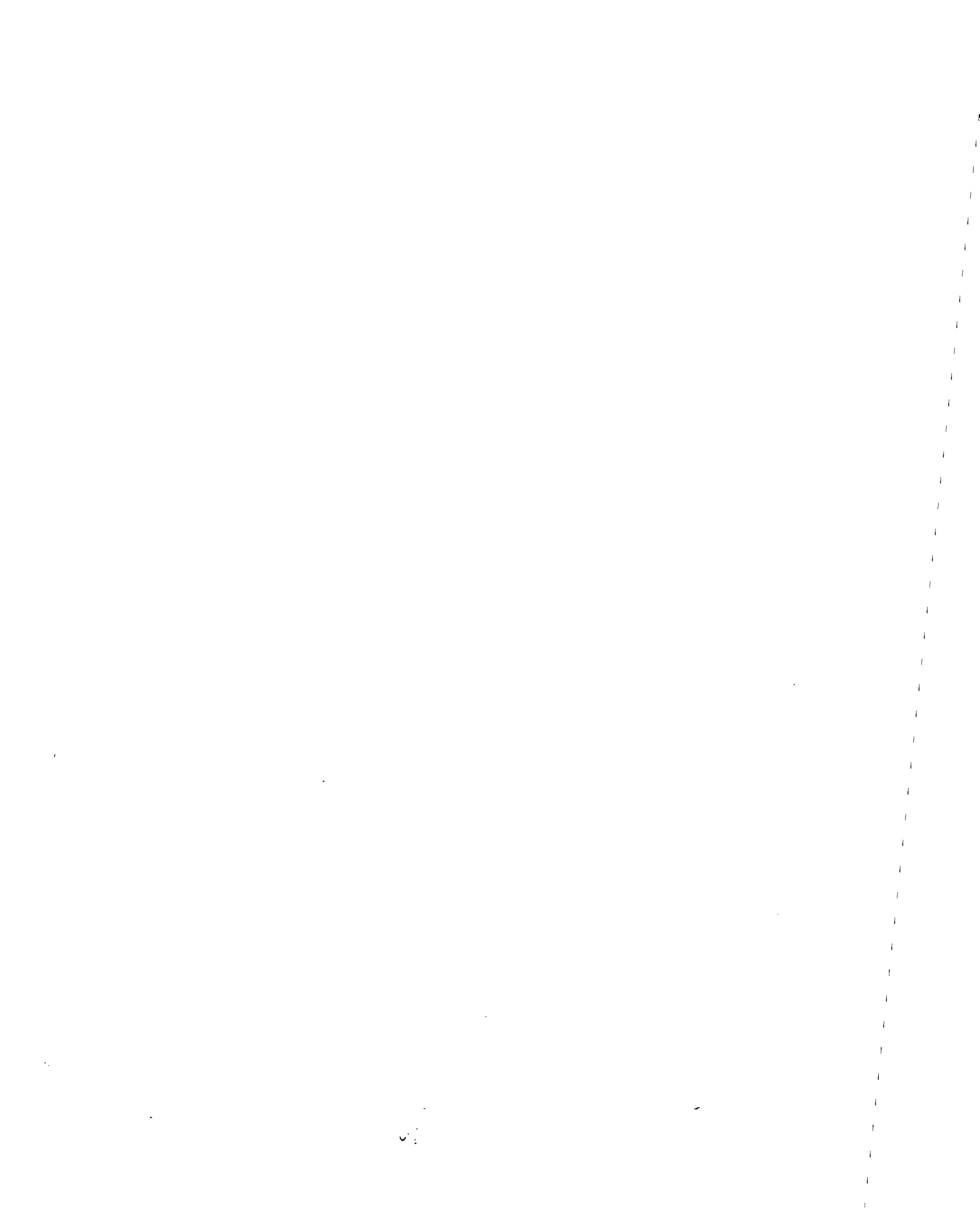
The manual includes:

- 1) Introduction and review of the general principals concerning cone penetrometer testing.
- 2) Individual design chapters which address topics such as: pile design, shear strength estimation, settlement calculation and compaction control.
- 3) Appendices which present previously published, pertinent information on cone penetrometer testing.

While the supply lasts, copies of the manual can be obtained from:

Federal Highway Administration  
Implementation Division (HDV-22)  
Washington, D.C. 20590

Copies of the video tape are also available on a loan basis from the same office and the FHWA Regional Offices.



GUIDELINES FOR CPT PERFORMANCE AND DESIGN  
Prepared for FHWA by Dr. John H. SCHMERTMANN

TABLE OF CONTENTS

	<u>Page</u>
1. INTRODUCTION	1
1.1 Purpose	1
1.2 Advantages and disadvantages	1
1.3 Sounding data to which Guidelines apply	1
1.4 Soils in which CPT useful	2
1.5 Associated soil sampling	2
1.6 References	2
1.7 Notation	3
1.8 Appendix I, factors affecting interpretation of CPT data	3
1.9 Appendix II, ASTM CPT standard	3
1.10 Appendix III, 1975 CPT state-of-the-art	3
1.11 Appendix IV, examples of pile capacity calculations	3
2. SOIL EXPLORATION FOR PRELIMINARY DESIGN	4
2.1 End bearing, $q_c$	4
2.2 Sleeve friction ( $f_s$ ) and friction ratio ( $R_f$ )	4
2.2.1 Local correlation needed	6
2.2.2 Mechanical tip calculation for $R_f$	6
2.2.3 Bearing on local friction sleeve	8
2.2.4 Sleeve surface roughness	8
2.2.5 Soil ductility controls $R_f$	8
2.2.6 Special pore pressure effects	8
2.3 Critical depth from surface or interface	9
2.4 Uniformity of soil conditions, stratigraphy	9
2.5 Position of the water table	10
2.6 Sand; estimating relative density	13
2.7 Clay; estimating sensitivity and overconsolidation	15
2.7.1 Sensitivity	15
2.7.2 Overconsolidation	15
2.8 Correlation with SPT	18
3. CPT FOR COMPACTION CONTROL	22
4. PILE DESIGN	24
4.1 Driven, displacement, straight-sided piles	24
4.1.1 End bearing	24

	<u>Page</u>
4.1.2 Side friction	26
4.1.2.1 Sand, with friction-cone $f_s$ data	26
4.1.2.2 Sand, without $f_s$ data	28
4.1.2.3 Clay	28
4.1.3 Negative side friction	31
4.1.4 Tension piles	31
4.2 Corrections for shape of pile and method of pile insertion	31
4.3 Factors of safety	33
4.4 Lateral loading	33
4.5 Pile settlement	36
4.6 Group action	37
4.7 Data for wave equation analysis	37
5. ESTIMATING SHEAR STRENGTH	38
5.1 Sand	38
5.1.1 Bearing capacity	38
5.1.2 Estimating $\phi'$	38
5.2 Clay	42
5.2.1 Undrained strength, $s_u$	42
5.2.2 Remolded undrained strength	44
5.2.3 Drained strength	44
5.3 Mixed soils	47
6. ESTIMATING SETTLEMENTS	49
6.1 Sand layers	49
6.2 Clay layers	54
6.2.1 Schmertmann method	54
6.2.2 Sanglerat method	55
6.3 Differential settlement	55
6.4 Rate of settlement	56
7. LIST OF REFERENCES	58
8. NOTATION AND ABBREVIATIONS	62
APPENDIX I - FACTORS AFFECTING INTERPRETATION OF CPT DATA	65
I.1 Theories for CPT behavior	66
I.2 Effect of vertical effective stress at constant $K'$	66
I.3 Effects of varying radial effective stress at constant vertical effective stress	68
I.4 Compressibility: density, cementation, large particles	68
I.5 Shape of the penetrometer tip	69
I.6 Method of penetration	70
I.7 Pore pressure effects	73
I.8 Layering and tip diameter effects	77

	<u>Page</u>
APPENDIX II - TEST OF ASTM D-3441-75T, STANDARD FOR CPT	80
APPENDIX III - CHAPTER 3. ON CONE PENETRATION TEST (CPT) from Schmertmann (1975) SOA paper; includes list of references	89
APPENDIX IV - EXAMPLES OF CALCULATIONS FOR PILE END BEARING AND FRICTION CAPACITIES USING NOTTINGHAM METHOD (from Nottingham and Schmertmann (1975))	120



# GUIDELINES FOR CPT PERFORMANCE AND DESIGN

Prepared for the FHWA by  
Dr. John H. Schmertmann  
February, 1977

## 1. INTRODUCTION

### 1.1 Purpose

This guidelines manual has the purpose of providing assistance to engineers interpreting the quasi-static cone penetration test (CPT), also known as the "Dutch cone test", data for design purposes. This purpose includes: a) Evaluation of site or route stratigraphy; the types, layering, uniformity, continuity, permeability and strength of various soils encountered, b) Control of the removal of poor soil materials and the proper placement and compaction of stabilized soils, c) Designing footing and pile foundations for both bearing capacity and settlement criteria, and d) Designing slopes and fills.

This manual has the further objective of encouraging uniformity within the various engineering organizations concerning their interpretation of such data. It also provides a focus for criticism, research, and suggestions for improvements in the field hardware, sounding techniques, and design interpretation of CPT data.

### 1.2 Advantages and Disadvantages

Relative to other soil engineering methods for exploring site stratigraphy and obtaining data for preliminary design, the CPT has the outstanding advantages of often providing better speed and economy, more detailed and precise data, and data better suited to many ordinary soil engineering design problems. It has the outstanding disadvantages of not obtaining a soil sample for visual/lab inspection, and of a sometimes severely limited depth capability.

### 1.3 Sounding Data to Which Guidelines Apply

These guidelines apply only to the quasi-static method (2 cm/sec or less penetration rate) of performing a sounding. They apply primarily to the 10 cm<sup>2</sup> penetrometer tips of either the Fugro-Cesco, Inc. (Dutch engineering firm) electrical types, with a cylindrical shape with cone-base diameter above the cone, or the Delft mechanical mantle or Begemann friction-sleeve types. ASTM D-3441-75T describes these tips in detail -- see Appendix II.

#### 1.4 Soils in Which CPT Useful

Generally, because of more limited alternatives, the CPT has proven most useful in the coarser, more permeable, soils such as sand. However, worldwide experience has shown that the CPT can also provide useful data for design in most of the types of soil wherein the equipment can penetrate. As with any other soil engineering investigative tool, the engineer must use appropriate judgement as to how to best interpret CPT data from different soils for design purposes. The writer hopes this manual will aid such judgement.

In relatively permeable soils, such as fine and coarser sands, pore pressure effects during penetration at standard rates often have a negligible influence and the CPT measures approximately fully drained behavior. In homogeneous, plastic clays the CPT measures approximately fully undrained behavior. Mixed soils produce in-between behavior.

The CPT cannot investigate all soils. Layers of very dense, and/or cemented sand often require penetration forces that exceed the thrust or reaction capability of the CPT equipment. As a rough guide to penetration limit, 10 ton equipment can just penetrate a 5 ft layer of Standard Penetration Test (SPT)  $N = 100$  sand at a depth of 25 ft. Significant amounts of gravel-sized particles can render CPT data very erratic and difficult to interpret quantitatively. The presence of cobbles can stop penetration and damage equipment. Rock usually stops penetration, but some of the softer and/or weathered rocks permit penetration and evaluation via the CPT.

#### 1.5 Associated Soil Sampling

The CPT method does not provide soil samples for visual inspection. However, the CPT data does permit an estimate of the soil types penetrated and provides accurate data for the subsequent precise locations of critical soils that might require sampling. Various types of samplers may be used with the various types of CPT rigs in use. Samplers that advance via punching, as do the CPT cone tips, can be used directly with the CPT hydraulic thrust machines and require no borehole. Other CPT equipment involves using a special set of adapters on an otherwise ordinary SPT drill rig. In this case the rig can easily reconvert to boring and sampling. Although engineers with much CPT experience in a local area sometimes conduct site investigations without actual sampling, in general one must obtain appropriate samples for the proper interpretation of CPT data. But, prior CPT data can greatly reduce sampling requirements.

#### 1.6 References

Where appropriate, the text indicates references in parentheses by author and year. In Section 7, and at the end of Appendix III the reader will find lists of references alphabetically by author and date of publication.

## 1.7 Notation

Section 8 lists, in alphabetical order, the various notations used herein. Usually a notation will be defined where first used.

## 1.8 Appendix I, Factors Affecting Interpretation of CPT Data

Any "Guidelines" for interpreting CPT data must include some discussion of the important variables that influence such data. Appendix I presents such a discussion. Note that six appendix figures follow the text.

## 1.9 Appendix II, ASTM CPT Standard

The ASTM has a new tentative standard, D-3441-75T, for the performance of the CPT. Appendix II to these Guidelines include this Tentative Standard. Engineers are encouraged to use D-3441-75T.

## 1.10 Appendix III, 1975 CPT State-of-the-Art

The writer previously prepared a state-of-the-art paper on insitu testing for shear strength, which included a chapter on the CPT. For easy reference, these Guidelines include this chapter and its associated figures and references, as Appendix III.

## 1.11 Appendix IV, Examples of Pile Capacity Calculations

In Appendix III the writer presented the essence of Nottingham's research results and recommended methods for computing ultimate pile bearing. Section 4 herein includes recommendations to use these methods. This Appendix presents examples of hypothetical and actual situations and ultimate pile bearing and friction computations using the Nottingham methods.

## 2. SOIL EXPLORATION FOR PRELIMINARY DESIGN

### 2.1 End Bearing, $q_c$

The soil in the immediate vicinity of a passing penetrometer tip experiences a complicated sequence of changes in stress and strain. No one has yet solved this problem theoretically. Some recent attempts show promise (see Durgunoglu and Mitchell, 1975, and Baligh and Scott, 1975). However, as described in Appendix I, we do know about some of the variables that influence CPT data and this helps interpret CPT logs.

As a guide, Figure 1 illustrates a simplified form of different  $q_c$ -profiles and suggests possible interpretations. In general, as illustrated by parts (a) and (b), clays have considerably lower  $q_c$  than sands, due to lower  $\phi'$  and pore pressure effects. Note that some overlap exists between loose sands and highly overconsolidated clays.

Part (c) shows that a normally consolidated sand would increase in  $q_c$  with depth while an overconsolidated sand might have an approximately constant  $q_c$  with depth from additional  $q_c$  due to additional lateral stress from the overconsolidation. The overconsolidated state might be confused with a normally consolidated state for the case when density decreases with depth. This illustrates a fundamental uncertainty when interpreting  $q_c$ -profiles -- increased stress and increased density produce similar  $q_c$  effects. Part (d) suggests different possible interpretations for, among other things, an unusually high  $q_c$  layer over a much weaker layer.

As further illustrated in parts (a) and (b), the passage of the penetrometer tip probably does not produce a smooth, continuous failure phenomena. More likely, penetration produces a succession of failures which involve a slip, a recovery of cone bearing strength and/or pushrod friction with simultaneous pushrod advance, another slip, etc. Perhaps in clays this succession occurs so rapidly that the  $q_c$  profile appears relatively smooth. However, in sands, and particularly dense sands, a pattern may also result from layering and variations in sand densities and perhaps lateral stresses inherent in the variable, intermittent deposition of sand deposits. Such zig-zag effects will be more pronounced with continuous recording when using Fugro tips than with the incremental operation of the mechanical tips. As explained in I.7 and I.8 of Appendix I, it will also be more pronounced the smaller the diameter of the tip and the greater the pore pressure effects.

### 2.2 Sleeve Friction ( $f_s$ ) and Friction Ratio ( $R_f$ )

As first introduced by Begemann (1953, 1965), the measurement of local friction by a special sleeve in the penetrometer tip has greatly

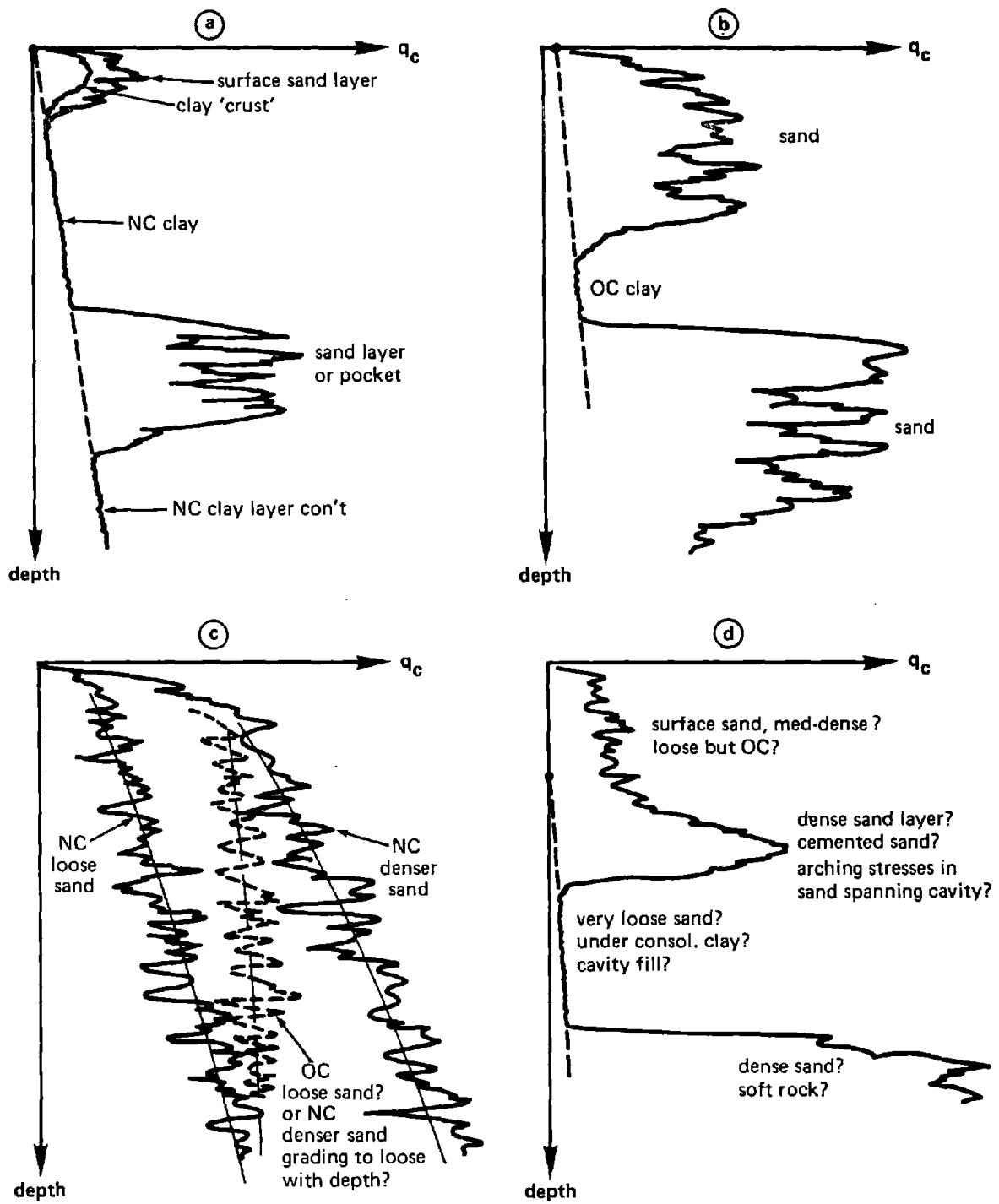


FIGURE 1 – SIMPLIFIED EXAMPLES OF  $q_c$ -LOG PROFILES SHOWING LIKELY AND POSSIBLE INTERPRETATIONS FOR SOIL TYPES AND CONDITIONS

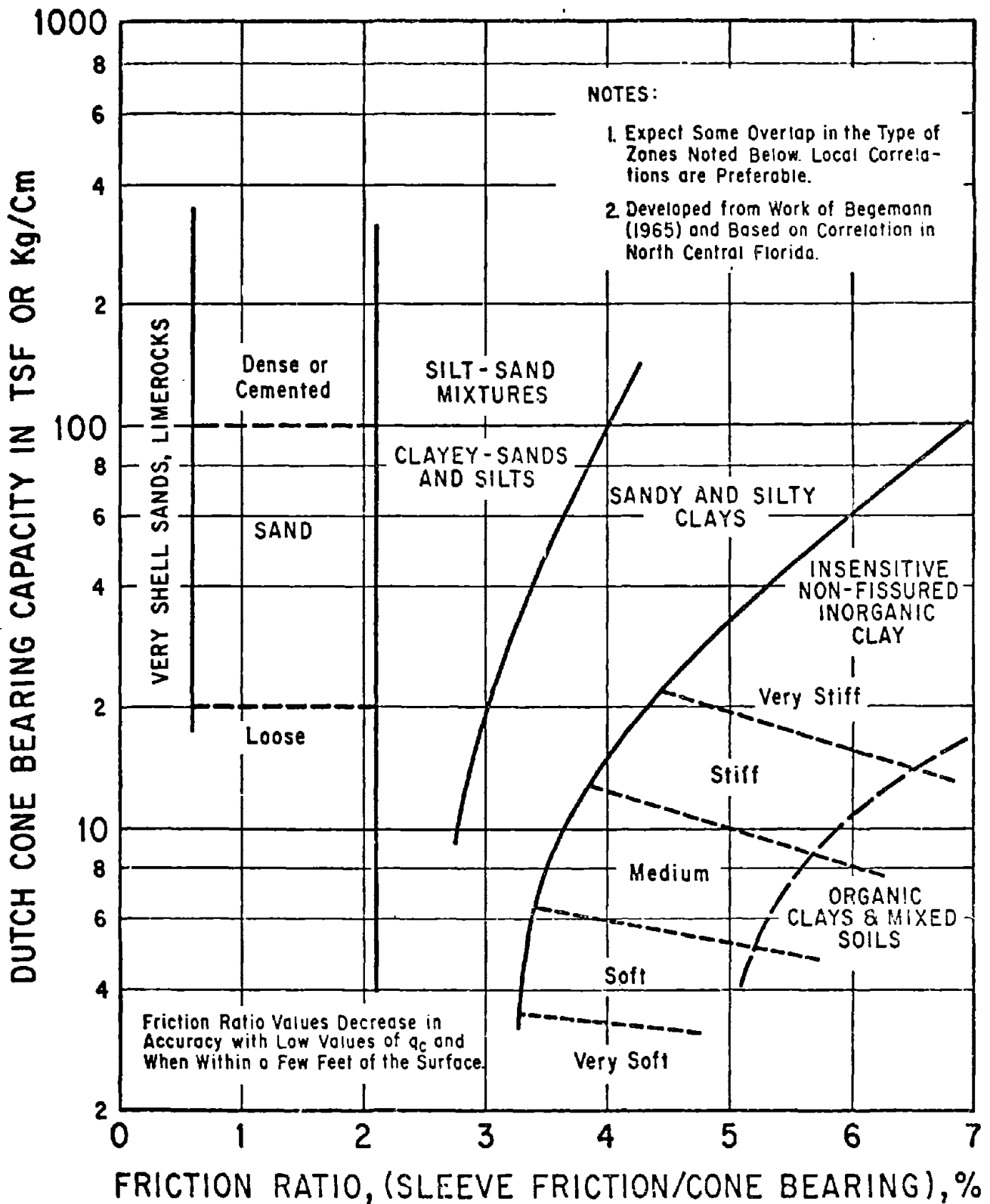
increased the value of CPT data. Besides providing friction data of superior value in the design of friction against piles, the dimensionless ratio of sleeve friction to bearing often, after local correlation, provides a means to help identify the soil types penetrated.

Figure 2 represents one correlation between soil type and CPT data, based on using the Begemann mechanical tip in Florida. A recent case history site investigation using the CPT (Alperstein and Leifer, 1976) showed fair agreement with Figure 2. Friction ratios will likely reduce when using the Fugro tip in sands -- from about 1 1/4% typical for the Begemann mechanical tip to about 1/2%. Four to seven percent represents a typical  $R_f$  in insensitive clays for both tips and present evidence is ambiguous as to which produces lower  $R_f$ 's. When using Figure 2, or similar types of correlations, observe certain precautions as follows:

2.2.1 Local Correlation Needed: Correlations may well be significantly different in different geologic areas. For example, structural sensitivity reduces friction ratios. In the case of quick clays the writer has measured  $R_f$  as low as 0.1% using a Fugro tip.

2.2.2 Mechanical Tip Calculation for  $R_f$ : When using the Begemann friction-cone tip, the operator takes a succession of two gage readings at each test depth -- the point only thrust,  $G$ , followed by the thrust to move both the point and friction sleeve,  $G + \Delta G$ . Assuming no change in  $G$  during the additional 1 to 4 cm penetration to obtain  $G + \Delta G$ , subtraction gives the  $\Delta G$  to overcome sleeve-soil friction. But, when comparing  $q_c$  with local friction for an  $R_f$  determination of soil at a specified depth, proper account must be taken of the elevation difference between the base of the cone, elevation "n", and the midheight of the sleeve, elevation "n-1". When using the Begemann tip, with its approximate 20 cm elevation difference between n and n-1 and also the usual 20 cm depth test interval, one must compare the current additional thrust to move the friction sleeve (see Appendix II, Figure 5),  $\Delta G_n$ , with the previous (20 cm higher) point-only thrust gage reading,  $G_{n-1}$ , to obtain the  $R_f$  at elevation n-1. Equation 1 presents the formula for  $R_{f(n-1)}$  when using the Begemann tip with its 150 cm<sup>2</sup> friction sleeve, and when using the Goudsche Machinefabriek CPT load cell that has Bourdon gages that register one half the pressure on the cone tip, or 1/2  $q_c$ .

$$R_{f(n-1)} (\%) = 6.6 \frac{\Delta G_n}{G(n-1)} \quad (\text{Eq. 1})$$



**GUIDE FOR ESTIMATING SOIL TYPE FROM DUTCH FRICTION-CONE RATIO (BEGEMANN MECHANICAL TIP)**

(AFTER SCHMERTMANN, 1969) - unpublished

2.2.3 Bearing on Local Friction Sleeve: Soil bearing on the bottom bevel of the mechanical friction sleeve may account for a significant portion of the apparent total sleeve friction force. For example, Begemann suggests 50% in sands. Some comparative tests in Florida sands indicated about 65% due to bevel bearing. Thus, the actual sand-steel friction,  $f_s$ , or friction ratio,  $R_f$ , in sands equals only about 1/2 to 1/3 that measured using the Begemann tip. This bevel bearing error seems much less significant in clays; therefore tentatively neglect it in clays.

2.2.4 Sleeve Surface Roughness: The nature of the surface on the steel friction sleeve plays a major part in determining the magnitude of  $f_s$ . The ASTM D-3441 Standard in Appendix II includes requirements for material and roughness. The engineer should replace sleeves that have worn noticeably smoother or rougher than specified.

2.2.5 Soil Ductility Controls  $R_f$ : Some recent research by Al-Awkati (1975) indicates that a soil's ductility (say expressed by its strength/modulus ratio) represents the most important property controlling  $R_f$ . Clays have a relatively high  $R_f$  because of their relatively high ductility. Sands have a relatively low  $R_f$  because of their relatively low ductility. However, be alert for special cases. For example, the Piedmont micaceous, residual silts have a very high  $R_f$  because of their high ductility resulting from the modulus-reduction effects of the mica. Shelly sands have a very low  $R_f$  because of their low ductility resulting from the brittle-breakage of the shell fragments.

2.2.6 Special Pore Pressure Effects: Special pore pressure effects can also change  $R_f$ . For example, the writer has noted very high  $R_f$  values in loose, silty sands when using the Begemann friction cone tip. This probably results from partial liquefaction during the  $q_c$  measurement, followed by rapid pore pressure dissipation. By the time the friction sleeve tests for  $f_s$  during the next 20-cm increment, the shear strength of the sand has increased substantially, thus producing a too-high  $R_f$ . Note that the electric tip of the Fugro type, with its continuous penetration and the friction sleeve immediately above the base of the cone, cannot cause such a distortion of  $R_f$ .

### 2.3 Critical Depth from Surface or Interface

The concept of a critical depth in a  $q_c$  profile has been advanced by several engineers, including Kerisel, DeBeer and Schultze. It involves the idea that as a penetrometer tip advances downward from the surface, or through a weak to strong layer interface,  $q_c$  at first increases rapidly until the point is deep enough to no longer sense the interface above it. Then the tip achieves the "deep foundation" state wherein  $q_c$  supposedly becomes approximately constant with further depth penetration. The relative depth, in diameters, to reach this constant condition increases with increasing  $\phi'$ . However, discussions at the 1974 Stockholm ESOPT showed this concept is controversial.

The initial, rapid increase in  $q_c$  from a surface or interface is well known. However, the elastic-plastic slip field used to explain theoretically this behavior is in dispute because some engineers claim it ignores the dominant effect of soil compressibility on penetration behavior. This dispute continues over whether or not  $q_c$  then becomes constant with increasing depth of penetration in a uniform soil. All lab chamber tests produce data of the type illustrated in Figure I.1, indicating  $q_c$  continues to increase with greater  $\sigma'_v$ , but at a progressively reduced rate due to grain crushing. Some engineers have also challenged the quality of the research data used to support the critical depth concept. Others point out that other explanations not previously considered, such as illustrated in Figure 1(c) and discussed in 2.1, might explain a profile showing constant  $q_c$  below a certain depth.

Engineers should recognize that a cone penetrometer requires a penetration of about 8d to no longer sense an overhead interface -- as discussed in I.8 and subsequently when estimating pile tip bearing capacity. After this penetration, expect  $q_c$  to continue to increase with increased  $\sigma'_v$ , if all other variables are held constant, although at a decreasing rate. Keep in mind the alternate explanations for the shapes of various  $q_c$  profiles.

The available evidence, admittedly sparse, suggests that  $f_g$  also increases from the surface, or other interface, in a manner similar to  $q_c$ . Tentatively assume that in the same soil the  $R_f$  remains constant as the cone penetrometer, or a pile, penetrates from an interface to a depth where it no longer senses this interface.

### 2.4 Uniformity of Soil Conditions, Stratigraphy

Because of the speed of making a sounding and the detail provided in the  $q_c$  and  $R_f$  logs, the CPT is an especially valuable tool to investigate the uniformity of soil conditions under a structural area or between widely spaced preliminary borings. Figure 3, from Begemann (1963), illustrated this for one site in Holland.

Figure 4 illustrates the use of the CPT to more accurately define a local condition -- in this case the size of the soil-limestone interface cavity found from 9 to 11 m at S-3. After sounding S-3 located a cavity the additional four adjacent soundings quickly showed the limited size and slot-shape of the cavity and the probable ease with which the overlying sands could arch across.

## 2.5 Position of the Water Table

There seems to be no convincing evidence to indicate that the position of the water table can be determined consistently by noting significant changes in the  $q_c$  profile at the level of the water table. Theoretically, the capillarity and the resulting negative pore pressure above the water table should stop when passing thru the water table, perhaps producing a discontinuity in the rate of increase of vertical effective stress at the water table. From I.2 in Appendix I there should be a similar discontinuity in the  $q_c$  profile. However, in practical circumstances other partial saturation effects and the natural variations in cone bearing seem to often mask this discontinuity in the  $q_c$  profile.

In some soils, particularly those older and relatively free draining, a higher- $q_c$  layer forms around present or past groundwater levels. The ordinary fluctuations around some average level produce many cycles of wetting and drying, which may produce chemical precipitation, which produces cementation between grains, which produces a distinctly higher- $q_c$  layer. One can sometimes use this phenomenon to explain some high- $q_c$  layers.

In clays, past or present groundwater levels are usually associated with overconsolidation above groundwater level from drying and the resulting capillary stresses, forming a "drying crust." One can sometimes identify probably drying crusts from  $q_c$  profiles (as in Figure 1 (a)) and use such to either help locate past or present groundwater levels or help explain the profile.

Some engineering firms, such as Fugro, also sometimes use cone penetrometer tips that incorporate a piezometer. If pore pressure determinations during penetration, or at equilibrium with no penetration, and/or knowing the position of the water table are important, then use this type of piezometer cone tip. In cases where the hole made by an ordinary penetrometer tip remains open after withdrawing the penetrometer, then lowering an electric water level probe into this hole provides a convenient means for determining the highest piezometric water level along this hole. Determine the level of the water in the penetrometer hole immediately after completing the sounding and at convenient time intervals thereafter until reaching equilibrium.

In the first place one can determine quickly the trend of the layers in the vertical and horizontal directions.

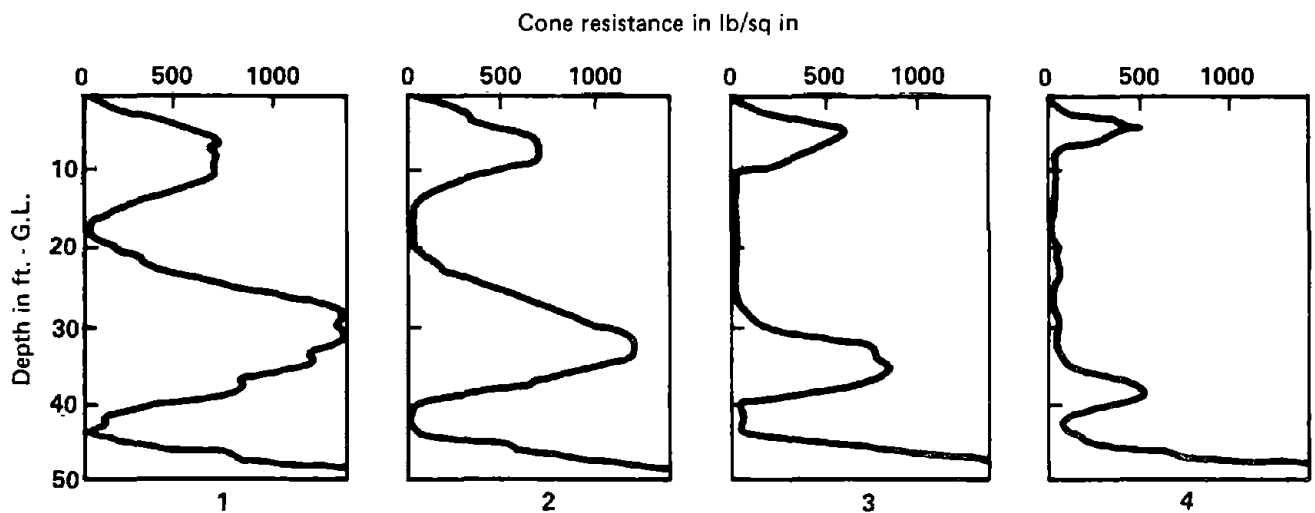
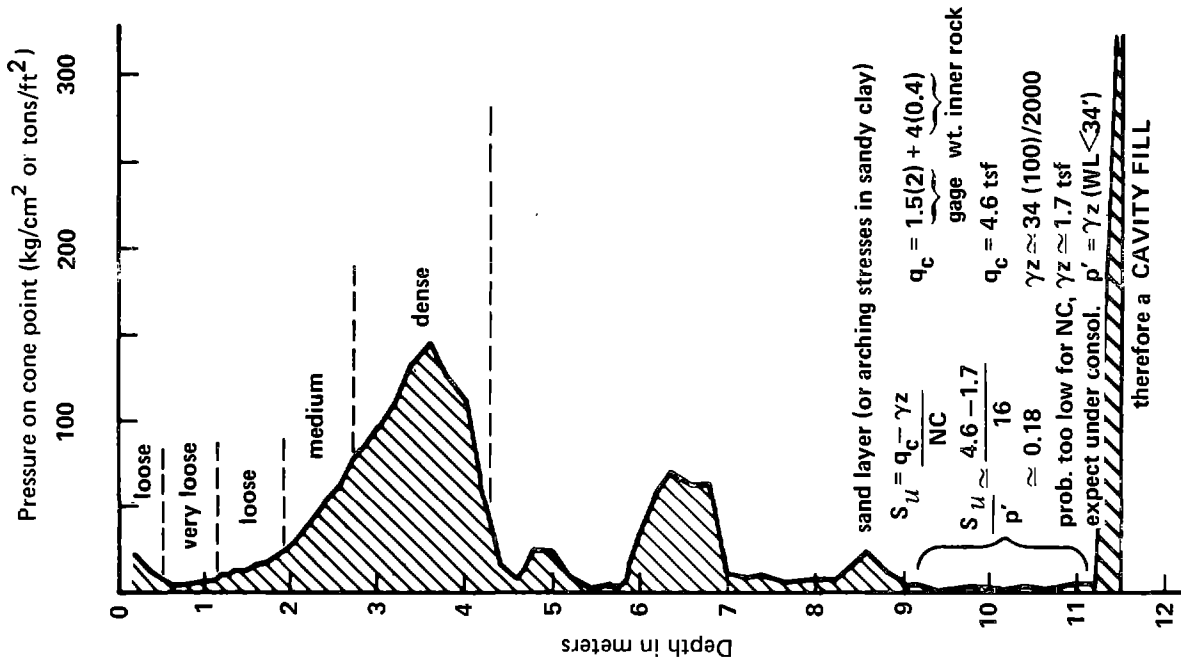


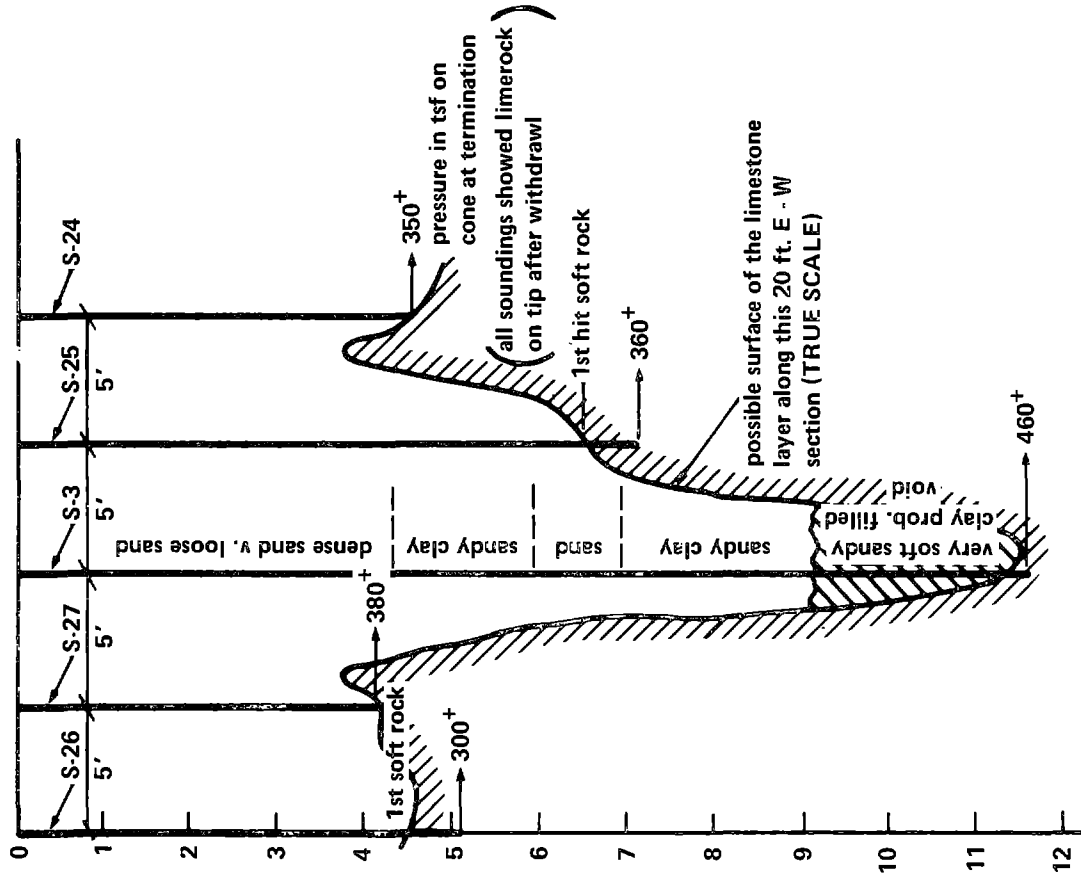
Fig. 4

This will be clear from the following simple example (see Fig. 4). In this case, a light building could be founded on the upper sand layer, although it will be immediately clear that more settlement will take place at sounding 4 than at sounding 1 owing to the greater thickness of the soft layers. For heavier buildings, a pile foundation will be necessary for which the second layer is nevertheless not suitable because of its small thickness at position 4 and its rather poor quality at 2 and 3. The piles should be placed in the third sand layer.

**FIGURE 3 – EXAMPLE (from Begemann, 1963) SHOWING THE USE OF CPT  $q_c$  PROFILES TO DISCOVER THE VARIATION IN THICKNESS AND QUALITY OF POTENTIAL PILE BEARING LAYERS ACROSS A SITE**



Above: Cone bearing log of S-3. Also illustrates calculated low  $s_u/p'$  ratio indicating probable cavity fill.



Note: Soundings S-24, -25, -26 and -27 made with Dutch mantle cone tip, advanced without gage readings, for the purpose of quickly better defining the nature of the rock surface and the likely geometry, in section, of any cavities above this rock.

FIGURE 4. – EXAMPLE OF THE USE OF STATIC CONE SOUNDINGS TO QUICKLY CHECK ROCK SURFACE PROFILE AND CONFIRM POTHOLE AND PROBABLY UNDERCONSOLIDATED CLAY NATURE OF CAVITY FILL

## 2.6 Sand; Estimating Relative Density

Static cone bearing capacity provides an indicator of the relative density of sands. Unfortunately, grain size distribution, cementing, lateral stresses, and depth of overburden also significantly affect  $q_c$ , as well as the previously mentioned compressibility, tip shape, pore pressure and thin-layer effects. Previous investigations of the  $q_c$ - $D_r$  correlation have shown considerable differences, as illustrated by Mitchell & Gardner (1975, Fig. 30).

A recent series of about 80 correlation tests in the 4 ft diameter University of Florida triaxial,  $K_0$  calibration chamber had the aim of establishing a better  $q_c$ - $D_r$  correlation. We evaluated these tests in addition to those discussed on pp. 83-85 of Appendix III. Figure 5 presents our latest correlation, applicable to saturated, NC sands. The sands tested include 2 artificial fine sands with opposite-extreme crushabilities, 2 natural fine sands -- one with appreciable mica, and 1 natural and one artificial medium sand, with all sands with uniformity coefficients between 1.8 and 2.2, and a maximum of 9% passing the 200 sieve. We tested dry over a  $D_r$  range of about 50-100% for the medium sands and both dry and saturated over 20-80% for the fine sands, and used both the mechanical and electrical tips. We also used constant-stress and constant-volume chamber boundary conditions and assumed the field case, Figure 5, one-third from the constant-stress towards constant-volume case.

The use of CPT data, from quartz sands clean enough to be suitable for relative density evaluation, will produce a Figure 5 estimate of  $D_r$  with a std. deviation of about 10%.

For the case of overconsolidated (OC) sands, Figure 5 predicts relative densities that are too high. Use Figure I-2 as a basis for correcting for horizontal effective stresses greater than for the NC case. Considering that in situ horizontal stresses are rarely, and perhaps never, known accurately, an approximate procedure for accounting for lateral stress effects may prove adequate. Estimate the effects of OC by using Figure I-2. Equation (2) expresses a formula, also plotted in Figure I-2, to give an equivalent NC  $q_c$ ,  $q_{cNC}$ , if one knows the ratio  $K'_{oOC}/K'_{oNC}$ . You can estimate this ratio from the OCR by using Equation (3). Equations (2) and (3) are empirical. The available data suggest they will also work in clays.

$$q_{cOC}/q_{cNC} \approx 1 + 3/4 \left( \frac{K'_{oOC}}{K'_{oNC}} - 1 \right) \quad (\text{Eq. 2})$$

$$\frac{K'_{oOC}}{K'_{oNC}} \approx (\text{OCR})^{0.42} \quad (\text{Eq. 3})$$

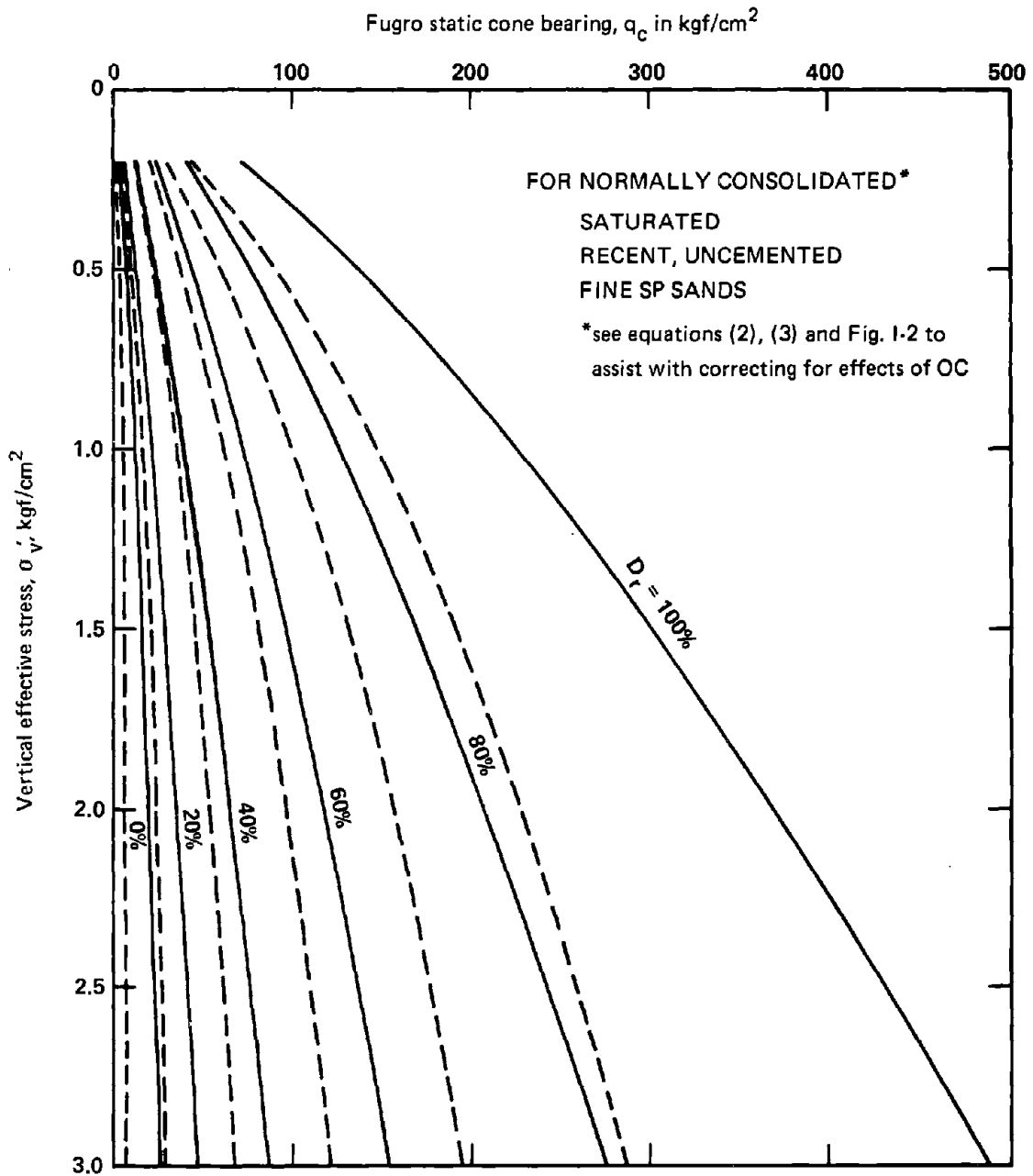


FIGURE 5 – UPDATED  $q_c$ - $D_r$  CORRELATION (solid)  
Previous correlation (dashed)

## 2.7 Clay; Estimating Sensitivity and Overconsolidation

2.7.1 Sensitivity: The sensitivity of a clay, defined as:

$$S_t = \frac{\text{max. undrained shear strength of undisturbed clay}}{\text{max. undrained shear strength of same clay after repeated applications of high shear strains (remolded)}}$$

$$= \frac{s_{uu}}{s_{ur}} \quad (\text{Eq. 4})$$

represents one measure of the "remoldability" of a clay's structure. Unfortunately, the magnitude of sensitivity,  $S_t$ , depends on the test methods used to obtain the undrained strengths. (See 5.2.1 for a more detailed discussion of undrained strengths.) We know that in the same type clay, the greater  $S_t$  the lower  $R_f$ . However, any accurate equation relating  $S_t$  to  $R_f$  should account for the stress-strain behavior of the undrained clay and the type penetrometer used. We do not know enough to do this at present. Equation (5) does provide a rough method for estimating the  $S_t$  of a clay, as obtained from a Geonor or Nillcon-type field vane, based on  $R_f$  from the Begemann tip.

$$S_{t_{\text{field vane}}} = \frac{15}{R_f\%} \quad (\text{Eq. 5})$$

2.7.2 Overconsolidation: An engineer can also use the CPT to estimate the extent of overconsolidation of a clay. We know from theory and experience that the undrained strength of a normally consolidated clay falls within a limited fraction of the effective overburden pressure on that clay. This fraction appears to vary primarily with the plasticity (PI) of the clay -- the higher the PI the higher the fraction. However, the geologic environment of deposition (for example, salt versus fresh water) and postdepositional changes (as with quick clays) have an influence. Secondary creep, or delayed compression, increases this fraction. Nevertheless, this fraction usually falls between 0.16 and 0.4, and rarely exceeds 0.6, based largely on field vane tests and  $K_0$  triaxial compression tests. Thus, if we find a clay's undrained

strength exceeds 0.6, or even 0.5, times its effective overburden pressure, we can say this clay is likely overconsolidated. From Ladd & Foott (1974) and Koutsoftas and Fischer (1976, p. 996) we now have sufficient data to make an estimate of the overconsolidation ratio of a clay based on its current  $s_u/p'$  ratio.

Figure 6 presents a correlation showing the ratio of undrained strength to undrained strength normally consolidated as a function of the overconsolidation ratio (OCR). Accepting an average normally consolidated  $s_u/p'$  of 0.33 as applicable to most post-pleistocene clays, and using the approximate numbers discussed in 5.2.1 to estimate undrained strength from  $q_c$ , we can determine the ordinate in Figure 6 and use the curve to estimate OCR. Of course, this would not apply exactly to all clays. For example, it would overestimate OCR for fresh water, montmorillonite clays and underestimate OCR for quick clays. Nevertheless, an estimate of OCR can be very useful to estimate compressibility and make preliminary settlement predictions (see 6.2.1) and by Eq. (3) to estimate in situ lateral stresses resulting from overconsolidation.

The reader should recognize that the above method to estimate OCR can lead to large error. The determination of  $s_u$  depends on the method used. For example, unconfined tests on undisturbed samples often produce different  $s_u$  than field vane tests. Even different types of field vanes can produce significantly different  $s_{uv}$ . One can also err significantly when estimating  $p'$  because of uncertainties in unit weights and in situ water pressures. For example, assume  $s_u/p' = 0.66$  is "correct." A -25% error in  $s_u$  due to poor vane test technique or unconfined test sample disturbance, combined with a +25% error in estimating  $p'$ , would produce  $s_u/p' = 0.33$ . Because 0.33 represents a good average for the NC case, the engineer would likely judge this clay as NC, while, from Figure 6, with accurate data he would estimate an OCR = 2.3. Further, if this clay had an actual, but unknown, NC  $s_u/p'$  ratio = 0.22, the estimated OCR would increase to 4.0.

Consider the following as an alternate method for estimating the OCR in clay layers sufficiently thick and homogeneous: sometimes the  $q_c$ -depth profile in a single clay layer, or a succession of seemingly similar clay layers, will define an apparent linear increase in  $q_c$  with depth -- as shown in Figure 7. Extrapolating this  $q_c$ -depth line to  $q_c = 0$  defines an intersection point "o" which can be taken as the highest probable past ground surface -- suggesting past erosion of "d" depth of soil and overconsolidation due to this D. However, this assumes "origin cohesion,"  $c_o = 0$ , and therefore an "origin  $q_c$ ,"  $q_{c0} = 0$ . The available data indicate  $c_o$  for many clays = about 0.05

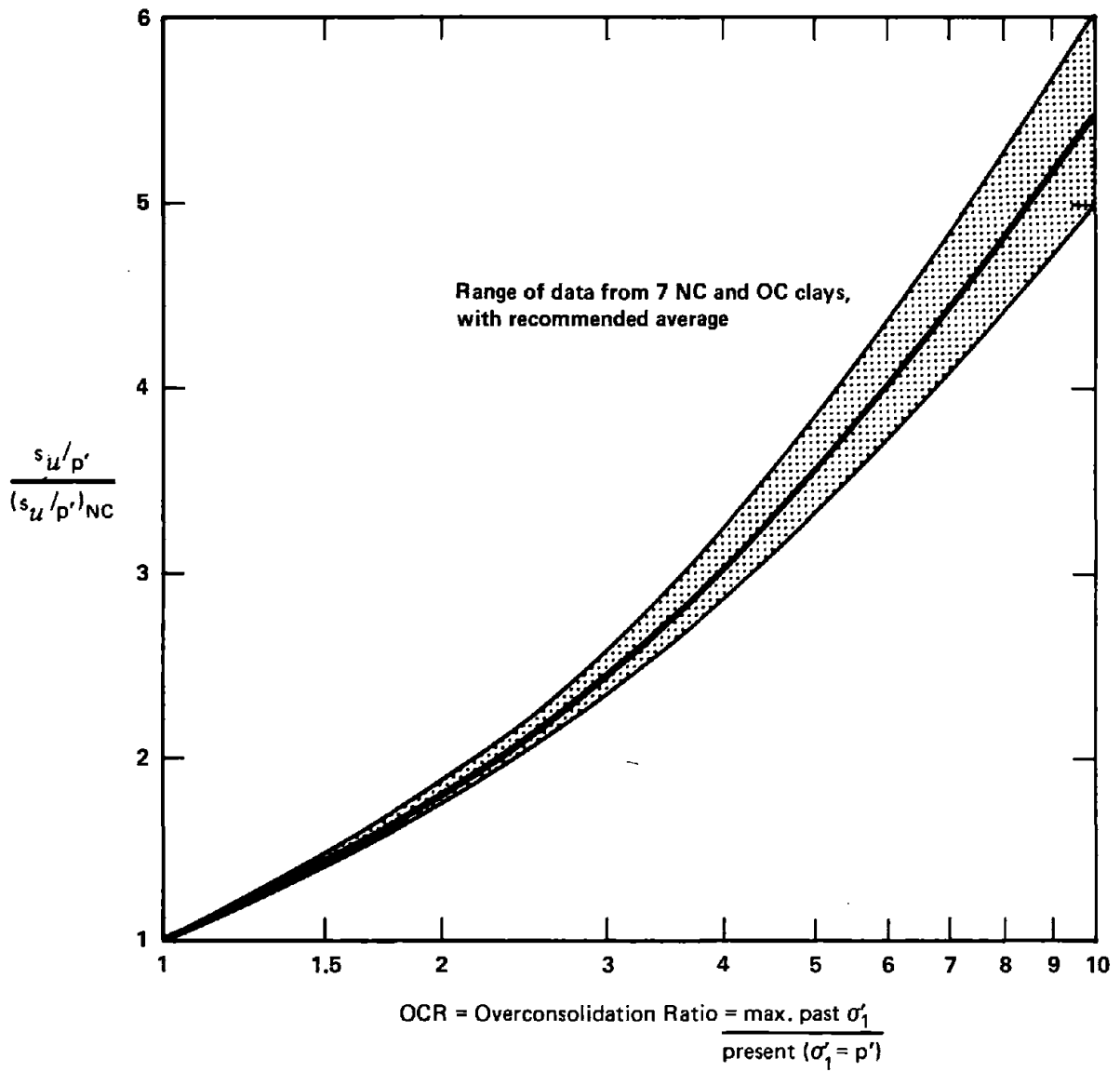


**FIGURE 6 – NORMALIZED  $(s_u/p')$  RATIO VS. OCR FOR USE IN ESTIMATING OCR FROM  $q_c$  IN CLAYS**

to  $0.10 \text{ kg/cm}^2$ , thus producing a maximum  $q_{c0}$  for about  $1.0 \text{ kg/cm}^2$ . Obtaining the  $q_c$ -depth extrapolated line intercept with  $q_c = 1.0 \text{ kg/cm}^2$  would produce a more conservative value for "d", as shown in Figure 7, and is recommended.  $D = 0$  suggests normal consolidation and a negative  $D$  underconsolidation. Note that because of the usually small closure angle,  $\alpha$ , this method is sensitive to different clay layers erroneously assumed homogeneous, to layers too thin or too  $q_c$ -erratic for accurate extrapolation, and to poor penetrometer load cell calibration for the  $q_c = 0$  line.

## 2.8 Correlation with SPT

The extensive use of the standard penetration test (SPT) in the United States makes it of interest to attempt a correlation between the SPT blow count values (N-values) and  $q_c$  in  $\text{kg/cm}^2$  or  $\text{tons/ft}^2$ . Sanglerat (1972, section 9.5) discusses these correlations in some detail. Schmertmann (1971, 1974 c) presented a theoretical correlation between the SPT and cone sounding data. Among other things, this work showed that N-values in most soils should correlate better with  $f_s$  than with  $q_c$ . Sanglerat (1971, 1972-9.5) discusses Schmertmann and notes that the  $q_c/N$  ratio should decrease with increasing cohesiveness of the soils tested. Meyerhof (1956) suggested that  $q_c/N$  equals approximately 4 in sands. The more detailed correlation presented by Schmertmann (1970), presented here as Figure 8, showed that a value of 4 was a reasonable average but that the scatter was very great. Table 1 presents previously suggested, purely empirical, approximate values of the  $q_c/N$  ratio for different soil types. Use Table 1 with appropriate caution.

Some recent (Schmertmann, 1976) research at the University of Florida, involving the stress wave dynamics of the SPT and expended-energy matches with parallel CPTs, has demonstrated that the  $q_c/N$  ratio varies with incident rod energy in the SPT, with  $R_f$ , and with the magnitude of  $q_c$ . Figure 9 presents a semi-theoretical correlation between these variables for the 50% level of incident energy ( $140 \text{ lb} \times 30 \text{ in} \times \frac{1}{2}$ ) -- an approximate average level attained by typical, cathead and rope type, US SPT rigs. The use of Figure 9 requires a knowledge of  $R_f$  as obtained from a Begemann type tip. If one has only SPT data available, then the ratios of ( $N_{0-6 \text{ in}}/N_{12-18 \text{ in}}$ ) and/or ( $N_{6-12 \text{ in}}/N_{12-18 \text{ in}}$ ) can provide a measure of  $R_f$ . The insert Table 2 below Figure 9 lists the theoretical values of these ratios for various  $R_f$ , based on Schmertmann (1971) but modified for SPT samplers designed for liners and used without them.

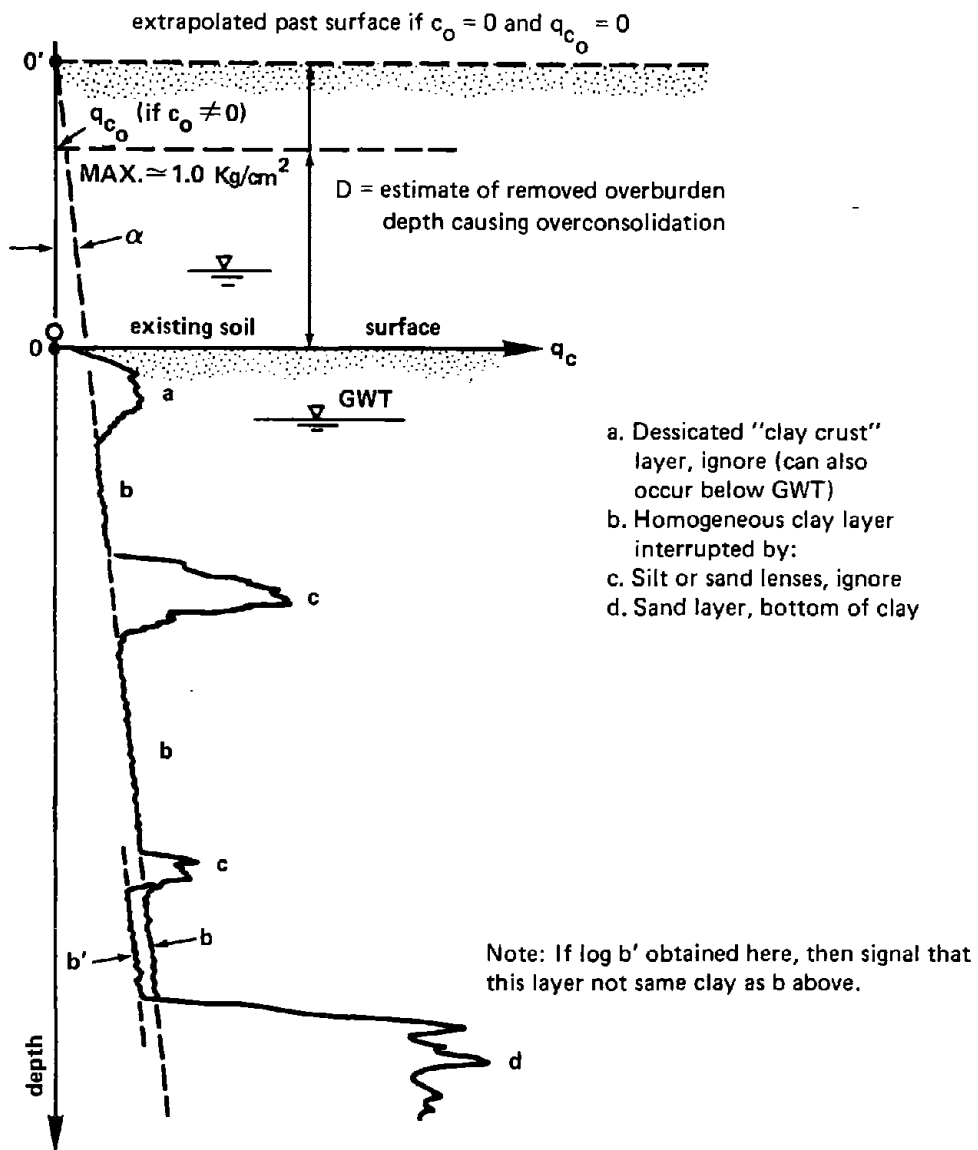
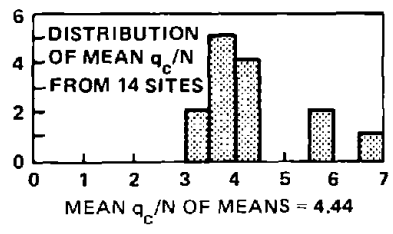
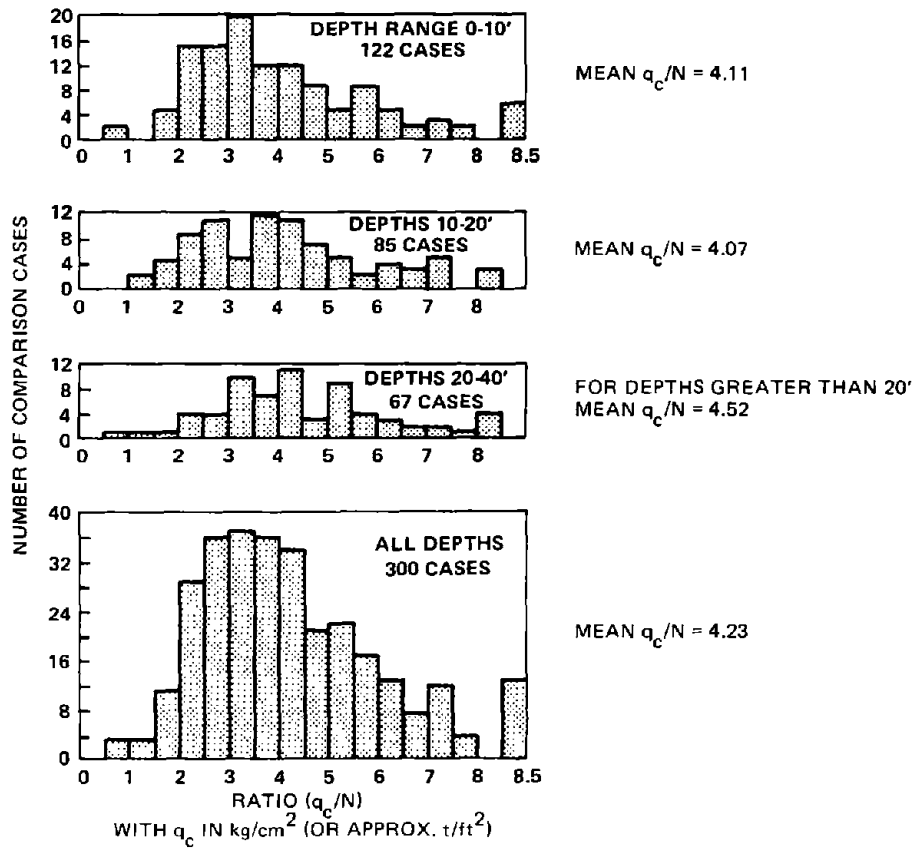


FIGURE 7 – EXTRAPOLATION OF THE  $q_c$ -PROFILE AS AN ALTERNATE METHOD TO ESTIMATE OVERCONSOLIDATION IN THICK, HOMOGENEOUS CLAY LAYERS

PLOTTED BELOW ARE FREQUENCY DISTRIBUTIONS  
SHOWING THE EFFECT OF DEPTH



EFFECT OF MAGNITUDE OF SPT N-VALUE

RANGE	LEAST SQUARES LINE	CORREL. COEFF.
$0 < N < 10$	$q_c = 4.88 N$	0.43
$0 < N < 30$	$q_c = 4.13 N$	0.72
ALL N	$q_c = 18.3 + 2.9 N$	0.80

FIGURE 8 – DATA FOR CORRELATING N AND  $q_c$  IN SILTY TO MEDIUM SANDS  
(Comparison holes 3-10 ft. apart; all  $q_c$  by University of Florida; N by 7 firms at 14 sites, 13 of which in Florida; all N are uncorrected.)  
(from Schmertmann, 1970)

TABLE 1 – Typical  $q_c$  ( $kg/cm^2$ )/N(SPT blows/ft) Ratios

Type soil	Fugro tip	Delft mechanical tips
sand & gravel mixtures	8	6
sand	5	4
sandy silts	4	3
clay-silt-sand mixtures	2	2
insensitive clays	1	1½
sensitive clays	ratios can get very high because N → 0	

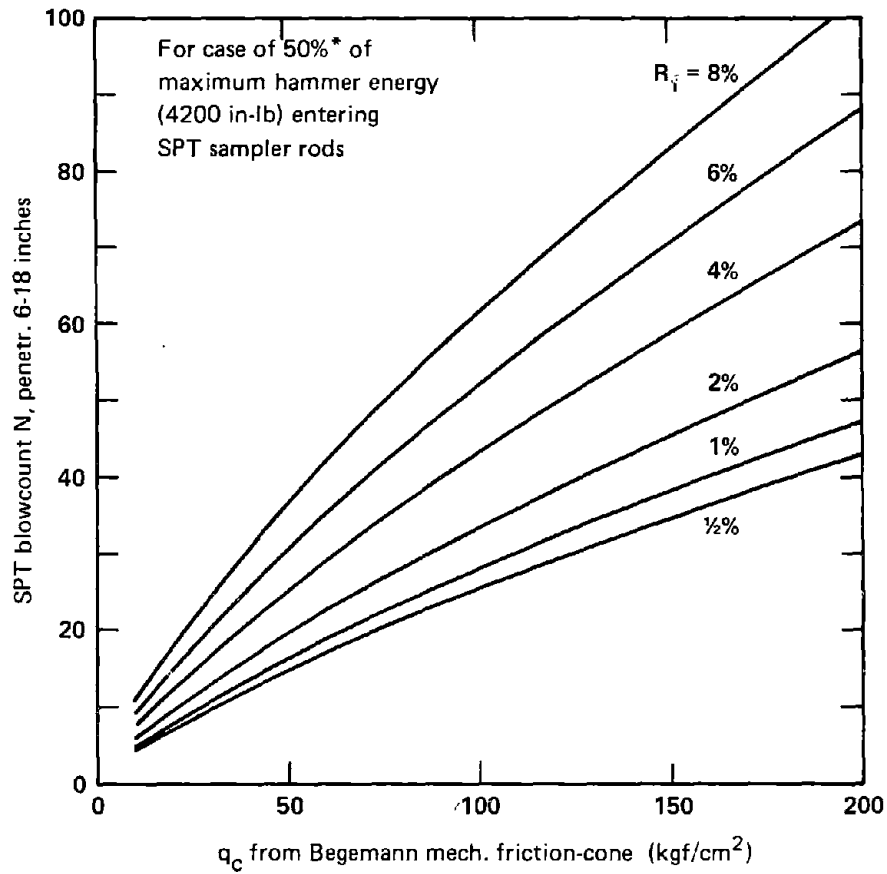


**FIGURE 9 – EXPERIMENTAL-THEORETICAL RELATIONSHIP BETWEEN  $q_c$  AND N, USING LINER SPT SAMPLER WITHOUT LINERS AND DELFT MECHANICAL CONE**  
 \*(current data indicates 50% approx. US ave.)  
 (from Schmertmann, 1976)

**TABLE 2 – Method for estimating  $R_f$  from 6" incremental SPT data using same equipment as in Fig. 9 (from Schmertmann, 1976)**

$R_f\%$	$\Delta N_{0-6''} / \Delta N_{12-18''}$	$\Delta N_{6-12''} / \Delta N_{12-18''}$
1/2	0.85	0.93
1	0.76	0.88
2	0.65	0.83
4	0.53	0.77
6	0.46	0.73
8	0.425	0.71

### 3. CPT FOR COMPACTION CONTROL

Because of the relatively large cone diameter, the CPT is not especially suitable to check the compaction of the surface 12 inches (30 cm) of compacted soil done from either the surface or built up in layers. One cannot easily check the compaction of a single, surface 6 to 9 inch lift with the CPT. However, engineers have found  $q_c$  quite suitable for checking deeper compaction. Within the top 12 inches the magnitude of the  $q_c$ -depth gradient provides a more suitable measure of compaction. Alternatively, the value of  $q_c$  at a specified depth from the surface, say 6 or 12 inches might prove useful. Figure 10 presents a page of examples using the CPT to check the compaction of sands using heavy vibratory rollers from the surface and the vibroflotation process. One must have local experience and obtain local correlation with dry density, relative density, % compaction, CBR, etc. before deciding on combinations of acceptable depth- $q_c$  compaction standards.

As explained in section I.3 of Appendix I, and noted in section 2.6,  $q_c$  increases not only with the increased density resulting from compaction but also from the increased lateral stresses from the overconsolidation produced by the compacting rollers. These stresses may later diminish, for example due to adjacent excavation. To obtain the relationship between  $q_c$  and density you must correlate locally, using the same or similar compaction equipment, to eliminate that portion of the  $q_c$  increase due to increased stresses.

The writer has had only one opportunity to check the possible relationship between  $q_c$  and the CBR -- in a vibratory-roller-compacted fine sand in Florida. In this case he found that  $CBR = q_c$  (tsf at 6 inch depth)/3.

The CPT has also proven especially useful for checking the adequacy and completeness of excavating undesirable materials and replacing with suitable materials. For example, peat layers left inadvertently beneath a sand fill may be easily located. The CPT has also proven useful to check the general adequacy and uniformity of a placed fill.

CPT soundings can also be used to locate undesirable obstructions such as boulders, old footings, old piling, etc.

Section 3.35, pp. 97-99 in Appendix III, also discusses the use of the CPT for testing soil compaction and presents another example.

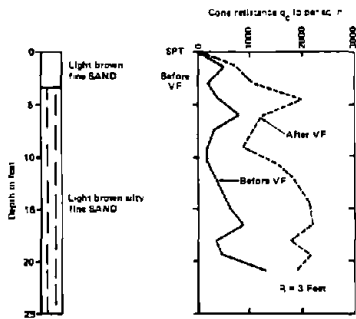


Fig. 3. — Example of in situ test results obtained during preconstruction and compaction control testing of aeolian sands—factory site

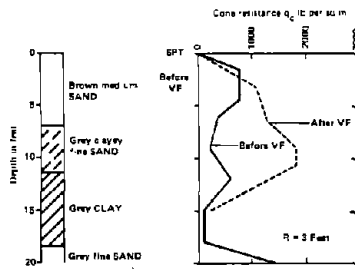


Fig. 4. — Example of in situ test results obtained during preconstruction and compaction control testing of dune sand—oil tank site

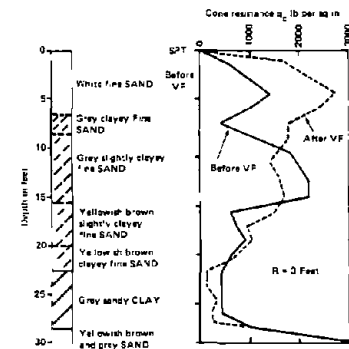


Fig. 2. — Example of in situ test results obtained during preconstruction and compaction control testing of clayey alluvial sands—sugar silo site

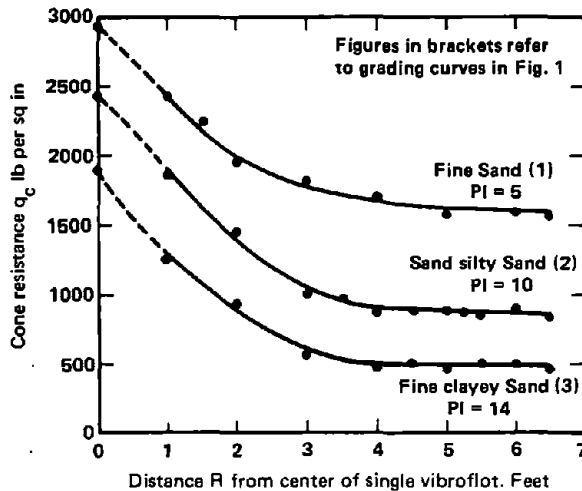


Fig. 5. — Variation of cone resistance with distance from center of compaction—clayey alluvial sands—sugar silo site

Ref:  
 D.L. Webb and R.I. Hall "Effects of vibroflotation on clayey sands"  
 ASCE Journal SM&FD Nov. 69, pp. 1365-1378  
 J.H. Schmertmann Discussion of: "Sand densification by heavy vibratory compactor"  
 ASCE Journal SM&FD Jan. 70, pp. 363-365

Figure Nos. from above refs.

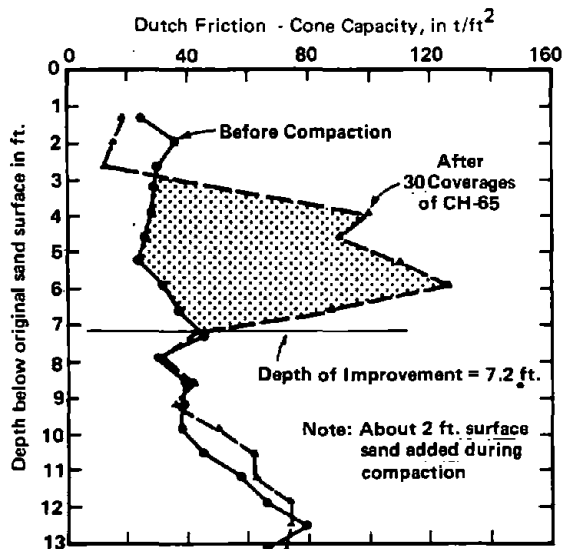


Fig. 11. — Static cone penetrometer definition of effect of roller compaction in fine sand and silty sand below water table

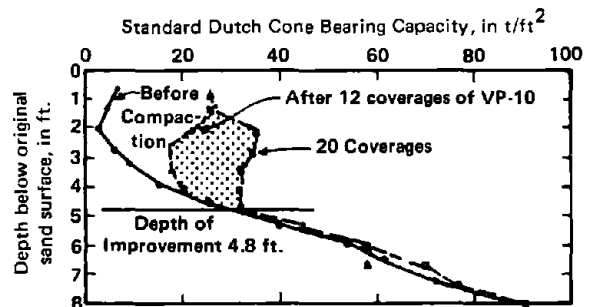


Fig. 10 — Static cone penetrometer definition of effect of surface roller compaction in fine sand above water table

**FIGURE 10 — EXAMPLES OF USING THE STATIC CONE PENETRATION TEST TO MEASURE THE EFFECTS OF VIBROFLOTATION AND VIBRATORY ROLLER COMPACTION IN SAND**

## 4. PILE DESIGN

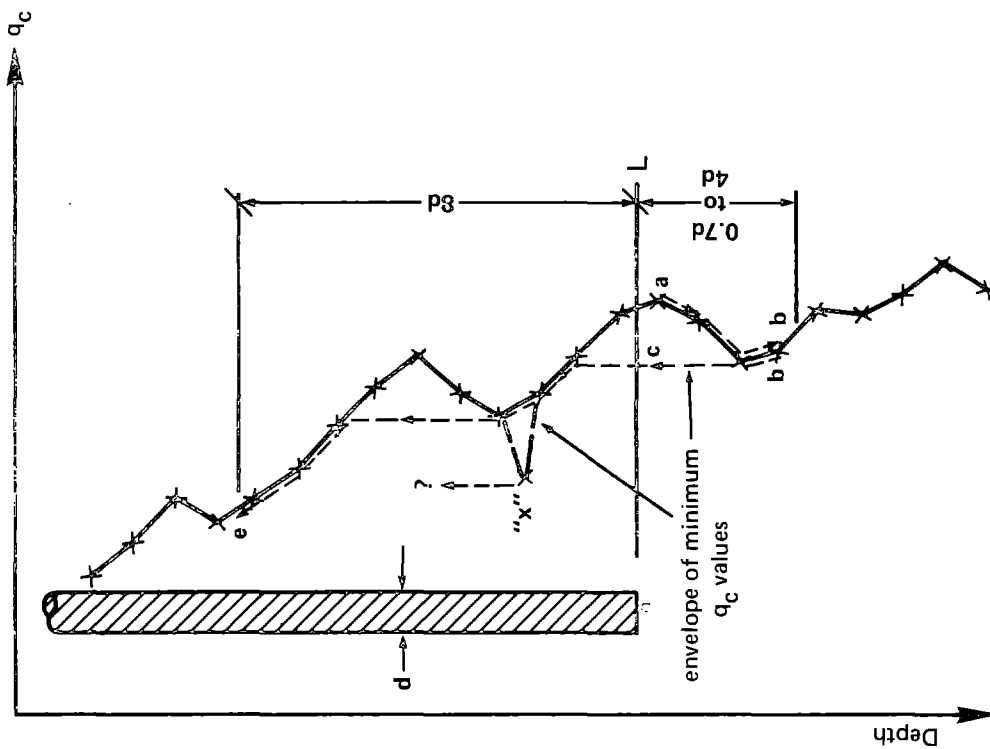
The modern CPT to which these Guidelines apply evolved from the work in the Netherlands that began over 40 years ago. The Dutch developed the CPT primarily as a model pile for the efficient positioning of piles in sand layers below thick compressible deposits and to more accurately estimate their static capacity when bearing in these sands.

### 4.1 Driven, Displacement, Straight-sided Piles

4.1.1 End Bearing: Figure 11 details the basis for the computation of ultimate pile end bearing resistance using Fugro-type tip penetrometer data. The procedure remains the same for the pile tip embedded in either sand, clay or mixed soils. The zone of pile tip support includes 0.7 to 4d below the tip and 8d above the tip. For all soils the engineer searches over this 0.7 to 4d range for the lowest below-tip contribution to end bearing, using the method in Figure 11. However, if a much weaker layer exists between 4d and 10d, and seems significant, then use appropriate judgement to reduce  $q_p$  accordingly. If the continuous  $q_c$  profile above pile tip shows a relatively few, abrupt "x" reductions and recoveries of  $q_c$  below the "envelope of minimum values," ignore them in all steps of the computation. Appendix IV has examples of the Fig. 11 method.

Because of possible uncertain size effects, differences in the settlement-rate of  $Q_p$  and  $Q_s$  mobilization, negative pore pressure during CPT penetration of very dense fine and silty sands, grain crushing and high pressure creep effects, it has been customary in Holland to employ both a  $q_c$  and a  $q_p$  cutoff level. When computing pile  $q_p$  using the method outlined above and in Figure 11, all  $q_c$  above the cutoff magnitude are reduced to the cutoff magnitude. The Dutch engineers often use a cutoff of 300 kg/cm<sup>2</sup>, and a maximum ultimate  $q_p$  of 150 kg/cm<sup>2</sup> in sands and 100 kg/cm<sup>2</sup> in very silty sands.

Because the problem does not often arise, engineers know relatively little about the allowable end bearing in clays. The research by Nottingham (1975), summarized by Nottingham and Schmertmann (1975), and even further digested in section 3.24 of Appendix III, suggests the Dutch end bearing calculation method will also work well in NC or lightly OC clays with



DUTCH PROCEDURE FOR PREDICTING PILE TIP CAPACITY

FIGURE 11

$$q_p = \frac{q_{c1} + q_{c2}}{2}$$

$q_{c1}$  = Average  $q_c$  over a distance of  $8d$  below the pile tip (path a-b-c).  
 Sum  $q_c$  values in both the downward (path a-b) and upward (path b-c) directions. Use actual  $q_c$  values along path a-b and the minimum path rule along path b-c. Compute  $q_{c1}$  for  $y$ -values from 0.7 to 4.0 and use the minimum  $q_{c1}$  value obtained.

$q_{c2}$  = Average  $q_c$  over a distance of  $8d$  above the pile tip (path c-e).  
 Use the minimum path rule as for path b-c in the  $q_{c1}$  computations. Ignore any minor "x" peak depressions if in sand, but include in minimum path if in clay.

$s_u = 1000$  psf or less. However, the end bearing in such clays will usually represent only a minor part of the total capacity of a pile.

Occasionally, engineers drive piles that bear in very strong, highly OC clays and the Dutch calculation for end bearing produces a significant fraction of the total capacity of the pile. But, pore pressure dissipation effects, high pressure creep, and soil-structure weakness on a larger scale caused by cracks, fissures, slickensides, etc., all argue for reducing ultimate end bearing from that calculated in such clays. In the absence of better data, the writer suggests using the "Woodward" adhesion ratio reduction factor,  $\alpha$ , presented in Figure 12 to reduce end bearing as computed by the Figure 11 method. Figure 11 applies to all pile materials.

4.1.2 Side Friction: Evaluating side friction from the results of a friction-cone CPT involves an experience and back-up research record much less than that for end bearing resistance. The development of the friction-cone tip, with its local sleeve to measure soil-steel friction at the tip, has greatly improved the accuracy possible for the prediction of soil-pile side friction. Friction on the tip friction sleeve can be greatly reduced if its diameter is less than that of the base of the cone point. This is especially true for the Fugro tip with the sleeve immediately above the cone. Check all penetrometer tips periodically to assure that the sleeve always has a slightly larger diameter.

4.1.2.1 Sand, with friction-cone  $f_s$  data: The research results by Freed (1973) and Nottingham (1975) provide the most comprehensive data on the use of  $f_s$  data to predict  $Q_s$  = the ultimate pile side friction capacity. Nottingham and Schmertmann (1975) gave the detailed design methods resulting from this work. In Appendix III, pp. 101-104 herein, the reader will find a summary of these methods. Use Equation (5) on p. 102. Note the depth-of-embedment correction over the initial 8B of pile penetration from the surface (in accord with section 2.3). However, for simplicity, Nottingham does not recommend similar corrections when crossing layer interfaces. For reasons similar to  $q_c$ , the Dutch engineers usually use limit values of  $f_s = 1.2$  kg/cm<sup>2</sup> in sands and  $f_s = 1.0$  kg/cm<sup>2</sup> in very silty sands when computing  $Q_s$ .

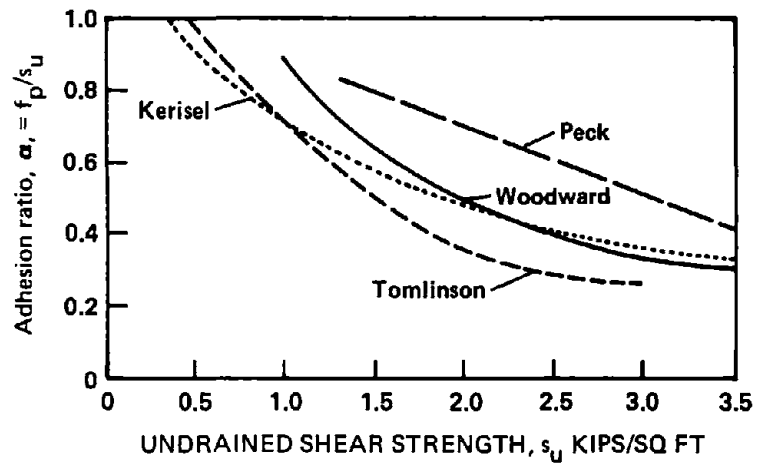


FIGURE 12 – CORRELATIONS OF CLAY ADHESION-PILE RATIO,  $\alpha$ , WITH UNDRAINED SHEAR STRENGTH  $s_u$

4.1.2.2 Sand, without  $f_s$  data: The following Table 3 lists the suggested values for "C" in Equation (6), which expresses some Dutch current practice for estimating ultimate pile friction in sand layers when having only  $q_c$  data. The  $q_c$  value of each  $q_c$  depth interval determines the contribution to  $Q_s$  over that interval.

$$Q_s = C \sum q_c A_s \quad (\text{Eq. 6})$$

With Table 3 as a guide, use appropriate judgement when selecting values of C for other types of piles. Note that the 4.1.1 cutoff level of 300 kg/cm<sup>2</sup> for  $q_c$  also applies to Equation (6).

Table 3 - "C" VALUES SUGGESTED  
FOR USE IN EQUATION (6)

Type Pile	C	Notes
a. Precast concrete	0.012	
b. Precast, enlarged base	0.009	only along shaft in a dense group of piles
c. Cast in situ displacement	0.018	Steel driving tube removed
d. "Vibro" pile	0.018	Steel driving tube removed
e. Timber	0.018	
f. Steel displacement	0.012	
g. Open ended steel pipe	0.008	

4.1.2.3 Clay: Presently the design concepts for the drained side friction of piles in clay are in a state of transition as the profession moves from the empirical concepts using undrained strengths to more rational concepts involving drained shear strength behavior. Three methods using CPT data are suggested herein. All require evaluating the undrained strength,  $s_u$ . Section 5.2.1 explains further how to estimate  $s_u$  from CPT data.

The first method involves an empirical correction factor by which to multiply  $s_u$  to obtain unit pile side friction. Figure 12 presents various investigator's estimates of this factor as a function of  $s_u$  itself -- the stiffer the clay the greater the reduction from  $s_u$ . The writer recommends using the "Woodward" curve.

The second method incorporates effective stress by including the average effective overburden pressure in the computations, in accord with Eq. (7).

$$Q_s = \lambda(\bar{p}' + 2\bar{s}_u) A_{st} \quad (\text{Eq. 7})$$

where:

$Q_s$  = predicted ultimate positive pile side friction force

$\bar{p}'$  = average overburden vertical effective stress along pile length

$\bar{s}_u$  = average undrained shear strength along pile length

$A_{st}$  = total side area of pile

The key  $\lambda$ -term was evaluated empirically (Vijay and Focht, 1972). Nottingham (1975) reviewed their data considering its probable validity for typical Foridal DOT pile lengths and sizes. As a result he plotted relative pile embedded length,  $L/B$ , vs.  $\lambda$ , resulting in Figure 13. The writer recommends using this modified form of the  $\lambda$  correlation. The use of Eq. (7) and Figure 13 requires a computation for the effective vertical overburden pressure, which one can usually estimate with satisfactory accuracy by estimating soil unit weights and the position of the water table.

The third method involves the direct use of  $f_s$  in clays, as suggested by Nottingham (Appendix III, pp. 102-105 herein). Because his research did not include clays with  $s_{uv} > 0.5 \text{ kgf/cm}^2$ , and because of the negative pore pressure and other effects noted previously and subsequently in stiff clays, also reduce  $f_s$  in accord with the "Woodward" curve in Figure 12. This again involves first estimating  $s_u$  (see section 5.2.1).

The rationale behind method 1 above is that driving piles in stiffer clays results in imperfect contact between clay and pile throughout the length of the pile, and that this contact becomes more imperfect the stiffer the clay; therefore, reduction factors should increase with stiffness. In addition, stiff clays can produce negative pore pressures during driving and these dissipate

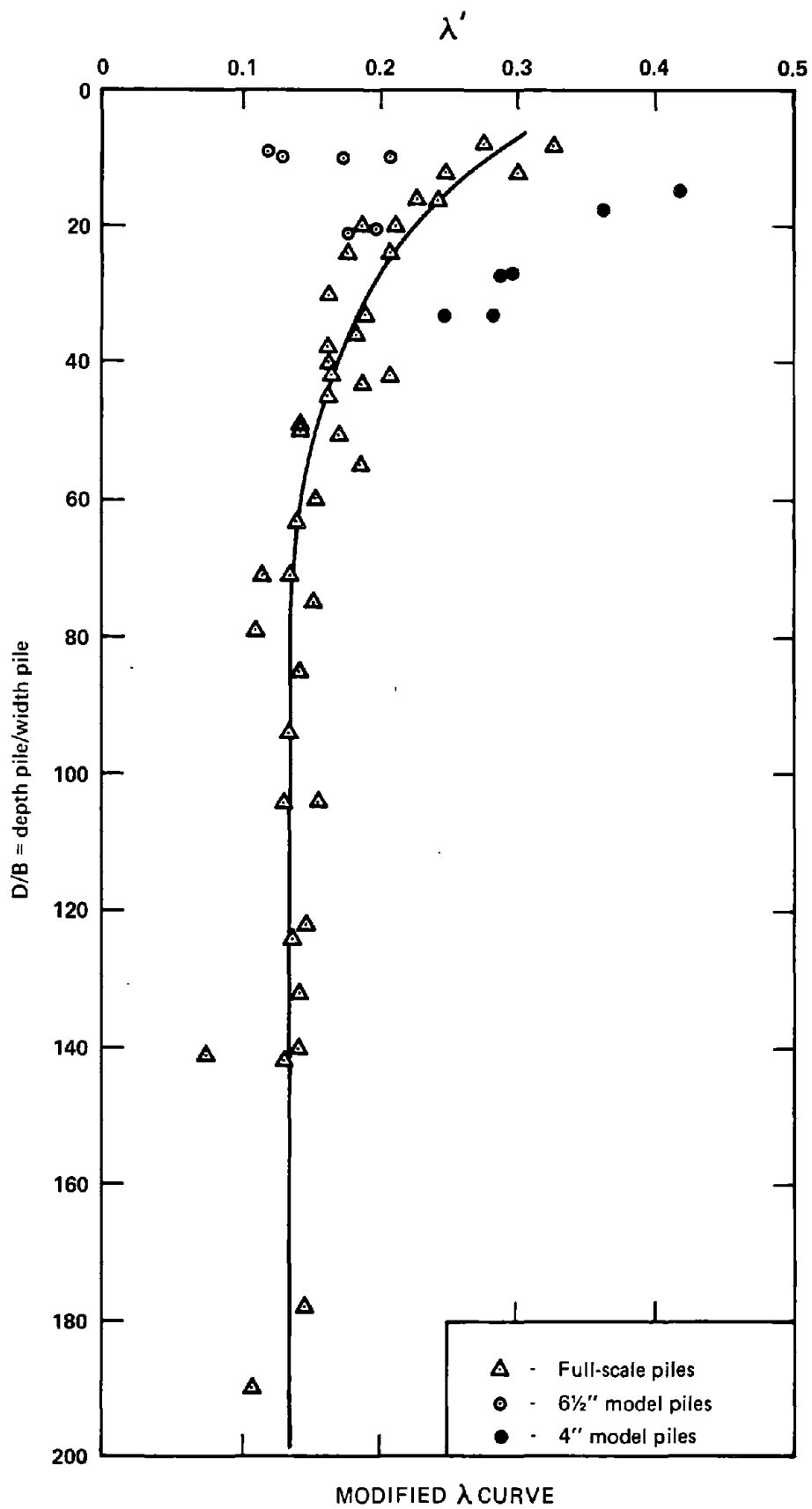


**FIGURE 13 – CORRELATION OF MODIFIED FRICTION CAPACITY COEFF.,  $\lambda'$ , WITH RELATIVE PILE PENETRATION (use  $\lambda'$  instead of  $\lambda$  in Vijay & Focht formula) (from Nottingham, 1975)**

with time and the clay weakens. The rationale behind method 2 is that the friction against the pile must depend on the lateral pressure against the pile, which in turn depends on the Rankine passive pressure,  $2s_u$ , for the undrained conditions during driving. The rationale behind method 3 is that it takes advantage of an actual in situ measurement of soil adhesion. Check your problem using all appropriate methods and use the answer that seems most reasonable considering local experience.

4.1.3 Negative Side Friction: The above section 4.1.2 applies to positive friction in which the friction force against the pile acts in the upward direction and the pile loads the soil and produces higher effective stresses in the vicinity of the pile sides and tip due to this loading. When the soil moves down, as by settlement, relative to the pile side, side friction forces reverse direction and the pile tends to support the soil, thereby reducing effective stresses against the pile, and thereby also reducing side friction. To estimate negative friction use 2/3 of the positive friction values computed above for a single pile.

4.1.4 Tension Piles: Again because of the resulting change in effective stresses due to the change in friction direction, use 2/3 of the computed compression friction for ultimate tension friction. For the special case of severely fluctuating tension loads, use only 1/3 of this computed tension friction over the middle 1/2 of the pile.

#### 4.2 Corrections for Shape of Pile and Method of Pile Insertion

It appears from the work of Begemann (1965) that the type of soil penetrated and the shape of the pile point can significantly change pile friction. Sharp points increase friction and flat points reduce friction. Because the cone has a relatively sharp  $60^\circ$  point, side friction is a near-maximum due to point effects when compared to real piles. Because this effect is not well understood for ordinary compression piles (Begemann's work was with tension piles), and empirical correlations have been with ordinary piles, do not attempt to treat this effect separately but consider it included in the high safety factors suggested in 4.3.

In general, piles driven with vibratory hammers produce reduced friction, presumably because they produce lower lateral stresses against the pile. On the other hand, hammer-injected piles, such as the Franki type, produce greater lateral effective stresses than driven, straight-sided piles and therefore have greater friction than computed above. At present little is known quantitatively about these effects and as a

rough approximation, halve friction for vibratory piles and double friction for hammer-injected piles.

Driven, tapered piles can produce much higher apparent side friction than equivalent straight-sided piles. As an approximation for the tapered effect, divide the pile into suitable segments of length, with constant section, such that each segment has the same total side area as the real tapered pile over the length of the segment. This will produce imaginary "steps" with horizontal bearing area between the constant-section segments. Such steps are real for step-tapered piles. The bearing on these steps adds directly to the side friction computed by the above methods for straight-sided piles. For such computation use the L/B ratio applicable to each constant-section segment where L = depth below ground surface to the bottom of that segment and B = diameter of that segment. To estimate this added bearing, take the  $q_c$  value at the elevation of each such step and multiply it by the area of the step. Then further multiply by the factor "S" given by Nottingham in Appendix III, p. 104 herein, Table 12, to obtain the total ultimate side resistance contributed by each step. Should a step occur within  $0 \leq L/B \leq 8$ , further multiply by the ratio  $(L/B)/8$ .

Concerning drilled-in-place or bored piles, again effective stresses against the sides of the piles are less than when driven, thus reducing friction. However, the very rough soil-concrete interface obtained with such piles tends to increase friction. As an approximation, assume the friction of bored piles equal to 3/4 that of driven piles. You need not further reduce side friction if the bored piles are made with the use of drilling mud, or if the piles are underreamed. Remember that full side friction probably develops with only about 0.1-0.3 inches relative settlement of the pile, while full end bearing will probably require 5-15% of shaft or bell (if any) diameter.

For the case of isolated piles driven with enlarged bases, we then have acting against the pile shaft above the base the equivalent of the radial active pressure compared to the radial passive pressure against a driven pile. Considering the very great difference between plane active and passive pressures in soils, and the probably even greater difference between radial passive and active, plus the possibility of reconsolidation and negative skin friction effects in the soils that squeeze back against the pile after driving with an enlarged tip, assume a side friction of zero for design purposes. For the special case of closely spaced groups of piles with enlarged bases, the driving of the adjacent piles will reestablish soil frictional contact along the shaft immediately above the enlarged base. For this case, and only within a sand bearing layer, allow (factor of safety included)  $0.003 q_c$  shaft friction.

Concerning H-piles, they usually develop a perhaps surprising amount of side friction. To account for this, analyze them for both friction and bearing as if you had a concrete pile with the dimensions of the rectangle that just encloses the H-pile.

#### 4.3 Factors of Safety

Nottingham's work (1975) showed about equal accuracy for both end bearing and side friction predictions. Individual CPT local friction measurements have greater error possibilities, but the overall integral effect over the entire sides of a pile tends to compensate errors. He also showed that predictions using an electrical tip have greater accuracy than those made on the basis of mechanical CPT data.

The following safety factors apply to the ultimate capacity of axially loaded single piles. Use of these factors should provide a factor of safety of at least 2.0 with respect to the yield-point loading of a pile (point where soil-support deformations change from primarily elastic to primarily plastic):

Use F.S. = 2.25 with electric tip data  
Use F.S. = 3.00 with mechanical tip data

FOR BOTH FRICTION AND BEARING.

#### 4.4 Lateral Loading

The usual lateral load problem involves transient loading due to wind, waves, vehicles, etc. In clays this type of lateral load problem involves their undrained properties. The problem often becomes one of estimating deformations and not merely assessing safety against lateral load failure. Thus the problem also involves the stress-strain properties of soils. The soil along a laterally loaded pile does not mobilize its strength simultaneously along its length -- progressive action becomes important. The problem also involves the transient stress-strain properties of soils over the full range of stress-strain behavior, including post-peak.

CPT data, by itself, can make only a partial contribution to such a complex problem. Perhaps the key to this contribution is to relate the CPT to the pressuremeter test (PMT) which also involves enlarging a cylindrical cavity. The uniform radial expansion in the PMT theory then needs to be related to the one-sided cavity expansion due to a laterally moving pile.

Table 4 presents the correlations suggested by available data relating  $q_c$  to Young's modulus,  $E$ , and to the limit pressure from a pressuremeter test,  $P_L$ , for both sands and clays. Knowing  $q_c$ , use this table to estimate  $E$  and  $P_L$ . The correlations in Table 4 apply to data obtained using the Delft mechanical tips. The writer has not

seen similar correlations attempted for the cylindrical tips of the Fugro type. For cylindrical tips the writer suggests estimating their equivalent mechanical tip  $q_c$  from Figure I-4 and then using these equivalent  $q_c$  in Table 4.

TABLE 4 -- GUIDE FOR ESTIMATING PRESSUREMETER E AND  $P_L$  FROM  $q_c$  USING DELFT MECHANICAL TIPS

Soil Type	$E/q_c$	$q_c/P_L$
sand, dense	1	10
sand, loose	1.5	5
silt	2	6
clay, insensitive	3	3
clay, v. sensitive	20	1.5

- NOTES: a. Above typical values only -- depends on soil stress-strain curve.  
 b. Error easily  $\pm 25\%$ , maybe  $\pm 100\%$ .

Assume that with a laterally loaded pile, where failure usually occurs first in the surface layer, that deformations are large enough that the surface soil behind the pile pulls away from the pile. The average horizontal pressure  $p_h$  exerted by the soil to resist the load is then, at failure, the horizontal force on the soil imposed by the pile (per unit length of pile) divided by the width of the pile. Assume that at failure this is 1.10 x the limit pressure.\* Figure 14 illustrates and Eq. (8) expresses this assumption.

$$(p_h)_{\max} = 1.1 P_L \quad (\text{Eq. 8})$$

Analysis for the deflections, shears, and moments in laterally loaded piles usually makes use of the Winkler hypothesis which represents the soil mass by a series of non-interconnected, parallel springs -- in this case, horizontal springs along the length of the pile. The Terzaghi (1955) horizontal subgrade modulus,  $k_h$ , denotes the inverse of the spring constant for these springs. The problem becomes how to estimate  $k_h$  from cone data. Table 4 shows how to estimate E. The following equation (Eq. 9), taken from Poulos (1971), permits an estimate of  $k_h$  from E.

$$k_h = 0.8 E/d \quad (\text{Eq. 9})$$

---

\* For depths below 4d.

At  $z = 0$  use 1/3 above  $(p_h)_{\max}$ , and linear variation to max at 4d.

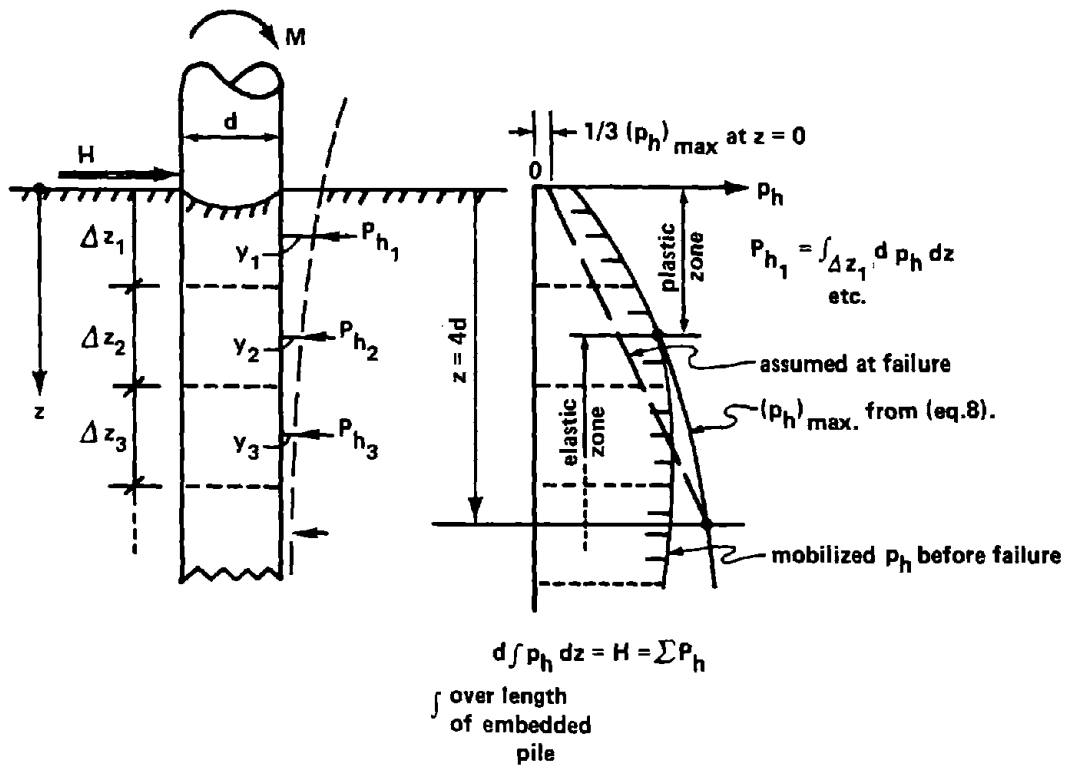


FIGURE 14 – ILLUSTRATION OF THE VARIOUS HORIZONTAL PRESSURES AND FORCES USED FOR THE ANALYSIS OF HORIZONTAL PILE MOVEMENTS UNDER LATERAL LOAD

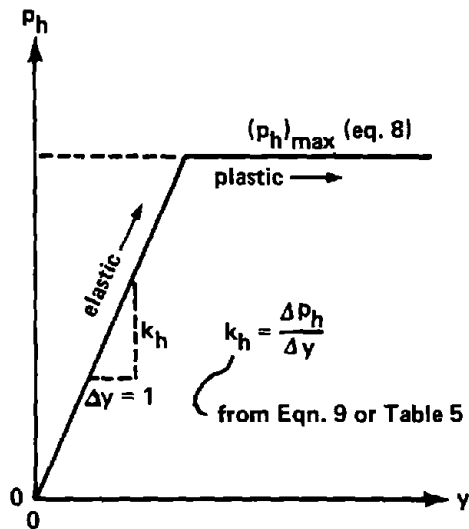


FIGURE 15 – (p-y) DIAGRAM FOR USE IN FINITE DIFFERENCE APPROX. ANALYSIS WHEN USING HORIZONTAL SUBGRADE REACTION THEORY (different diagram for ea.  $\Delta z$ )

where:

E = pressuremeter pseudo-elastic modulus  
d = diameter of pile  
(derived for pile with  $L/d = 25$ , Poisson's ratio = 0.5)

Or, the following Table 5 from Ménard provides an alternate, semi-empirical, method for estimating  $k_h$  from E:

TABLE 5 -- MENARD'S (c. 1965) ESTIMATES OF  $k_h$   
(in  $\text{kg/cm}^2/\text{cm}$ ) FROM  $E_{pm}$  (in  $\text{kg/cm}^2$ )

	E/ $k_h$ for pile diameters, in cm		
	30	60	120
clay:	19	38	60
silt:	13	26	37
sand:	9	18	22

Comparing the  $k_h$  values suggested by (Eq. 8) and Table 5 shows Ménard's  $k_h$  greater by a factor of about 2 to 2.5 in clay (Poulos used  $\nu = 0.5$ ). However, Poulos noted that using horizontal subgrade reaction theory (Winkler hypothesis), and his  $k_h$  values, he predicted horizontal displacement at the ground surface about 20% too large for very rigid piles and 250% too large for very flexible piles compared to the presumed more accurate elastic 1/2-space theory predictions. Thus, use (Eq. 9) for rigid and Table 5 for flexible piles.

Knowing  $k_h$  and the pile limit pressure permits the construction of an approximate p-y curve as illustrated in Figure 15. Construct such curves to apply to suitable positions along the pile embedded length. Then use these curves for the finite difference analysis for pile deflections, etc.

Obviously, Figure 15 provides only approximate information for preliminary design. Modify the shape of the p-y curves thus obtained in accord with any other soils data available.

#### 4.5 Pile Settlement

It has been demonstrated in France that an engineer can estimate the load-settlement performance of single driven or bored piles by using appropriate theory and pressuremeter test results. The writer has not studied the details of the computation methods. Perhaps study of the references noted below can enable the interested reader to make such computations.

Gambin (1963) presented a numerical procedure for evaluating both the end bearing and the frictional contributions to the settlement of the top of a single pile. Cassan (1966) suggested a simpler procedure, which he then improved in Cassan (1968). Both authors suggest methods for estimating the entire load-settlement curve, and both note the great importance of friction-induced settlement under normal working loads. They base the practical application of their analysis methods on  $E$  and  $P_L$  results from pressuremeter tests using the then-current Ménard equipment. For the approximate, and probably conservative, application of these methods to CPT data, use Tables 4 and 5 herein.

#### 4.6 Group Action

The above methods for interpreting CPT data with respect to pile design apply only to single piles. When dealing with piles in groups close enough to interfere with each other (less than about 8 diameters) the engineer should make appropriate adjustments depending on the nature of the problem. For example, bearing and side friction might be controlled by the groups acting as large single piers. Settlement for the group would normally be greater than that for an individual pile with the same average load per pile. With the above predictions for single piles, estimate the settlement of pile groups for pile loadings within normal working load ranges by means of elastic theory as suggested by Poulos (1968). For some other references dealing with group effects, see Moorhouse and Sheehan (1968), and Poulos (1971b).

#### 4.7 Data for Wave Equation Analysis

One of the important inputs into any wave equation analysis of pile behavior during driving is the distribution of soil resistance against the pile due to friction and end bearing. CPT data from friction-cone soundings permit the engineer to estimate this distribution for the quasi-static rate of penetration. This should usually allow an adequate estimate for dynamic pile penetration.

## 5. ESTIMATING SHEAR STRENGTH

This section deals with estimating the shear strength of soils from CPT data for problems such as evaluating bearing capacity, slope stability, compaction control, pile design, etc.

### 5.1 Sand

5.1.1 Bearing Capacity: Although settlement usually controls design, an engineer must check bearing capacity as well. Use the Terzaghi bearing capacity equation (Eq. 10), applicable to about  $D/B \leq 1.5$ :

$$q_{FS=1} = \gamma \frac{B}{2} N_{\gamma} + D N_q + cN_c \quad (\text{Eq. 10})$$

and estimate the bearing capacity factors  $N_{\gamma}$  and  $N_q$  as fractions of  $q_c$  (in  $\text{kg}/\text{cm}^2$ ) averaged over the depth interval 0 to  $1.5B$  below a foundation (Muhs and Weiss, 1971, p. 27). Equation (11) expresses this approximation.

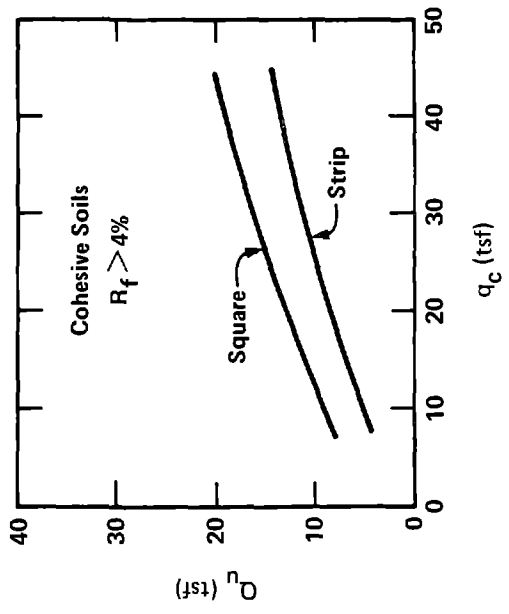
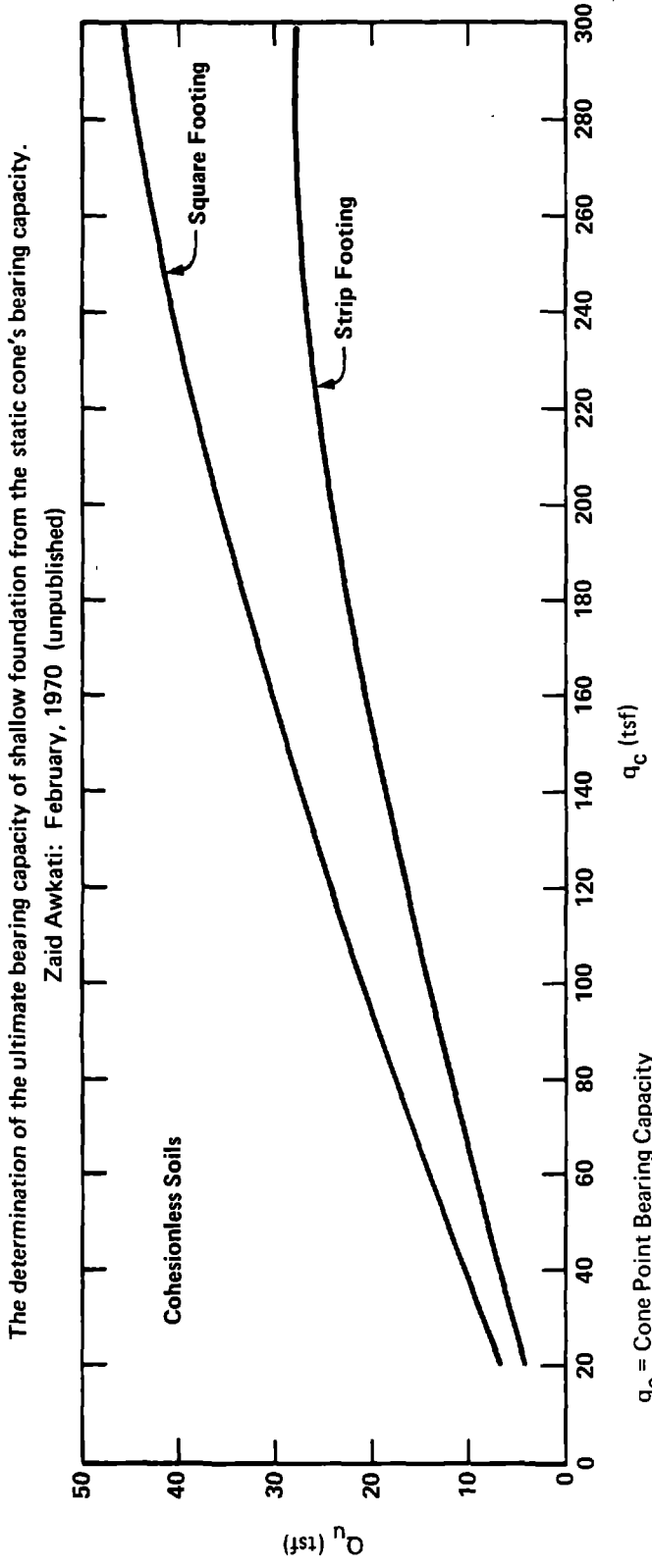
$$0.8 N_{\gamma} \approx 0.8 N_q \approx \overline{q_c}_{0-1.5B} \quad \text{in } \text{kgf}/\text{cm}^2 \quad (\text{Eq. 11})$$

Then use an appropriate safety factor, usually between 2 and 3, to obtain allowable bearing. Because  $q_c$  increases with depth in a homogeneous sand, the above method provides for a bearing capacity increase with embedment greater than that supplied only by the D-factor in the second term in Equation (10).

As a check for near-surface footings, you may also use Figure 16 prepared by Awkati (1970), or Figure 17 by Meyerhof (Sanglerat, 1972, p. 118).

5.1.2 Estimating  $\phi'$ : Engineers do not ordinarily estimate  $\phi'$  from CPT data but instead use these data to estimate the desired behavior directly -- such as bearing capacity in section 5.1.1. However, one method of estimating  $\phi'$  is via the intermediate parameter of relative density, which can be estimated using Figure 5. Then go to a correlation such as Figure 18 (Burmister, 1948) and obtain an estimate of  $\phi$  from relative density.

Another method involves the use of Equation (11) to obtain  $N_{\gamma}$  or  $N_q$ , and then using any of the published charts relating these to  $\phi'$ . Figures 8 and 9 on page 93 of Appendix III present still other methods of estimating  $\phi'$  from CPT data.



Note: These charts are valid for a footing with an embedment,  $h$ , defined as

$h \geq 1.5' + \frac{B'}{2}$  when  $B$ , the minimum width of the footing is less than 3 feet.

or

$h \geq 4' +$  When  $B$ , the minimum width of the footing is more than 3 feet.

**FIGURE 16 – CHART FOR ESTIMATING THE ULTIMATE BEARING CAPACITY OF SHALLOW FOOTINGS ON SAND OR CLAY, USING AVERAGE  $q_c$  FROM MECHANICAL TIPS OVER DEPTH 1.5B BELOW FOOTING**

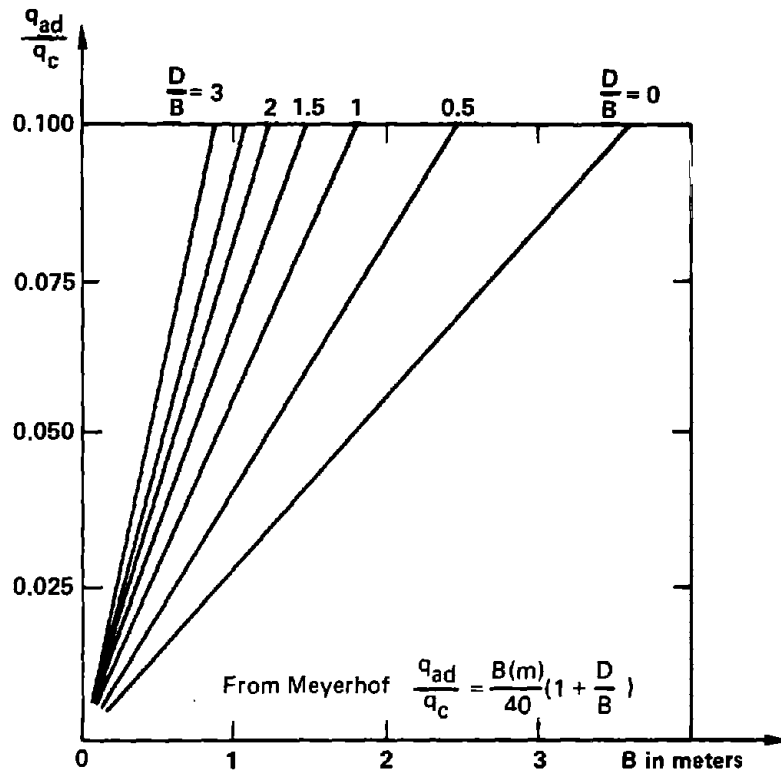


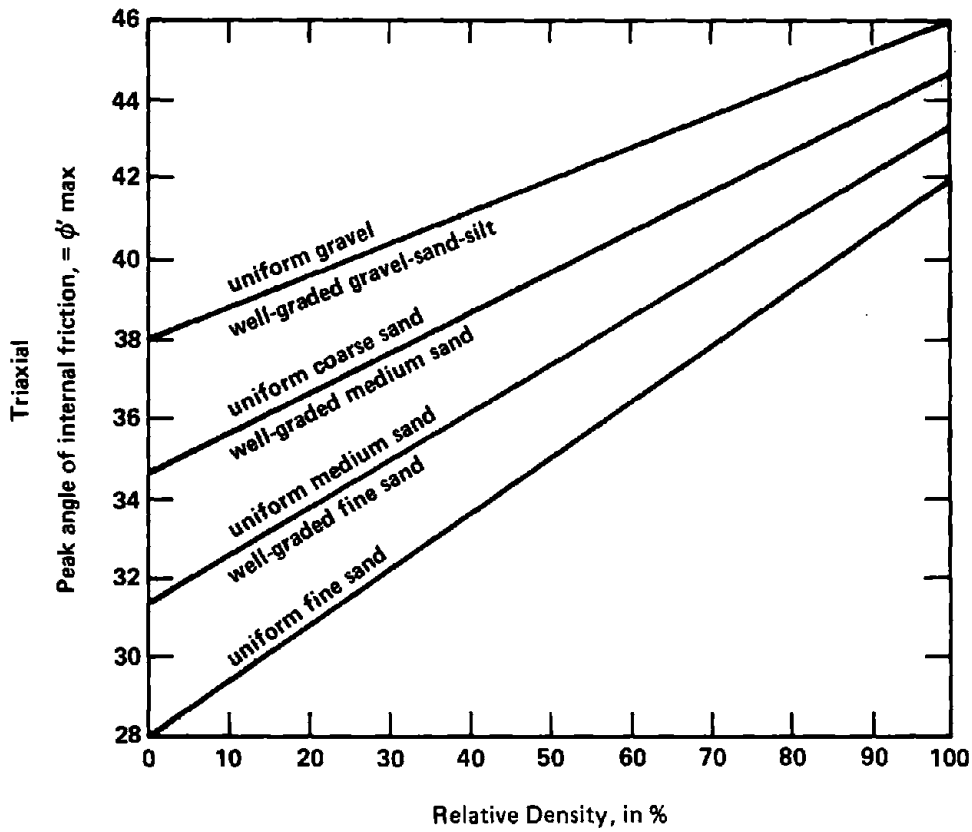
Fig. 77. Meyerhof's chart for shallow footings.

B: width of designed shallow footing; D: embedment of footing;  $q_c$ : cone resistance of static penetrometer;  $q_{ad}$ : allowable capacity.

**FIGURE 17 – ALLOWABLE FOOTING BEARING CAPACITY  
BASED ON CPT DATA (settlement not incl.)  
(from Sanglerat, 1972)**

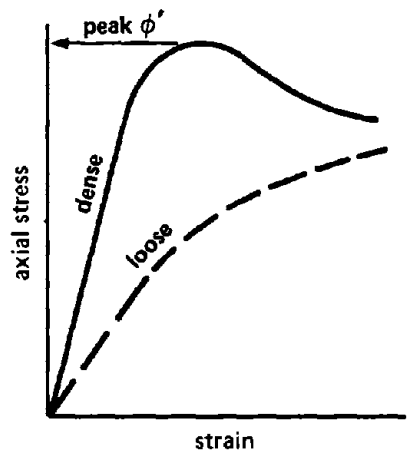
**BEARING CAPACITY ON COHESIONLESS SOILS:**

Chart for the approximate evaluation of the peak angle of internal friction after the relative density has been evaluated. Modified from: Burmister, Donald M., "The Importance and Practical Use of Relative Density in Soil Mechanics," ASTM Proc., Vol. 48, 1948



**Note of caution:**

In problems where the sand may strain past the peak strength value before a general failure occurs, then a reduced value of φ must be used (particularly in the denser cohesionless soils).



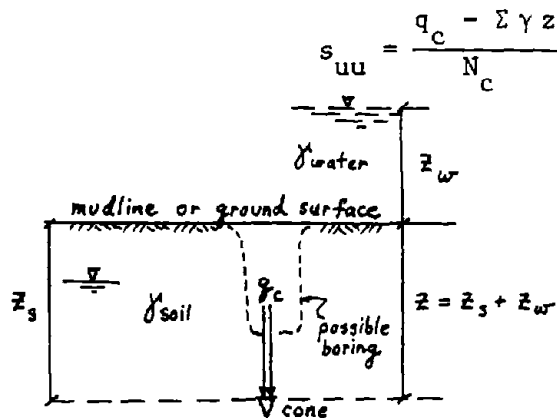
**FIGURE 18 – ESTIMATING SAND φ' FROM ESTIMATE OF RELATIVE DENSITY**

Durgunoglu and Mitchell (1975) presented a theory which has some promise for estimating a sand's  $\phi'$  from  $q_c$  for shallow depths, say to 1-2 meters.

Remember that all of these methods will produce likely incorrect estimates of  $\phi'$  if pore pressure effects contribute significantly to  $q_c$ . Negative pore pressures, if ignored, may produce a too-high estimate of  $\phi'$ , and positive too-low. If you wish drained friction, then reduce penetration rate until further reduction no longer changes  $q_c$ .

## 5.2 Clay

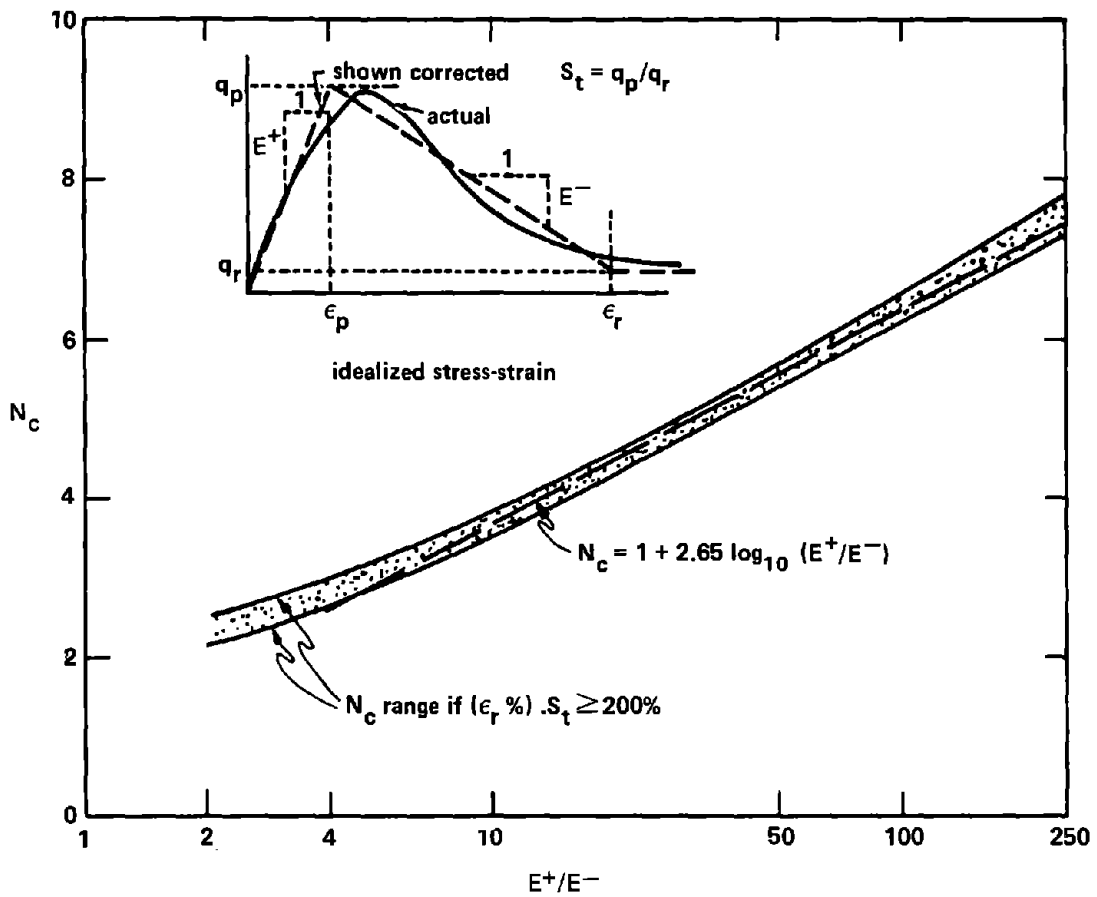
5.2.1 Undrained Strength,  $s_u$ : Note that the undrained strength of a clay depends significantly on the type of test used, the rate of strain, the orientation of the failure planes, and probably other factors yet to be discovered. The more soil engineers learn about  $s_u$  the more they realize its empirical nature. Nevertheless, it remains important in many of today's design procedures. When evaluating  $s_u$  from cone tests use equation (12). Here  $N_c$  equals a Terzaghi-type bearing capacity factor for the cohesive contribution to bearing, but applied to the small-diameter, deep foundation case represented by CPT  $q_c$  data.



NOTES:  $\gamma$  = total (not effective) unit weight  
 Ignore borehole (if any) correction to  $\sum \gamma z$  but  $q_c$  questionable until below 3 borehole diameters below borehole.  
 Ignore  $z_w \gamma_w$  in  $\sum z \gamma$  if  $q_c$  set = 0 at mudline.

DIAGRAM TO EXPLAIN EMPIRICAL USE OF EQ. (12) (Water above or below ground surface)

Unfortunately,  $N_c$  is not a constant but varies with the stress-strain properties of the clay. Figure 19, adapted from Ladanyi (1967), clearly illustrates this point. In general, the more sensitive the clay the lower  $N_c$ , with limits of about 10 for an insensitive clay ( $E^- = 0$ ) and 1 for an infinitely



Theoretical variation of  $N_c$  for strip load within homogeneous clay and with progressive failure (based on B. Ladanyi, 1967)

FIGURE 19

sensitive ( $E^- = \infty$ ) clay.  $N_c$  also increases with rate of penetration. The design of the cone tip further influences  $N_c$  -- for example, any mantle above the cone permits clay friction to be measured as part of cone resistance and thus increases the  $N_c$  factor required. The literature reports most  $N_c$  ranging from about 5 to 20 for Fugro-type tips and from about 10 to 25 for the Delft mechanical tips. Average values for normal penetration rates in "average" clays are about  $N_c = 10$  and 16 for these tips, respectively.

Figures 20 and 21 from the Norwegian Geotechnical Institute (NGI) (1975), present some results from a joint research project in Scandinavian clays by Fugro and the NGI, wherein equation (12) was used to backfigure  $N_c$ . Lunne (1975) and Lunne et al. (1976) have now published some results from this joint calibration project. The NGI supplied the  $s_{uv}$  data from Geonor field vanes tests, and Fugro supplied the  $q_c$  data using Fugro tips. These data clearly suggest that the weaker the clay, the higher  $N_c$ .  $N_c$  approaches 10 in the stronger clay. As presented at the Stockholm ESOPT, similar tips produced results similar to Figure 20. If you are working with very weak clays you must increase  $N_c$ . Use Figure 20 as a guide. Some recent research in Scandinavia and France also suggests that  $N_c$  tends to decrease with increasing depth and also with increasing plasticity index.

In summary, it seems reasonable to first-estimate  $s_u$  by using the  $N_c$  values of 10 (cylindrical tips) and 16 (Delft mechanical tips). Koutsoftas and Fischer (1976), for example, obtained good results using  $N_c = 16$ . In some, perhaps many, cases your clays will produce questionable results and the engineer must make a local correlation for  $N_c$  using equation (12). A key question then arises: What  $s_{uu}$  to correlate against? Clearly, if possible we should correlate against actual  $s_{uu}$  values backfigured from failures. Given the scarcity of such  $s_{uu}$ , an engineer will likely have to correlate against the type of  $s_{uu}$  with which he has the most experience and confidence -- such as from unconfined, triaxial of various types, or vane tests.

**5.2.2 Remolded Undrained Strength:** One can estimate roughly the remolded undrained strength, as obtained by a field vane test, by assuming the adhesion strength along the friction sleeve of the friction-cone penetrometer tip as the average between  $s_{uu}$  obtained from equation (12) and  $s_{ur}$ .

**5.2.3 Drained Strength:** No practical method exists at present to estimate the undisturbed, drained strength parameters of a clay based only on CPT data. One method of possible use in higher permeability clays is to reduce the rate of penetration in steps to very slow rates. Then graph the changing  $q_c$  against rate and extrapolate to rate = 0. Then use equation (12) but reduce  $N_c$  by 10% and use the effective rather than the total unit weight of the soil.

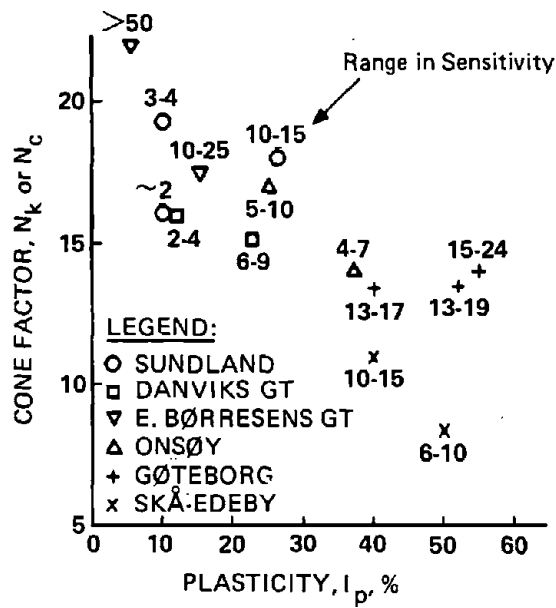
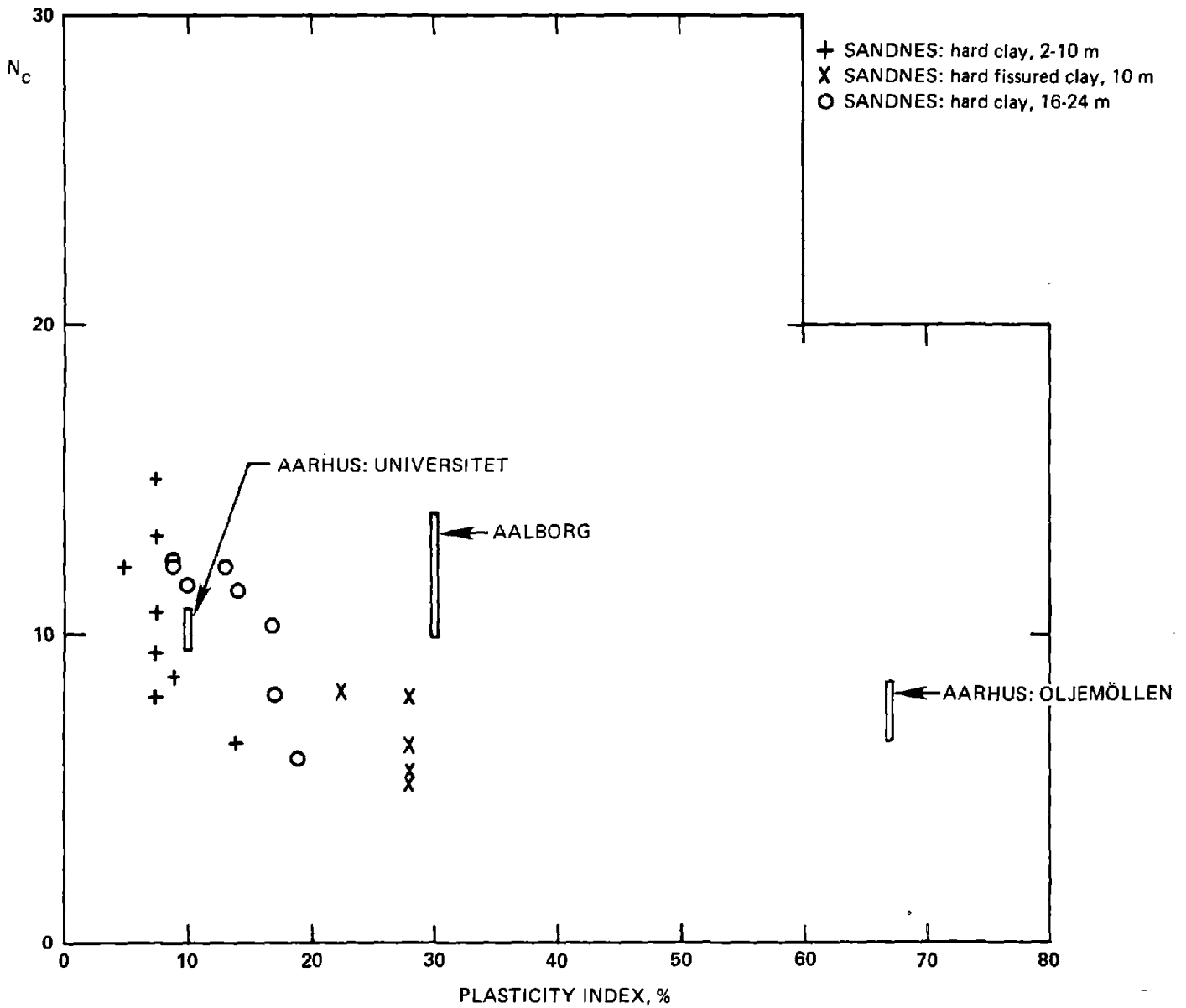


FIG. 8. SUMMARY OF  $N_k$  VALUES FROM ALL SITES.

TABLE 1. Summary of  $N_k$  values

Test site	Depth (m)	Range $\tau_f$ (t/m <sup>2</sup> )	Plasticity $I_p$ (%)	Sensitivity	Cone Factor $N_k$
Sundland	4-9	2-2.5	22-28	10-15	17-18
Drammen	9-14	2-4.5	~10	~2	20
	14-22	2.5-4	~10	3-4	15.5
Dansvigs gate	5-10	2-3	20-25	6-9	14-15
Drammen	11-30	2-4	10-11	2-4	14-16
Børresens gate	5.5-12	3-2	~15	15-25	16-20
Drammen	12-30	1.3-2.5	~5	50-160	20-24
Onsøy	1-9	1.2-1.4	20-30	5-10	16-18
	10-20	1.8-4.8	35-40	4-7	13-18
Skå-Edeby	1-4	0.6-1.2	45-80	6-10	8-9
	4-12	0.8-2.0	30-50	10-15	10-12
Gøteborg	3-10	1.5-2.5	50-60	15-24	13.5-14.5
	10-21	2.5-4.2	50-55	13-19	13-14
	21-30	4.5-5.5	~40	13-17	13-14

FIGURE 20 – EXAMPLE OF A LOCAL CORRELATION FOR  $N_c$  (Fig. and Table from Lunne et. al., 1976, when using Fugro electric cone tip and Geonor vane in normally consolidated Scandinavian clays)



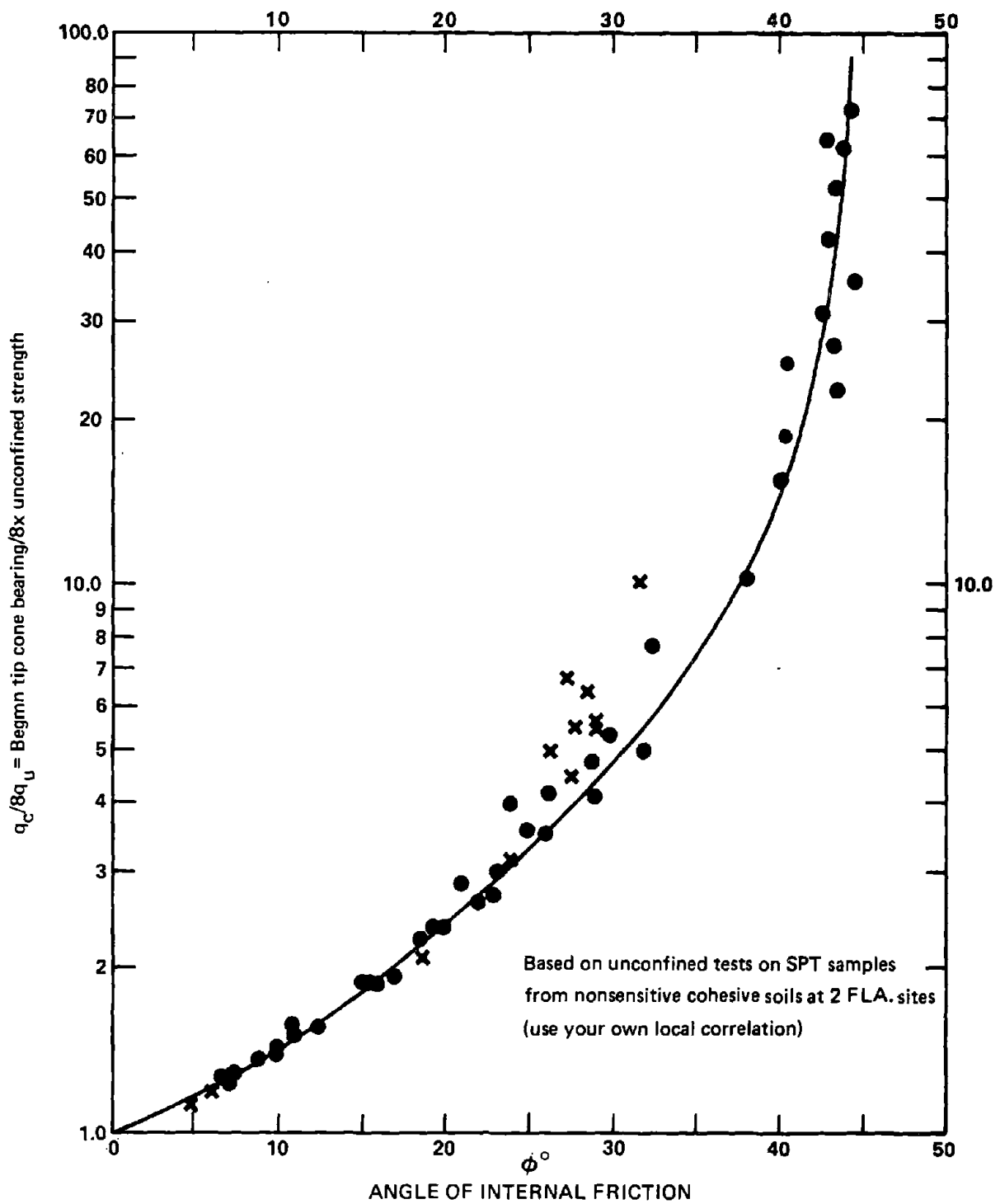
CONE PENETRATION TESTS IN CLAY	Date: 23.4.75	Drawn by: C.D.
$N_c$ AGAINST PLASTICITY FOR ALL SITES	Approved:	
	Project no.:	52155
Norwegian Geotechnical Institute	14	

FIGURE 21 – CORRELATION BETWEEN FUGRO CONE  $q_c$   
 AND GEONOR VANE  $s_{uv}$ , OVERCONSOLIDATED  
 CLAYS IN SCANDINAVIA

### 5.3 Mixed Soils

Soils with mixed cohesion and friction properties, such as clayey sands, sandy and silty clays, etc., present a difficult problem for engineering properties assessment from cone penetration test data. With the aid of local experience an engineer can often identify such soils by using a friction-cone, determining friction ratio profiles, and using a correlation such as in Figure 2. As an approximation, he can treat the penetrometer data as if it came from a theoretically cohesionless and then from a perfectly cohesive soil. Then he must interpolate for the properties of the real, mixed soil. Unfortunately, this often leaves much room for error.

Supplemental data can help greatly. For example, if the soil has enough cohesion (not due only to partial saturation and capillarity) to permit performing an unconfined test, and samples for such tests are available from soils in the same layer as tested for  $q_c$ , then Figure 22 can aid in determining an undrained  $\phi$  for that soil. Note that Figure 22 is based on tests from only two sites, both in the same area of Florida. Also, as described in detail by Prochaska (1967), extracting  $\phi$  from such data involves several approximations and assumptions that make the method undesirable for general use. Areas with other soil mineralogy and/or environments of soil formation, other relative degrees of disturbance in the unconfined test sample, and using other types of penetrometer tips will likely produce a different correlation. If possible, establish a local correlation -- preferably by more direct means of evaluating  $\phi$ , such as undisturbed sampling and triaxial tests or in situ borehole shear tests.



**FIGURE 22 – RATIO OF CONE BEARING CAPACITY TO THEORETICAL BEARING CAPACITY IN CLAY VERSUS THE COMPUTED ANGLE OF INTERNAL FRICTION.**

## 6. ESTIMATING SETTLEMENTS

This section deals primarily with estimating the settlement of structural foundations including footings, mats and pile groups. However, it may also be used to estimate the settlements under fills and large loaded areas such as oil and water tanks.

### 6.1 Sand Layers

The writer, and Sanglerat (1972) recommend the use of the strain factor method reported by Schmertmann (1970) for estimating the settlement of footings over sand. Although the reader should study this 1970 paper to more completely understand the method, for completeness within these "Guidelines" the following presents a summary of how to use the method. It includes the same example problem as in the 1970 paper. When comparing the following with 1970, note that the writer has now modified the method to separate the plane strain (long footing) and axisymmetric (square footing) cases.

To get the settlement estimate, solve the following equation (13), (14) and (15):

$$\rho = C_1 C_2 \Delta p \sum_{1}^n \frac{I_z}{x q_c} \Delta Z \quad (\text{Eq. 13})$$

$$C_1 = 1 - 0.5 \left( \frac{p'_o}{\Delta p} \right) \quad (\text{Eq. 14})$$

$$C_2 = 1 + 0.2 \log_{10} \left( \frac{t_{\text{yr}}}{0.1} \right) \quad (\text{Eq. 15})$$

wherein:

- $\rho$  = settlement in units of  $\Delta Z$
- $C_1$  = correction factor for depth of embedment
- $C_2$  = correction factor for secondary creep settlement
- $\Delta p$  = net foundation pressure increase at bottom footing, in  $q_c$  units, after subtracting  $p'_o$
- $I_z$  = strain influence factor at the centerheight of each assumed constant- $q_c$  sublayer. See Fig. 23 for square and long footing  $I_z$ -depth diagrams
- $n$  = number of  $q_c$  sublayers to depth below footing =  $2B$  (square footing) or  $4B$  (long footing) or to assumed rigid boundary layer if this comes first.  $B$  = least width of loaded area
- $\Delta Z$  = thickness of each of the  $n$  sublayers
- $x$  = factor by which to multiply CPT  $q_c$  to obtain equivalent sand Young's modulus, - 2.5 for square and 3.5 for long footings

$p'_o$  = previous effective overburden pressure at the elevation of the bottom of the footing  
 $t_{yr}$  = time in years from application of  $p'_o + \Delta p$  on footing

To provide the information for these equations, use the following procedure:

(a) Obtain the static cone bearing capacity ( $q_c$ ) believed applicable for the footing location over the depth interval from the proposed footing contact level to a depth of 2B (square footing) or 4B (long footing), or to a boundary layer that can be assumed incompressible, whichever occurs first.

(b) Simplify the  $q_c$  log into a succession of layers of constant  $q_c$  to approximate the actual log. Figure 24 shows such a log after such a simplification. This example considers an actual bridge pier case -- No. 1 in Schmertmann (1970).

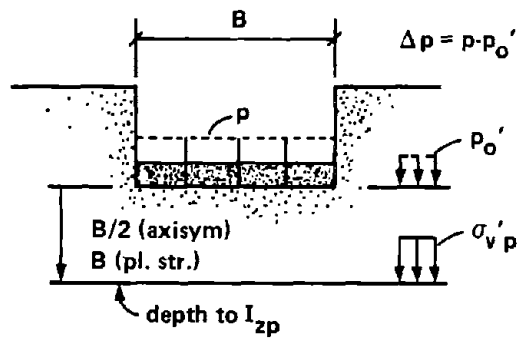
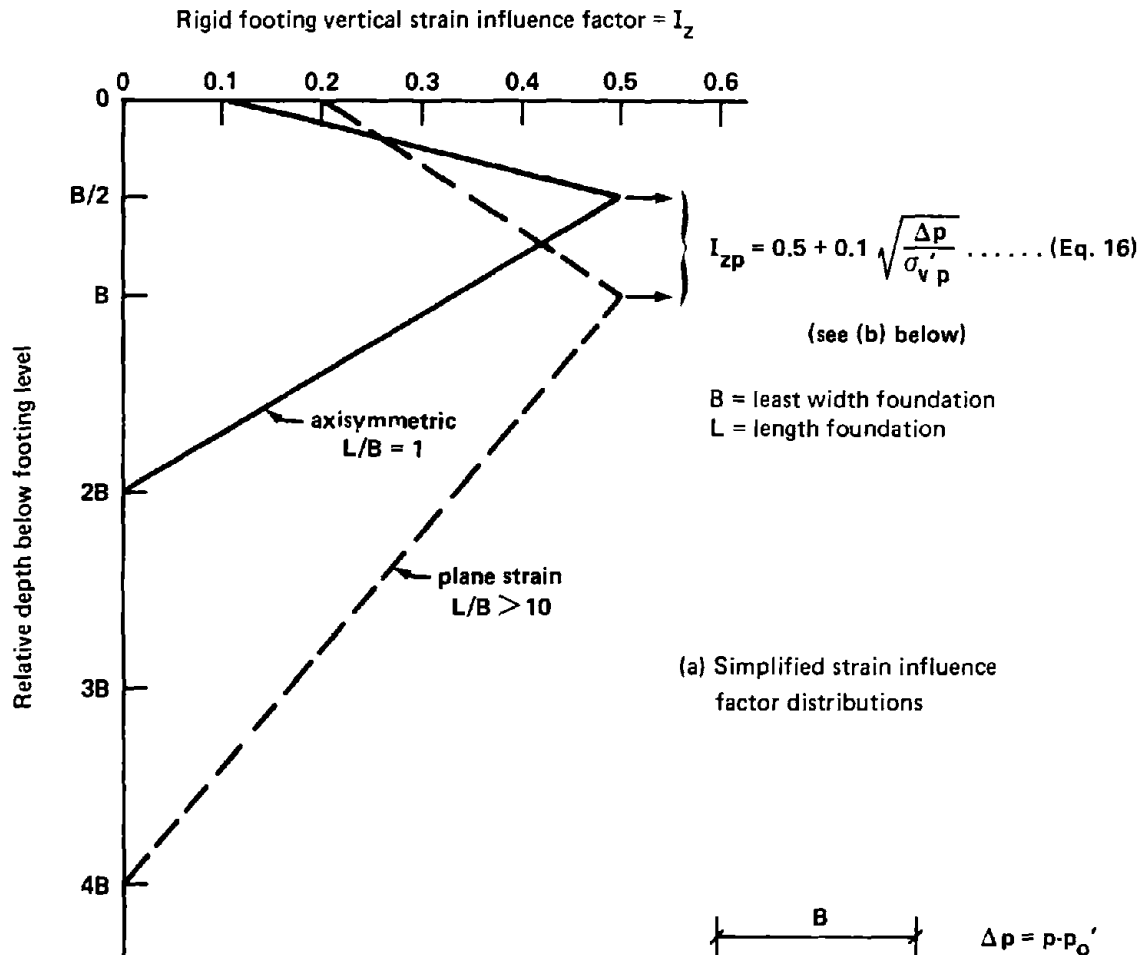
(c) Decide whether you have an axisymmetric (square footing) or plane strain (long footing -- say length/width =  $L/B \geq 10$ ) case. Superimpose the appropriate strain factor diagram, as described in Figure 23, over the  $q_c$  log. Figure 24 also illustrates this superposition for this plane strain example. Use equation (16), shown in Figure 23, to obtain the peak value of strain factor =  $I_{zp}$ . In this example  $I_{zp} = 0.5 + 0.1(1.5/0.58)^{1/2} = 0.66$ .

(d) Prepare a table with headings similar to those in Table 6 and fill in the columns with appropriate values from the above data, as shown

(e) Sum the last column in Table 6, compute  $C_1$  and  $C_2$  from equations (14) and (15), calculate  $\Delta p$  and then calculate the settlement,  $\rho$ , from equation (13). The above example shows these final computations below Table 6.

(f) For  $1 < L/B < 10$  the engineer can solve for both the axisymmetric and plane strain cases and interpolate.

The above methods should be used only with first-loading cases with adequate bearing capacity. If the sand has been prestrained by previous footings or other loads producing significant prior shear strain, then real settlements will likely be significantly less than predicted by the above method. Engineers suspect that overconsolidation, or preloading by other means, including roller compaction, will decrease the settlement of a preloaded sand under subsequent loading by a factor greater than the resulting increase in  $q_c$  would indicate. If such preloading has occurred, tentatively use 1/2 the above predicted settlement as probably still conservative. Or, other methods could then be more suitable, such as extrapolating plate bearing load tests or triaxial test stress path methods (see Lambe, 1967).



(b) Explanation of pressure terms in Eq. 16

**FIGURE 23 – MODIFIED STRAIN INFLUENCE FACTOR DIAGRAMS FOR USE IN SCHMERTMANN METHOD FOR ESTIMATING SETTLEMENT OVER SAND**

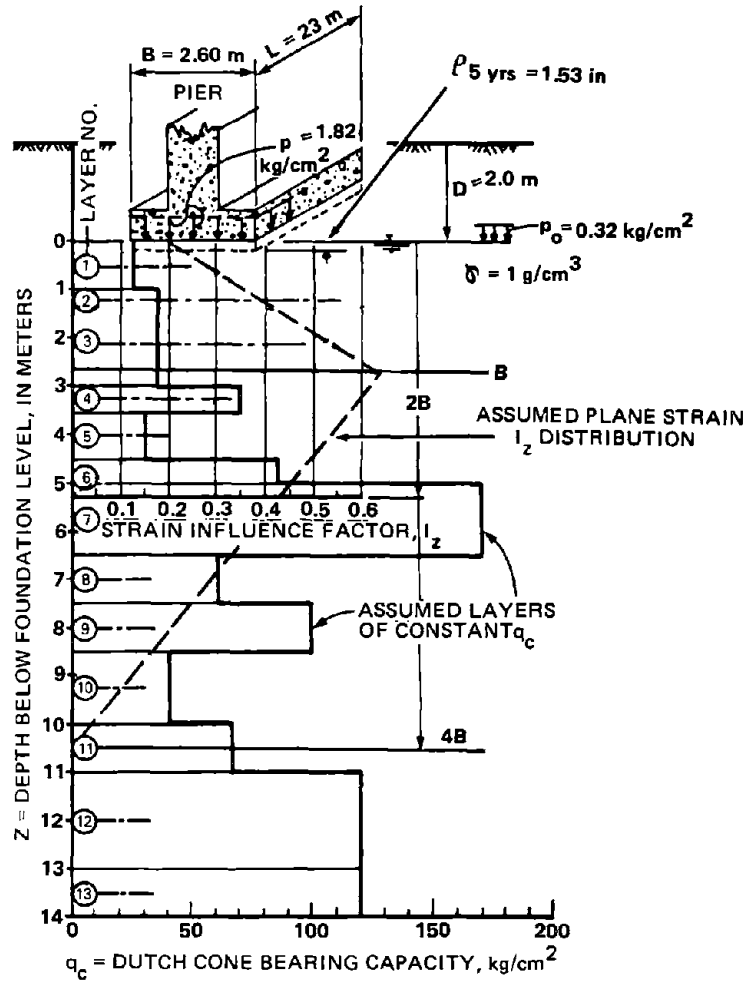


FIGURE 24- TEST CASE NO. 1 AS COMPUTATIONAL EXAMPLE

**TABLE 6** - Example computation for settlement on sand, from Figure 24

Note: L/B = 8.8 used long footing case, x = 3.5  
 B = 260 cm  
 $I_{zp} = 0.66$

layer	$\Delta Z$ (cm)	Z (cm)	$I_z$	$q_c$ (kg/cm <sup>2</sup> )	$I_z \Delta Z / 3.5 q_c$ (cm/kg/cm <sup>2</sup> )
1	100	50	0.29	25	0.331
2	30	115	0.40	35	0.098
3	170	215	0.58	35	0.805
4	50	325	0.61	70	0.124
5	100	400	0.54	30	0.514
6	70	485	0.47	85	0.111
7	130	585	0.38	170	0.083
8	100	700	0.29	60	0.138
9	100	800	0.20	100	0.057
10	150	925	0.10	40	0.107
11	40	1020	0.02	65	0.004

$$\Sigma = 1040 \text{ cm}$$

$$= 4B$$

$$\Sigma = 2.372$$

$$\rho = C_1 C_2 \Delta p \sum \frac{I_z \Delta Z}{E_s}$$

$$C_1 = 1 = 0.5 \frac{0.32}{1.50} = 0.89$$

$$C_2 = 1 + 0.2 \log_{10} \frac{5}{0.1} = 1.34$$

$$\Delta p = 1.82 = 0.32 = 1.50 \text{ kg/cm}^2$$

$$\rho = 0.89 (1.34) 1.50 (2.372)$$

$$= 4.24 \text{ cm}$$

$$= 1.67 \text{ in.}$$

Note also that the above method applies only to conventional static loading. Dynamic loading can produce many times the static settlement, at equal maximum footing pressures, if over loose sand and the vertical accelerations reach 1/2-1 times gravity. Dynamic loading, and also simple cyclic or repetitional loading, can also produce larger settlement due to the strength reduction resulting from a net generation-dissipation accumulation of pore water pressure and the consequent reduction of effective stress. Similar behavior can occur in clays. In cohesionless soils this action can lead to time intervals of near-zero effective stress and consequent large deformations. The best protection against dynamic or cyclic load induced settlements is a sufficiently high dry density or relative density and/or to prestress the soil.

## 6.2 Clay Layers

6.2.1 Schmertmann Method: This method is based on using the  $s_u/p'$  value as an indication of the overconsolidation ratio (OCR), as explained in section 2.7 and Figure 6. The CPT  $q_c$  provides a means of estimating  $s_u$ , as explained in section 5.2. The engineer can estimate the effective overburden pressure,  $p'$ , from estimates of soil unit weight and water pressure. Table 7 then provides a basis for estimating the compressibility coefficient of the soil as a function of OCR. Then put the compressibility of the soil into Equation (17), and use it to estimate the settlement of the clay,  $\Delta H$ .

$$\Delta H = \sum_1^n \left[ H_1 \left( \frac{C_c}{1+e_1} \right) \log_{10} \left( \frac{p'_1 + \Delta p'_{1-2}}{p'_1} \right) \right] \quad (\text{Eq. 17})$$

where:

n = no. of compressible sublayers used in analysis  
 for each sublayer  $\left\{ \begin{array}{l} C_c = \text{compression index} = \Delta e / \Delta(\log_{10} p') \\ e_1 = \text{initial void ratio} \\ p'_1 = \text{initial vertical effective stress} \\ \Delta p'_{1-2} = \text{expected increase in stress} \\ H_1 = \text{initial thickness} \end{array} \right.$

TABLE 7 - ESTIMATING THE CONSOLIDATION OF CLAYS FROM  $s_u/p'$

$s_u/p'$	approx. OCR	$C_c/(1 + e_1)$
0 - 0.1	less than 1	greater than 0.4 (still consolidating)
0.1 - 0.25	1	0.4
0.26 - 0.50	1 to 1.5 (assume 1)	0.3
0.51 - 1.00	3	0.15
1 - 4	6	0.10
over 4	greater than 6	0.05

The above method produces only an estimate. Special soil conditions or special problems, which perhaps become obvious from such an estimate, will require more exact methods such as undisturbed sampling and oedometer testing. Also note that the above Table 7 may need modification for different local soil conditions. For example, in Norway, various clays, with  $s_u/p'$  varying from 0.1 to 0.5 and all believed NC, have compressibilities that increase with  $s_u/p'$  (as does PI with these clays) rather than decrease as suggested in Table 5. Some NC, sensitive, cemented clays can have a compressibility exceeding 0.4.

6.2.2 Sanglerat Method: As an alternate to the above, or perhaps as a check, the following outlines a method based on extensive comparative  $q_c$  and oedometer testing, primarily in France (Sanglerat, 1976). The method uses the original method of Buisman, but with the  $q_c$  correlations from the more recent work.

In this method the engineer employs the following equation:

$$\Delta H = \sum_1^n \left[ H_1 \frac{\Delta p'}{2.3 q_c} \right] \alpha_o \quad (\text{Eq. 18})$$

with the following Table 8 providing a guide for the  $\alpha_o$  values to use:

TABLE 8 - SANGLERAT'S SUGGESTED VALUES FOR  $\alpha_o$

Type Soil	$q_c$ (kgf/cm <sup>2</sup> )	$\alpha_o$
Recent alluvium (CL)	less than 7	0.15 to 0.4
	7 to 20	0.4 to 0.8
	over 20	0.8 to 1.7
Recent alluvium (CH)	less than 20	0.5 to 1
	over 30	0.8 to 1.5
Peaty soils (OH)		w = 90-130%
		1.5 to 3
		w over 300% over 3

(See Sanglerat, 1972, sections 11.3 and 11.4, for more data.)

### 6.3 Differential Settlement

Given sufficient data, the writer suggests estimating differential settlements by making the above computations for settlement, using 6.1

for sand layers and 6.2 for clay layers, under different parts of the loaded area being considered, and thus obtain possible differential settlements. Make an appropriate reduction for estimated structural stiffness effects.

One can also use the statistical approach wherein it has been found by detailed investigations of settlement data, from a relatively few structures, that maximum differential settlements between adjacent load points in sand range from about 0.5 to 1.0 the maximum settlement. Take 0.75 as an average, usually conservative.

In clay soils experience shows soils more uniform and thus they produce less differential settlement. Take 0.33 the maximum settlement as the likely maximum settlement between adjacent load points. Caution -- if these estimates show a problem becomes critical, or for an unusual load configuration, use more accurate methods.

#### 6.4 Rate of Settlement

Ordinary CPT data produces no direct evaluations of permeability or pore pressure generation and dissipation, and thus nothing of direct use to estimate rate of drainage or settlement. However, continuous  $q_c$  logs might provide a good indication of drainage layers otherwise only detected by continuous sampling.

If an electric cone-piezometer tip is available -- either the Fugro tip designed for the purpose or the Geonor vibrating wire tip or some other that becomes available -- then permeability may be estimated by observing the rate of dissipation of pore pressure as measured by such a tip immediately after penetration has stopped. No well established theory exists at present to relate this rate of dissipation to permeability. The soil's compressibility also enters the problem as well as the variable sample disturbance effects around the tip, and the diameter and location of the porous sensing element on the tip. Use Figure 25 for a permeability estimate, based on very limited empirical data. Note that when using Figure 25 one should expect errors in  $k$  by a factor of 10.

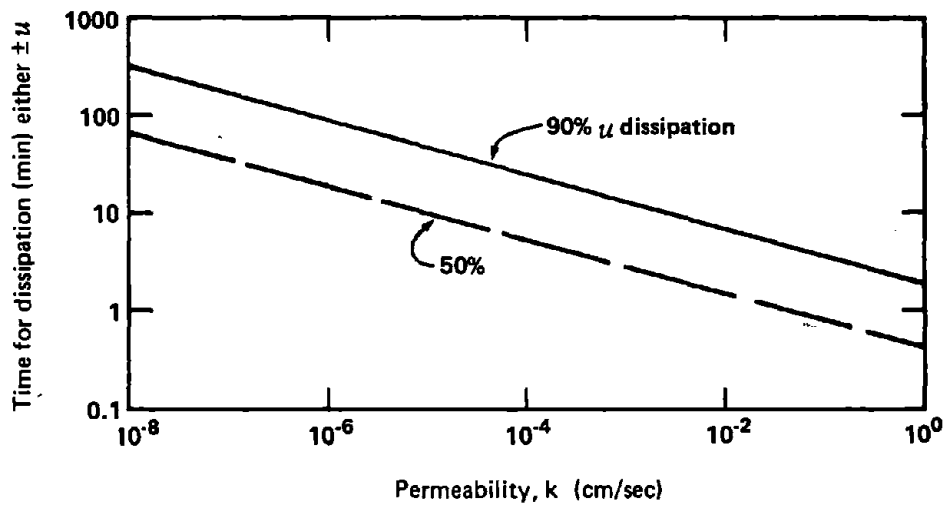


**FIGURE 25 – PRELIMINARY CORRELATION BETWEEN INSITU PERMEABILITY AND TIME FOR 50% and 90% DISSIPATION OF EXCESS HYDROSTATIC PORE PRESSURE AFTER STOPPING PENETRATION OF A CONE-PIEZ.**

## 7. LIST OF REFERENCES\*

1. Alperstein, R. and S. Leifer (1976), "Site investigation with static cone penetrometer," ASCE, J-GED, May, pp. 539-555.
2. Awkati, Z. (1970), unpublished, prepared for office use while employed by Soil Exploration Company, St. Paul, Minn.
3. Baligh, M. and R. Scott (1975), "Quasi-static deep penetration in clays," ASCE, J-GED, Vol. 101, GT11, Nov., pp 1119-1133.
4. Begemann, H.K. (1953), "Improved method of determining resistance to adhesion by sounding through a loose sleeve placed behind the cone," Proc. 3rd ICSM&FE, Vol. I, pp. 213-217.
5. Begemann, H.K. (1963), "The use of the static penetrometer in Holland," New Zealand Engineering, February, p. 42.
6. Begemann, H.K. (1965), "The friction jacket cone as an aid in determining the soil profile," Proc. 6th ICSM&FE, Vol. 1, pp. 17-20.
7. Begemann, J.K. (1965), "The maximum pulling resistance of a single tension pile calculated on the basis of results of the adhesion jacket cone," Proc. 6th ICSM&FE, Vol. II, p. 229.
8. Burmister, D. (1948), "The importance and practical use of relative density in soil mechanics," Proc. of the ASTM, Vol. 84, p. 1.
9. Cassan, M. (1966), "Le tassement des Pieux; Synthese des recherches recentes et Essais comparatifs," Sol Soils, No. 18-19, p. 43.
10. Cassan, M. (1968), "same as above, suite et fin," Sol Soils, No. 20, p. 23.
11. Dahlberg, R. (1974), "The effect of the overburden pressure on the penetration resistance in a preloaded natural fine sand deposit," Proc. ESOPT, Stockholm, Vol. 2.2, pp. 89-91.
12. Freed, D. (1973), "Prediction of pile side resistance of smooth and rough 4 inch square concrete model piles driven in sand using static cone penetrometer data," University of Florida M.S.C.E. thesis, December, 207 pp.

---

\*Also see reference list at end of Appendix III for a reference cited and not found in this listing, and also for the meaning of abbreviations used in both listings.

13. Gambin, M. Ph. (1963), "Computation of the settlement of a slender deep foundation in terms of pressuremeter test results, Sol Soils, No. 7 (in French).
14. Holden, J. (1971), "Research on performance of soil penetrometers," University of Florida Dept. of Civil Engineering internal report CE-SM-71-1, August.
15. Joustra, K. (1974), "Comparative measurements on the influence of the cone shape on results of soundings," Proc. ESOPT, Stockholm, Vol. 2.2, p. 199.
16. Kok, L. (1974), "The effect of the penetration speed and the cone shape on the Dutch static cone penetration test results," Proc. ESOPT, Stockholm, Vol. 2.2, p. 215.
17. Koutsoftas, D. and J. Fischer (1976), "In-situ undrained shear strength of two marine clays," ASCE, J-GED, Vol. 102, GT9, September, pp. 989-1005.
18. Ladanyi, B. (1967), "Deep punching of sensitive clays," Proc. 3rd PanAm Conference on SM&FE, Caracas, July.
19. Ladd, C. and R. Foott (1974), "New design procedure for stability of soft clays," ASCE, J-GED, July, p. 769.
20. Lambe, T. W. (1967), "Stress path method," ASCE, J-SM&FD, Vol. 93, SM6, November, pp. 309-331.
21. Lunne, T. (1975), "Correlations between vane shear strength and cone resistance in some Norwegian soft clays," Proc. ASCE, SC-IMSP, Raleigh, Vol. II, pp. 161-163 (a discussion).
22. Lunne, T., O. Eide and J. deRuiter (1976), "Correlations between cone resistance and vane shear strength in some Scandinavian soft to medium stiff clays," Canadian Geotechnical Journal, Vol. 13, pp. 430-441.
23. Massarsch, R. and D. Holtz, B. Holm, A. Fredriksson (1975), "Measurement of horizontal in situ stresses," ASCE, SC-IMSP, Raleigh, Vol. 1, p. 266.
24. Ménard, L. (1965), "Comportement d'une fondation profonde soumise a des efforts de renversement" (source not determined).
25. Meyerhof, G. G. (1956), "Penetration tests and bearing capacity of cohesionless soils," ASCE, J-SM&FD, Vol. 82, SM1, p. 5.
26. Moorhouse, D. and J. Sheehan (1968), "Predicting safe capacity of pile groups," Civil Engineering, ASCE, October, pp. 44-48.
27. Muhs, H. and K. Weiss (1971), "Study of the bearing capacity and settlement behavior of single, near-surface footings in non-uniform cohesionless soil," Degebo Heft 26 (in German).

28. Nottingham, L. and J. Schmertmann (1975), "An investigation of pile capacity design procedures," Final Report D629 to Florida Dept. of Transportation from Dept. of Civil Engineering, Univ. of Florida, Sept., 159 pp.
29. Norwegian Geotechnical Institute (NGI) (1975), Internal reports 52155-2 and -3, "A comparison between cone resistance and vane shear strength in some Scandinavian clays: Part A: Soft clays, Part B: Overconsolidated Clays," April.
30. Poulos, H. G. (1968), "Analysis of the settlement of pile groups," Geotechnique, Vol. 18, No. 4, pp. 449-471.
31. Poulos, H. G. (1971), "Behavior of laterally loaded piles: I- Single piles," ASCE, J-SM&FD, Vol. 97, SM5, May, p. 722.
32. Poulos, H. G. (1971b), ibid. Part II - Pile groups, pp. 733-751.
33. Prochaska, B. (1967), "J. Hillis Miller Health Center foundation feasibility study." Master's thesis presented to the Dept. of Civil Engineering, University of Florida, see Chapter 5 (unpublished).
34. Sanglerat, G. (1972), The Penetrometer and Soil Exploration, Elsevier Publishing Co., Amsterdam.
35. Sanglerat, G. (1976), "Talking Point," Ground Engineering, Vol. 9, No. 6, September, p. 2.
36. Schmertmann, J. H. (1970), "Static cone to compute static settlement over sand," ASCE, J-SM&FD, Vol. 96, SM3, May, pp. 1011-1043.
37. Schmertmann, J. H. (1971), Discussion to DeMell's SOA paper "The standard penetration test," 4th PanAm Conf. SM&FE, Puerto Rico, Vol. III, pp. 90-98.
38. Schmertmann, J. H. (1972), "Effects of in situ lateral stress on friction-cone penetrometer data in sands," Fugro Sondeer Symposium, pp. 37-39 (published by Fugro-Cesco, Inc., The Netherlands).
39. Schmertmann, J. H. (1974), "Penetration pore pressure effects on quasi-static cone bearing,  $q_c$ ," Proc. ESOPT, Stockholm, Vol. 2.2, p. 346.
40. Schmertmann, J. H. (1974b), "CPT to help understand SPT," Discussion to ESOPT, Stockholm, Vol. 2.1, p. 146.
41. Schmertmann, J. H. (1976), "Predicting the  $q_c/N$  Ratio -- Interpreting the dynamics of the Standard Penetration Test," University of Florida Final Report, Project D-636, to the Florida Dept. of Transportation, October, 34 pp. 38 Figures.

42. Terzaghi, K. (1955), "Evaluation of coefficients of subgrade reaction," Geotechnique, Vol. 5, pp. 297-326.
43. Torstensson, B-A (1975), "Pore pressure sounding instrument," ASCE, SC-IMSP, Vol. II, pp. 48-54.
44. Vijayvergiya, V. N. and J. A. Focht, Jr. (1972), "A new way to predict capacity of piles in clay," Offshore Technology Conference, Dallas, paper 1718.

## 8. NOTATION AND ABBREVIATIONS

$A_s$  = pile-soil side contact area per  $f_s$  or  $q_c$  determination  
 $A_{st}$  = total  $A_s$  in clay layers  
 $B$  = least width of a footing-type foundation  
 $c$  = undrained cohesion =  $s_u$   
c. = circa, or approximately  
 $c_o$  = origin cohesion =  $s_u$  when effective stress extrapolated to 0  
 $C$  = correction factor for  $Q_s$  when no  $f_s$  data  
 $C_c$  = compression index from oedometer test  
CPT = abbrev. for quasi-static cone penetration test  
CRB = abbrev. for Country Roads Board (Australia)  
 $d$  = diameter of cone point or pile tip  
 $D$  = pile penetration into sand layer  
    = thickness of overburden lost due to erosion  
    = depth of embedment of footing-type foundation =  $h$   
 $e_R$  = relative void ratio = relative density,  $D_r$   
 $e_1$  = initial void ratio  
 $E$  = Young's modulus  
 $E^+$ ,  $E^-$  = see Figure 19  
 $E_{pm}$  =  $E$  determined from pseudo-elastic part of a PMT  
 $E_s$  = equivalent  $E$  for sand due to vertical loading from a footing-type foundation  
ESP = effective stress path  
 $f_p$  = ultimate pile friction stress  
 $f_s$  = unit friction + adhesion stress on the friction sleeve  
FR or F.R. = friction ratio =  $(f_s/q_c) \cdot 100\%$ , also denoted  $R_f$   
FS = factor of safety  
 $h$  = footing depth of embedment, also denoted  $D$   
 $\Delta H$  = computed settlement  
 $H_1$  = initial thickness of a compressible soil layer  
 $I_z$  = vertical strain influence factor

$I_{zp}$  = maximum, or peak value of  $I_z$   
 $k$  = coefficient of permeability (velocity units)  
 $k_h$  = horizontal coefficient of subgrade reaction  
 $K$  = correlation factor for  $Q_s$  when using  $f_s$  data  
 $K'$  = ratio horiz/vertical effective stress =  $\sigma'_r/\sigma'_v$   
 $K_o$  =  $K'$  for in situ condition of no horizontal strain  
 $K_{oNC}$  =  $K_o$  if same soil was normally consolidated  
 $L$  = length of pile embedded in soil  
       = length of a rectangular foundation of width  $B$   
 $n$  = number of sand layers, including bearing layer, penetrated by a pile  
       = number of compressible layers included in a settlement analysis  
 $N$  = blowcount in a SPT  
 $NC, nc$  = abbrev. for normally consolidated  
 $N_\gamma, N_q, N_c$  = Terzaghi bearing capacity factors, functions of  $\phi$   
 $OC, oc$  = abbrev. for overconsolidated  
 $OCR$  = abbrev. for overconsolidation ratio  
 $p$  = ave. vertical pressure applied by footing at footing bearing level  
 $p'$  = vertical effective overburden pressure  
 $\bar{p}'$  = ave.  $p'$  along part of  $L$  in clay  
 $p_h$  = ave. horizontal pressure, across  $d$ , exerted on soil by a laterally loaded pile  
 $p_L$  = limit pressure from a PMT  
 $p'_o$  = original  $p'$  at footing bearing level  
 $\Delta p$  =  $p - p'_o$   
 $PI$  = abbrev. for plasticity index  
 $PMT$  = abbrev. for pressuremeter test  
 $q$  = bearing capacity  
 $q_c$  = cone bearing capacity from a CPT  
 $q_{cNC}$  =  $q_c$  when normally consolidated soil tested by vertical penetration  
 $q_{co}$  =  $q_c$  due only to  $c_o$

$\bar{q}_c$  = ave.  $q_c$  over some specified depth interval  
 $q_{pa}$  = maximum allowable pile point bearing stress  
 $q_u$  = unconfined compressive strength  
 $Q_p$  = total end bearing force at pile point (FS = 1)  
 $Q_s$  = total side friction force along pile (FS = 1)  
 $Q_u$  = ultimate bearing capacity force of a footing-type foundation  
 $R_p = q_c$   
 $s_u$  = undrained shear strength, undisturbed soil =  $s_{uu}$   
 $s_{ur}$  = undrained shear strength, remolded soil  
 $s_{uv}$  = undrained shear strength determined by field vane test  
 $\bar{s}_u$  = ave. undrained shear strength in all clay layers penetrated by a pile  
  
SPT = abbrev. for standard penetration test  
 $S_t$  = soil sensitivity (see Eq. 4)  
 $t$  = time  
  
TSP = abbrev. for total stress path  
 $u$  = excess hydrostatic pore water pressure  
  
UF = abbrev. for University of Florida  
  
 $V$  = volume  
  
 $w$  = weight water/weight dry soil = water content  
  
 $y$  = horizontal pile displacement due to lateral loading  
  
 $z$  = depth below soil surface  
  
 $\alpha$  = closure angle between  $q_c$  vs. depth and  $q_c = 0$  or  $q_{co}$  lines  
 $\alpha_o$  = coefficient used in Buisman settlement formulas  
 $\gamma$  = unit weight of soil  
 $\Delta$  = denotes "change in . . ."  
 $\rho$  = settlement  
  
 $\sigma'$  = effective major principal stress  
 $\sigma'_r$  = effective radial or horizontal stress  
 $\sigma'_v$  = effective vertical stress  
 $\sigma'_{oct}$  = effective octahedral stress =  $\frac{\sigma'_v + \sigma'_r + \sigma'_r}{3}$   
  
 $\phi$  = total stress Mohr-Coulomb friction angle  
 $\phi'$  = effective stress Mohr-Coulomb friction angle

APPENDIX I

FACTORS AFFECTING INTERPRETATION OF CPT DATA

## APPENDIX I - FACTORS AFFECTING INTERPRETATION OF CPT DATA

The user of these "Guidelines" would do well to become familiar with those variables that can significantly influence CPT data.

### I.1 Theories for CPT Behavior

At present we have two alternate ways of theorizing about the behavior of a penetrating cone. The oldest considers the problem as one of bearing capacity, and the newest considers the problem as one of cavity expansion. As discussed in Sections 3.36 and 3.21 of Appendix III both theories have produced practical insight. Because of its superiority by more naturally considering compressibility and pore pressure effects, the writer believes that the cavity expansion theories will ultimately dominate. The bearing capacity theories appear most useful for near-surface penetration into dense soils -- hence for the important case of compaction testing.

### I.2 Effect of Vertical Effective Stress at Constant $K'$

Laboratory chamber tests with controlled stress and density conditions in sand (Holden, 1971, Chapman, 1974, Veismanis, 1974) have shown that cone bearing capacity,  $q_c$ , varies with vertical effective stress approximately as indicated by Figure I-1. One finds a small intercept "a" at zero effective stress (sand surface), followed by essentially linear behavior to point "b". At point "b" crushing of the sand grains becomes noticeable and progressively more severe as vertical stress increases. The corresponding deviation from the a-b straight line becomes progressively greater but  $q_c$  still continues to increase at the approximately 4 kg/cm<sup>2</sup> vertical stress limit of the chamber tests. For "ordinary" quartz sands point "b" occurs at about  $q_c = 100$  kg/cm<sup>2</sup>, but in relatively non-crushable sands such as Ottawa sand, this point may exceed 300 kg/cm<sup>2</sup>. In very crushable sands it would be correspondingly less than 100.

Note that when an engineer performs CPT's in an area that will later be excavated or filled, or subject to an increase or decrease in groundwater level,  $q_c$  will then change. Dahlberg (1974) did formal research on this subject. Excavation and/or an increase in GWL will decrease  $q_c$ , while fill and/or a decrease in GWL will increase  $q_c$  at the same elevations. Assuming normally consolidated initial conditions, any increase in  $\sigma'_v$  will produce an approximately proportional increase in  $q_c$ . For conditions other than NC for geologic, compaction, or other reasons,  $q_c$  will change at a rate less than proportional to changes in  $\sigma'_v$ . See I.3, eq. 2, and Table 7 (in Section 6.2.1) for further discussion of OC effects.

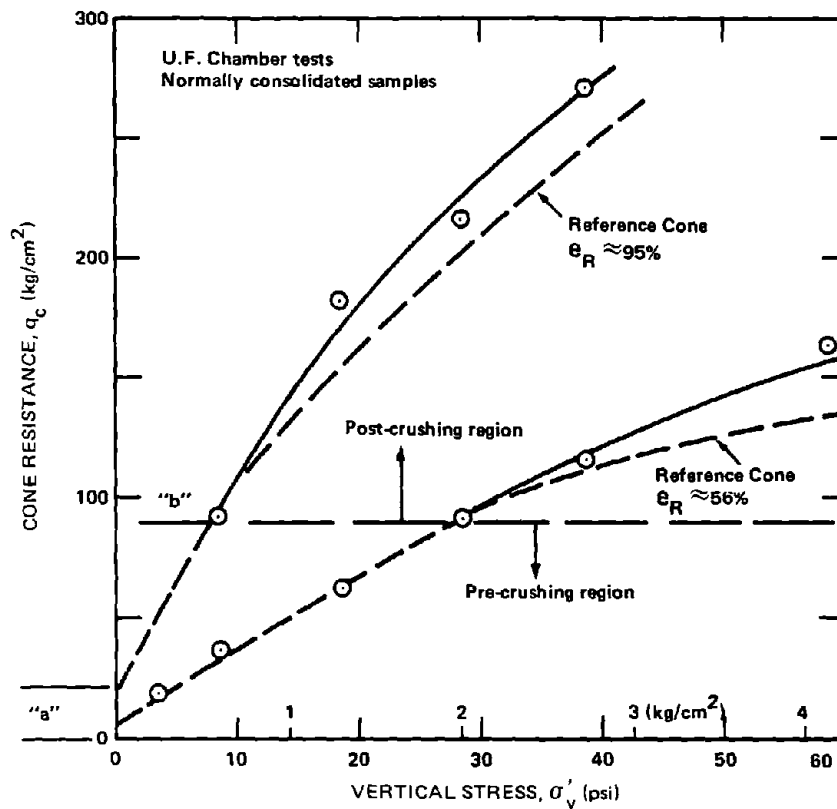


Fig. 8. Cone Resistance vs Vertical Stress. Edgar Sand. Model A Fugro Penetrometer

FIGURE I-1 – IMPORTANCE OF VERTICAL EFFECTIVE STRESS TO  $q_c$   
(data from Holden, 1971, Fig. from Veismanis, 1974)

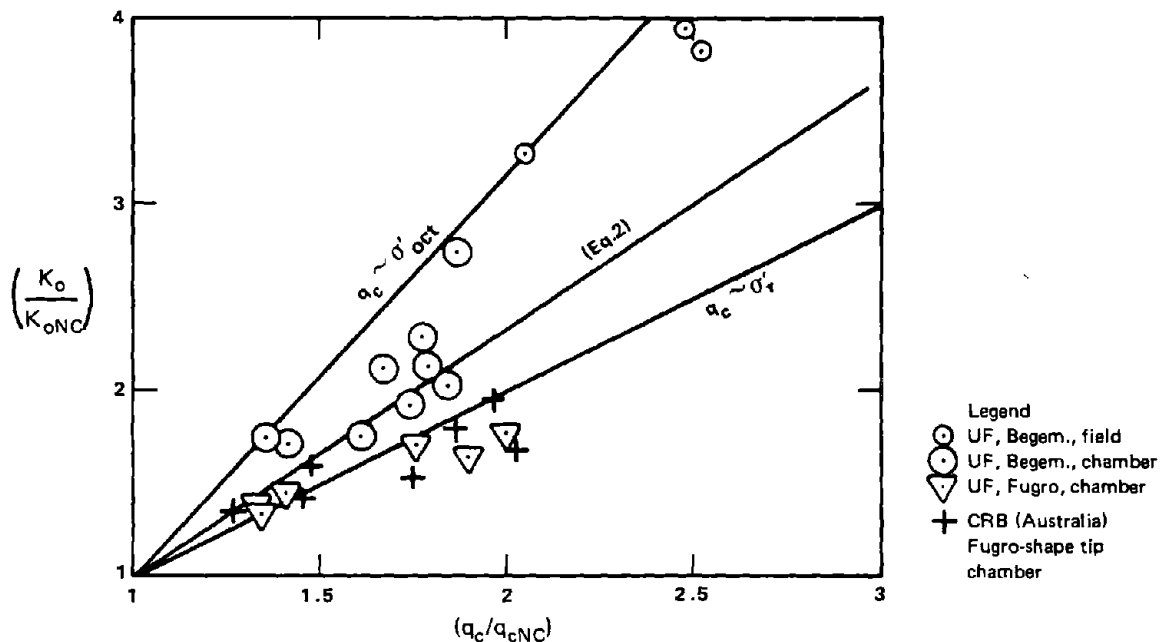


FIGURE I-2 – NORMALIZED COMPARISONS UF FIELD AND UF AND CRB CHAMBER TESTS, COMPARING  $q_c$  WITH ALL VARIABLES EXCEPT EFFECTIVE HORIZONTAL STRESS HELD CONSTANT (also see Schmertmann (1972))

### I.3 Effects of Varying Radial Effective Stress as Constant Vertical Effective Stress

The net result of the passage of the cone penetrometer on an axial soil element is a radial expansion of the element to the radius of the penetrometer tip. One should therefore expect the in situ radial effective stress,  $\sigma_r'$ , to have a significant effect on  $q_c$ . Chamber tests show dramatically that  $\sigma_r'$  after 1 cycle of  $K_0$  overconsolidation has a greater effect than  $\sigma_v'$  on the magnitude of  $q_c$ . Figure II-2 illustrates this via a normalized plot (Schmertmann, 1972 and 1974), as noted in the next paragraph.

The available evidence in Figure I-2 suggests that the Fugro tip (cylindrical shape) has its  $q_c$  controlled primarily by  $\sigma_r'$ , while the octahedral normal stress,  $\sigma'_{oct}$ , in which the radial stress has twice the influence of the vertical stress, more closely controls  $q_c$  when using the Begemann tip -- and probably also the mantle tip.

The available chamber-test evidence also suggests that the ratio of tip-sleeve friction to end bearing,  $f_s/q_c$ , herein termed the "friction ratio" and designated  $R_f$ , is also controlled primarily by the in situ radial stress.

The above shows very clearly the great importance of in situ radial stress, and therefore overconsolidation ratio (OCR) and a soil's geologic history, to any interpretation of static cone sounding data. Unfortunately, we have usually only quantitatively rough data concerning geologic history and the techniques for measuring in situ radial stress are just coming out of the research stage for cohesive soils (Massarsch, 1975) and remain unavailable for cohesionless soils. Note that  $\sigma_r'$  need not be equal in all horizontal directions.

We do know that excavation will produce an OC state in underlying soils and perhaps greatly reduce  $\sigma_r'$  in horizontally adjacent soils. Even an open borehole, if closer than about 10 (reduced from value of 20 noted in ASTM D-3441 due to recent research) hole diameters, may significantly reduce  $\sigma_r'$ . Both static and vibratory roller compaction or the use of compaction piles, or even ordinary displacement piles, can greatly increase  $\sigma_r'$ . Vibroflotation can also increase  $\sigma_r'$ , but sometimes, especially in the case of fine sands and using a fine sand vibroflot backfill, appears to decrease  $\sigma_r'$ . The engineer must consider, at least qualitatively, such effects when evaluating the results of CPT's for design.

### I.4 Compressibility: Density, Cementation, Large Particles

As noted in I.1, a soil's compressibility can significantly influence  $q_c$ . Because the advancing cone must either displace or densify the particle packing, the more compressible the soil the easier this displacement and/or densification and the lower  $q_c$ . Note that crushing the grains of a sand may significantly increase its compressibility.

Obviously, as is well known, the more dense the particle packing, expressed as a higher dry density or higher relative density or lower water content or lower porosity, the higher  $q_c$  because of the inter-related variables of reduced compressibility and greater strength. Note that because they affect  $q_c$  in similar ways, the engineer in the field usually cannot distinguish between effective stress and density effects when attempting to evaluate the reasons for different  $q_c$  in the same soil.

Cementation between particles, always a possibility in situ and the more likely the older a soil, also reduces compressibility and thereby increase  $q_c$ . Sometimes, if available, undisturbed samples will show the engineer he is dealing with cemented soil. However, significant cementing in sands, sensitive clays, etc. may be destroyed by ordinary sampling methods and the higher  $q_c$  may then be incorrectly attributed to other factors, such as stress or density.

When the particle size of the soil penetrated becomes a significant fraction of the cone diameter, then  $q_c$  can increase abruptly because of decreased compressibility due to having to displace these particles as rigid units. Research is scarce on this subject but it appears that this effect is not significant in medium and finer sands with cone tips of the sizes considered herein. However, gravelly sands tend to produce sharp peaks in the  $q_c$  profile when encountering the gravel. Static soundings often reach refusal when attempting to penetrate gravel layers. Intersecting very large particles unusually abruptly stops a sounding. Brushing against them can deflect and permanently bend a tip.

Review Section I.4 for other comments on limits to CPT penetration.

### I.5 Shape of the Penetrometer Tip

The shape of the tip can have an important influence on sounding data. See Appendix II for the details of tip shapes. A cylindrical tip of the Fugro type provides no partial relief of the volume displacement forced by the downward movement of the cone. On the other hand, mechanical tip designs of the Delft mantle and Begemann types do allow displacement relief because of their reduced diameter immediately above the cone. In all but the loosest soils such displacement relief also means effective stress relief and therefore a reduction in  $q_c$ . The mechanical tips have a mantle above the cone, which moves with the cone. Soil friction along this mantle registers as part of the cone bearing and tends to increase  $q_c$ .

Of particular importance in evaluating shape effects is the ratio of  $q_c$  and/or  $R_f$  between data obtained with the mechanical tips and data obtained with the Fugro-type electrical tips. The available evidence suggest that in very weak sands and also in normally consolidated clays the mechanical tip will produce higher cone bearing values (due to mantle friction) but that in dense sands the mechanical tips yield significantly

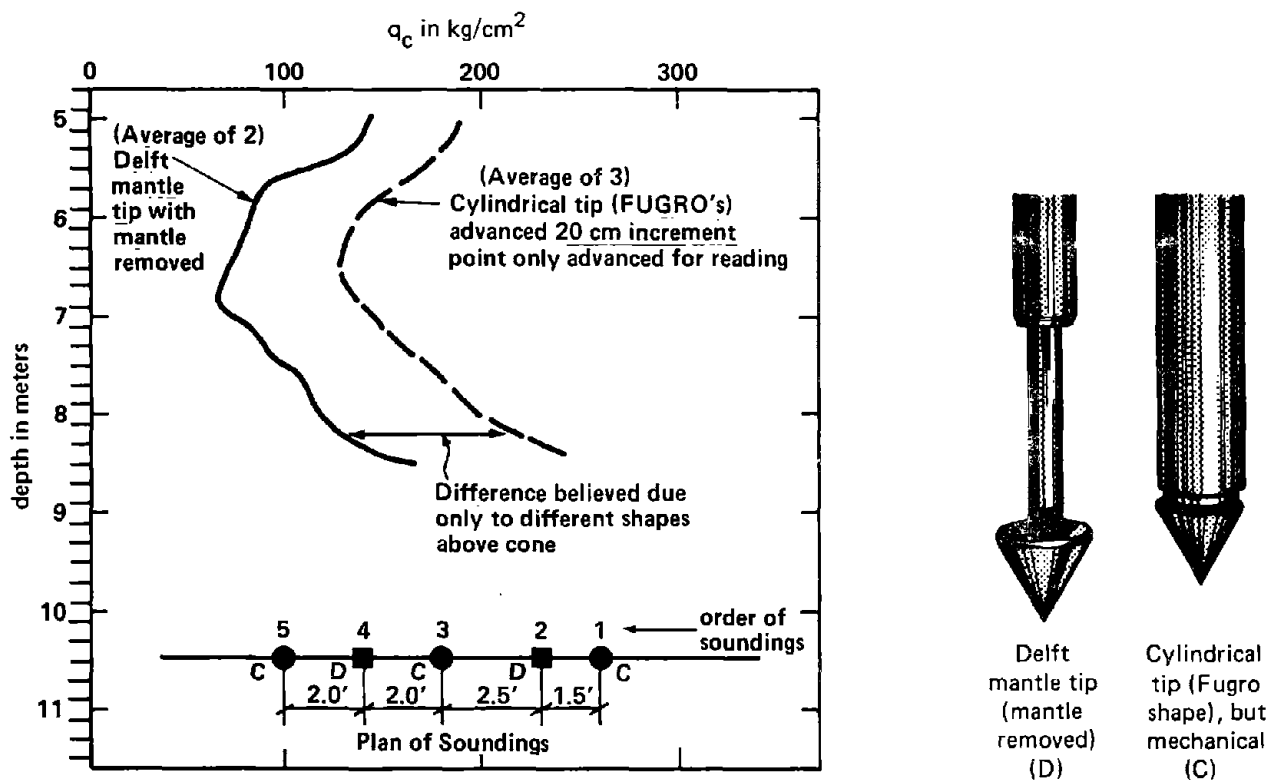
lower values of cone bearing due to stress relief. Figure I-3(a) illustrates this effect for two extremes in tip shape at one field site in dense sand, with all variables held constant except shape. Figure I-4 summarizes the data available to the writer to date concerning the ratio between  $q_c$  for the mechanical tip and  $q_c$  for the Fugro tip, primarily for sands. The writer indicates a trend line through these data. However, we need more data to more accurately define this trend. At present the available data do not clearly show, even qualitatively, the effects of possibly significant variables such as depth, in situ stress conditions, soil gradation, and penetration pore pressure effects (see I-7). It may prove very difficult to separate the interrelated effects of shape and pore pressure. Note that Figure I-4 includes only a few comparisons in cohesive soils.

Note that the Delft Soil Mechanics Laboratory, which developed the Dutch cone test, now uses an electric tip with a reduced shaft diameter immediately above the base of the cone point. They argue that this tip produces data that matches better in sands the data obtained from the older Delft mechanical tips (Heijnen, 1973, 1974). However, others (Joustra, 1974) have produced data indicating the Fugro-type cylindrical tip at least sometimes produces better matching data. Holden (1974) argued for the cylindrical shape. Section 3.2.1. of D-3441 (Appendix II) precludes the use of the Delft electric tip in favor of the cylindrical.

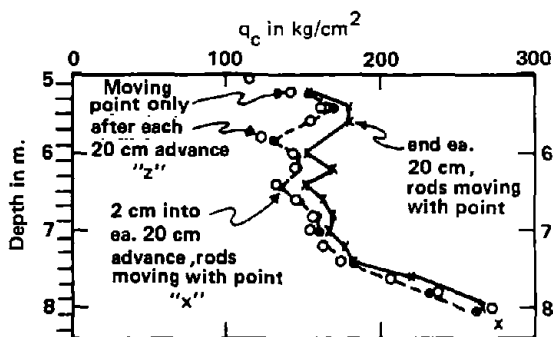
#### I.6 Method of Penetration

Engineers using electrical tips of the Fugro type usually advance them at a constant penetration speed of about 2 cm/sec. They advance mechanical tips in a discontinuous manner with alternate downward movement of both tip and push rod followed by an advance of the tip only. This results in a difference in overhead push rod friction on soil at the time of the  $q_c$  and  $f_s$  measurements. With continuous penetration push rod friction acts in a downward direction and should usually increase effective stresses. With the discontinuous operation there is no downward friction and there may even be a residual upward friction. Some theoretical studies and experimental work at the University of Florida and elsewhere suggests that a continuous penetration in dry sands or sands without significant pore pressure buildup results in a  $q_c$  increase of only about 0 to 10% compared to discontinuous penetration. At low  $D_r$  continuous penetration results in a slight decrease in  $q_c$ .

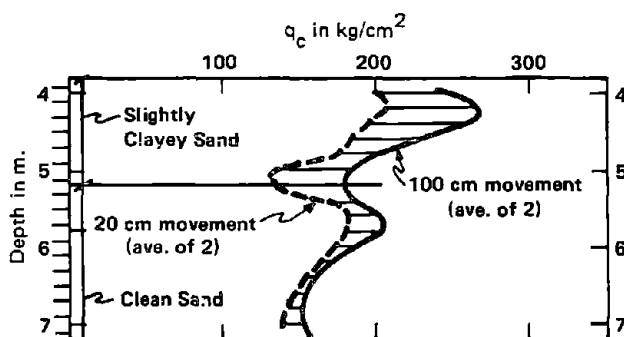
As one field research example, compare in Figure I-3(b) the  $q_c$  values shown by the "z" profile points when only the cone point of the cylindrical, mechanical tip moved, with those from the "x" profile (dashed line) when both cone and overhead rods moved simultaneously. Both "z" and "x" are from the same sounding, with "x" obtained only about 2 cm below each "z" -- enough to generate full overhead rod friction but not full pore pressure. The essentially equal "x" and "z"  $q_c$  values suggest, in this case, a near-zero overhead rod friction effect during simultaneous penetration.



(a) Effect of using different tip shapes at right in a saturated, dense sand

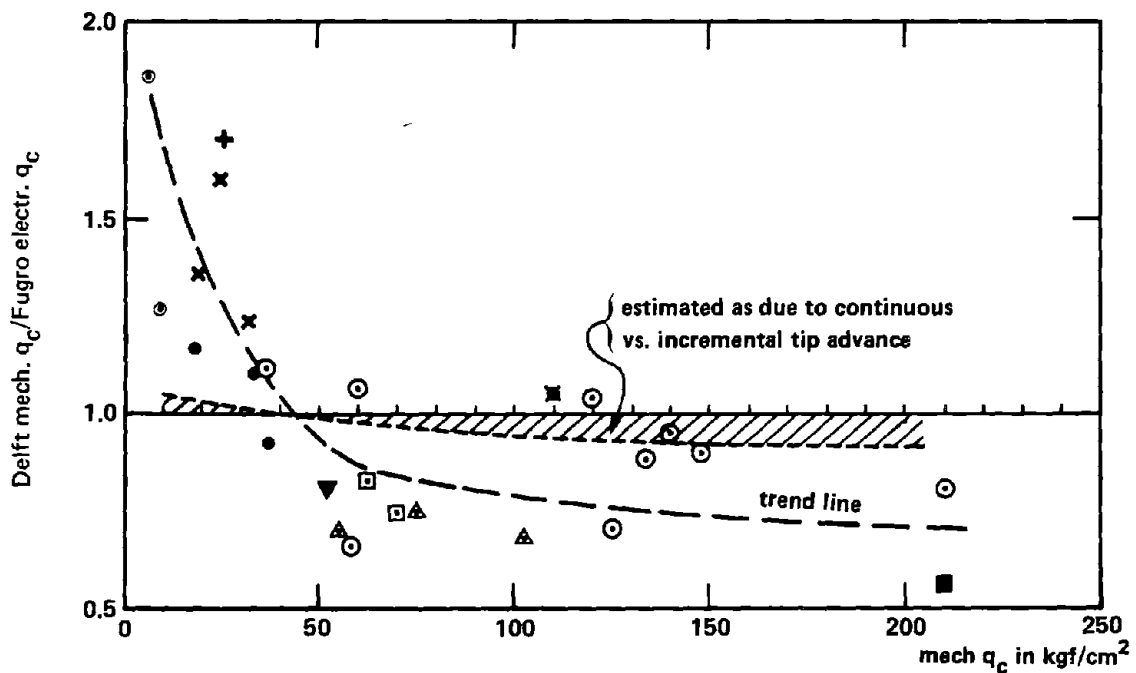


(b) — Example from a single sounding in dense sand below the water table showing increase in  $q_c$  with increasing penetration along the same sounding stroke using C tip



(c) — Comparison of  $q_c$  - profiles from 2 sets of soundings in dense sand showing decrease in  $q_c$  with interruption of the continuous penetration using C tip (soundings alternate 0.6 m apart on a line)

**FIGURE I-3 — SOME RESULTS FROM FIELD RESEARCH AT UNIV. OF FLORIDA IN A SLIGHTLY SILTY, FINE QUARTZ SAND (SP), BELOW WATER TABLE (AT 2.1 m DEPTH) ILLUSTRATING EFFECT OF TIP SHAPE, PORE PRESSURES AND CONTINUOUS ADVANCE**



- Legend: ○ Fugro tests, below WT (Joustra, 1974)  
 □ Delft tests, below WT (Heijnen, 1973)  
 ▲ Kok (1974), below WT  
 ■ U.F., field below WT  
 + U.F., field, below WT, sandy clay  
 ● U.F., field, above WT  
 ▼ U.F., chamber, dry uniform med. sand  
 ⊙ Ft. Pierce, Fla., silty sand below WT  
 × Raleigh, NC, above WT, residual silt  
 ⊠ Raleigh, NC, below WT, residual silt

All points represent averages of a layer at least 1.0 m thickness

FIGURE I-4 – COMPARISONS BETWEEN  $q_c$  OBTAINED WITH DELFT MECHANICAL AND FUGRO ELECTRIC STATIC CONE TIPS

Considering the variability of natural sands and the many possibilities for measurement errors, this systematic error of 0 to 10% seems negligible and the writer suggests disregarding it at present. Figure I-4 includes an estimate of this continuous versus incremental penetration effect.

Some research in the University of Florida chamber indicates that the sleeve friction,  $f_s$ , depends greatly on the magnitude and direction of overhead pushrod friction. Downward friction increases  $f_s$ . Because of the continuous penetration this effect must be more carefully controlled and standardized (with respect to the diameter, roughness, and projections from the pushrods) with the operation of the Fugro tips.

The rate of penetration may be of some importance. In sands the rate effect is usually minor and negligible over the ordinary range of tip advance rates. Even fine sands ordinarily generate only minor pore pressures, in relation to total stress magnitude, during CPT penetration. However, one important exception involves saturated, very loose, cohesionless deposits. They can liquefy, or almost liquefy, during penetration at ordinary rates and produce greatly reduced cone bearing resistance,  $q_c$ .

In clay there is approximately a 5 to 10% increase in  $q_c$  or  $f_s$  resistance with every 10-fold increase in the rate of penetration. However, in the mixed soils with permeabilities between clay and sand there may also be a significant rate effect due to water pressure generation. The more rapid the rate the less time for positive (or negative) water pressure dissipation, the lower (or higher) the effective stresses, and the lower (or higher)  $q_c$ .

In general use the 1-2 cm/s rate of penetration required by D-3441. Whenever rate of penetration effects are in question, including pore pressure effects, use at least two rates of penetration -- the standard 1-2 cm/sec and 1/10 of this. This should demonstrate the importance of rate in soils with  $k > 10^{-5}$  cm/sec, and may lead to slower rates of penetration than the standard for some soils for some investigations.

#### I-7 Pore Pressure Effects

The permeability, compressibility, saturation and dilatancy behavior of the soil penetrated, the method of penetration, and the shape of the penetrometer tip control the excess hydrostatic pore pressures developed in the immediate vicinity of the penetrometer tip during its advance. Water pressures govern effective stresses and, as has been shown in Figures I-1 and I-2, therefore have an important influence on  $q_c$  and  $f_s$  measured.

We do know that soils with +dilatancy (expanding structure) will decrease water pressure when subjected to shear strain. In the same way soils with -dilatancy (contracting structure) will increase water pressure with the application of shear strain. We usually associated positive dilatancy with dense or strong soils and negative dilatancy with loose and weak soils. Thus, soil dilatancy and the consequent water pressure effects make weak soils appear weaker and strong soils appear stronger in the CPT than their strengths when fully drained.

However, with higher confining pressure the tendency for +dilatancy decreases in all particulate materials. At very high confining pressures lab triaxial tests show only -dilatancy. Wissa and Ladd (1965) demonstrated that some quartz sands still showed +dilatancy at confining pressures of over 70 kg/cm<sup>2</sup>, even after grain crushing begins. See Schmertmann (1974 b, pp. 147) for a digest of their data. At present we do not know the  $\sigma_v'$  and  $q_c$  limits for possible +dilatancy, and therefore possible  $-\Delta u$ . The present data indicate  $-\Delta u$  effects may be very important in dense soils with  $k < 10^{-4}$  cm/s, and that the effect might be more important under high hydrostatic water pressures (as offshore) because greater  $-\Delta u$  can develop before cavitation occurs.

The mechanical tips with their reduction in diameter above the cone, plus their incremental operation, allow space and time for more water pressure dissipation relative to the continuously advance cylindrical Fugro tip. Therefore, the Fugro tips will produce higher peaks and lower valleys in the cone bearing and friction profiles than the mechanical tips. This will occur in addition to the similar effect produced by continuous electrical cone profiles compared to the incremental mechanical profiles.

At present not much is know about pore pressure effects on  $q_c$  and  $f_s$  in the field. The great dependence of  $q_c$  of radial effective stress suggests pore pressure effects may be very significant. Figures I-3(b) and I-3(c) present cone bearing profiles which seem to illustrate negative pore pressure effects in a dense fine sand below the water table using a mechanical cylindrical tip simulating the Fugro design.

For both the I-3(c) and I-3(b) comparisons all other variables except time, and presumably pore pressure, were held constant, as follows: Figure I-3(c) illustrates the significant increase (ave. 25% in slightly clayey sand and 8% in clean sand) in  $q_c$  when advancing the cylindrical tip continuously in 100 cm increments and stopping only to add another push rod, compared to also stopping every 20 cm to take a point-movement-only reading. Both  $q_c$  readings were taken during simultaneous cone-rod advance. The continuous 100 cm advance allowed less time for negative pore pressure dissipation, thus maintaining higher effective stresses and thus producing greater  $q_c$ . Comparing the "x" and "y"  $q_c$  profiles in Figure I-3(b) shows that after a stop the negative pore pressures generated during the subsequent 2 to 20 cm increment of simultaneous cone-rod movement increased  $q_c$  an average of

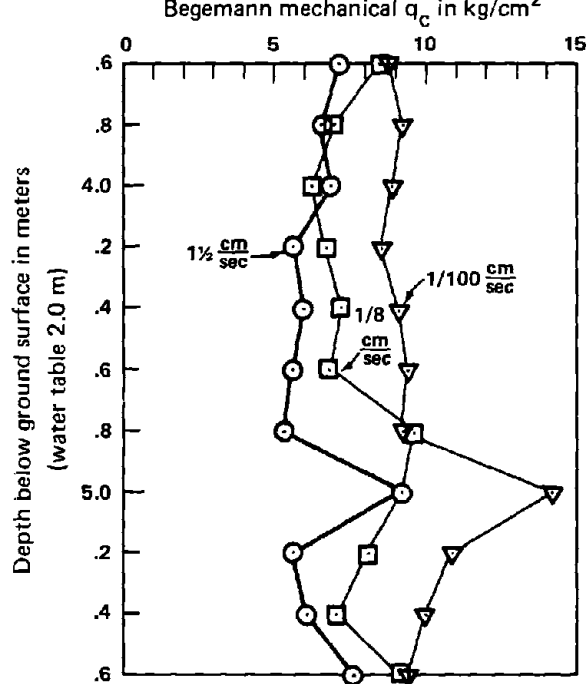
about 8%. Thus, Fugro-type testing with 100 cm increments of continuous advance would produce, in this case, at least an  $8+8 = 16\%$  increase in  $q_c$  in the clean sand compared to when pore pressure = 0. Similar ratios suggest at least a 30% increase for the slightly clayey sands.

On the other hand, Figure I-5 presents an example to show how positive pore pressure generated during tip penetration can decrease  $q_c$  -- in this case, to an estimated 40% of the fully drained  $q_c$ . This Florida organic clayey sand had a sensitive structure and a low enough permeability to generate significant excess hydrostatic pore pressure due to tip displacement. But, its permeability was also high enough for significant pore pressure dissipation during reduced rates of penetration. Part (a) of this figure presents the  $q_c$  profiles at the ordinary rate of advance for a mechanical tip and at two slower rates -- as described in the accompanying table (d). Part (b) shows the excess hydrostatic pore pressure decay in this layer as measured with an electric (Geonor, vibrating wire, 3.1 cm diam) piezometer advanced as an ordinary cone sounding and then stopped at time = 0. Note that even with  $k$  as high as  $10^{-5}$  cm/sec this decay takes at least 1 hour! Part (c) documents the relative positions of the five soundings involved here. Part (e) lists average soil layer properties as determined from laboratory tests on 2 inch diameter, fixed-piston, undisturbed samples.

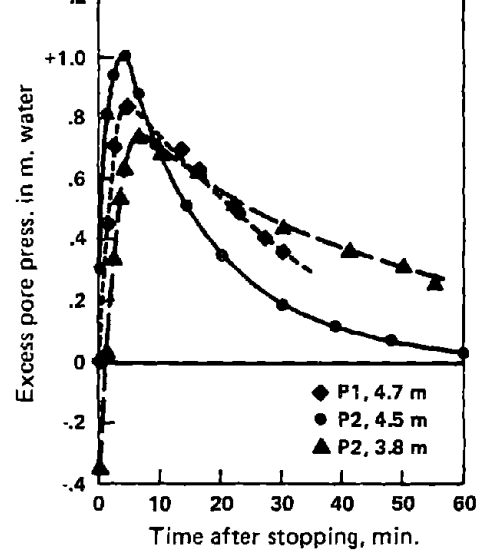
A paper by Wissa et al. (1975) describes a piezometer probe designed like a cone penetrometer tip, but with a 20 degree point angle and a small, cylindrical water pressure sensing element projecting from the point of this tip. These authors describe finding both + and -  $\Delta u$  during penetration into a variety of soils, with extremes of +19 m excess water pressure in a soft, sandy clay and -14 m water in a dense silty sand. A discussion by Tortensson (1975) presents similar, but independent results from concurrent research in Sweden. A recent paper by the writer (Schmertmann, 1974) presents evidence that suggests both + and - excess hydrostatic pore pressure can exist simultaneously at different locations around an advancing cone penetrometer tip.

These examples indicate that pore pressure effects may have great significance in the engineering interpretation of data, and particularly when attempting to compare data obtained with tips that generate significantly different pore pressure response.

The reader should expect penetration-generated pore pressures and tip shape and method of tip advance to be interrelated in a complicated way -- depending on, at least, soil dilatency and permeability, rate and manner of penetration, and in situ stress conditions. See Appendix III, section 3.34, for some additional discussion of pore pressure effects.



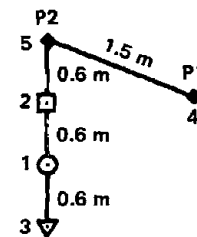
(a) – Effect of reducing rate of penetration in a sensitive organic clayey sand (plan Fig. 8)



(b) – Rise and decay of excess hydrostatic pore water pressure after stopping penetration of a cone-piezometer in sensitive, organic clayey sand

(d)  
Fig. (a) Penetration Rate Procedures

Symbol	○	□	▽
Pushrod penetr. (cm/sec)	5	5	5
Wait (sec)	5-10	60-90	5-10
Cone penetr. for $q_c$ (cm/sec)	1-2	1/8 ave. 1/100 (15-30 sec for ea. $\approx$ const. $\Delta q_c$ step to $q_c$ )	
Total time per $q_c$ determ. (sec)	10	90	360



(c) – Plan of soundings and cone-piezometer tests in sensitive, organic clayey sand, with order of penetration

(e) Average soil layer properties

- #40 sieve = 85% with LL = 37%, PL = 18%
- #200 sieve = 20%, -2 microns = 3%
- organic = 6%, carbonates (mostly shells) = 26%
- OCR = 2.0,  $K_o = 0.50$
- $k = 10^{-5}$  cm/sec, pp param.  $B = 0.85$  ( $S = 97\%$ ),  $A_f = 1.4$
- $S_t = 15+$ ,  $s_u/p' = 0.34$ ,  $\phi' = 38^\circ$ ,  $c' = 0$
- $w = 35\%$

FIGURE I-5 – EXAMPLE FROM ST. PETERSBURG, FLORIDA, OF RATE OF PENETRATION AND PORE PRESSURE DISSIPATION EFFECTS ON  $q_c$  IN A SENSITIVE, ORGANIC CLAYEY SAND WITH  $k = 10^{-5}$  cm/s

## 1.8 Layering and Tip Diameter Effects

When interpreting CPT data one must consider the effects when the penetrometer passes through the boundaries between soil layers.

Figure I-6(a) shows a sequence of  $q_c$  readings when a Fugro-type penetrometer passed from a lower to a higher relative density layer of the same sand. Figure I-6(b) illustrates the reverse. Holden (1971) obtained similar data with a Fugro electric cone advanced continuously. Note that the cone tip required between 5 and 10 cone base diameters to sense the interface and then another 5 to 10 to pass completely through it. The total effect of the interface, in these cases, involves  $q_c$  through about 15 diameters of depth. Thus, the smaller the cone diameter the thinner the layer that can be fully measured. For the 10 cm<sup>2</sup> cone this thinnest layer in sand equals about 15 diameters, or about 50 cm or 20 in. Also, the smaller the cone diameter the more sensitive the tip to local variations with depth. Larger diameter tips, including piles, tend to average the effects of all layers with a bias toward developing failure zones in the weaker layers. Note that the pile driving record often shows that a pile, during driving, senses an underlying layer, particularly if weak, at a greater vertical distance than when subsequently loaded statically. The Figure I-6 data were obtained from dry sand under laboratory conditions. Undrained bearing theory predicts that the complete  $q_c$  transition will occur more rapidly (2 to 4 diameters) in clays.

Note that the above 15 diameters for sands represents the minimum layer thickness needed to reach full  $q_c$  within that layer. However, a cone penetrometer tip, especially if advanced with continuous recording, will sense much thinner layers -- but not fully. The greater the difference in strength and compressibility between the layer to be sensed and its adjacent soil, the thinner the layer that one can detect in the  $q_c$  profile. The writer knows of no extensive research on this subject. But, experienced engineers believe they can detect isolated sand layers as thin as 1 cm in clay when using electric tips and continuous recording.

It sometimes becomes desirable to increase penetration capability by using tips of the same shape but of smaller size, or to increase tip size to increase sensitivity or to increase structural strength and allow supplementary dynamic driving of the penetrometer. The available field and chamber test evidence indicates that cones with end areas from 5 to 20, and perhaps even to 40 cm<sup>2</sup>, produce about the same CPT data as the standard 10 cm<sup>2</sup> cone in all soils. As explained above, decreasing the cone diameter will increase layer detection sensitivity and increasing the diameter will decrease this sensitivity.

$K_0$  NC to 15.00 psi at bottom, then tested with reference tip in 1" depth increments. Penetration rate  $\approx 0.65$  in/min. End bearing transducer chart recorded after 1 min penetration and plotted below at corresponding depth. Point always collapsed to original length.

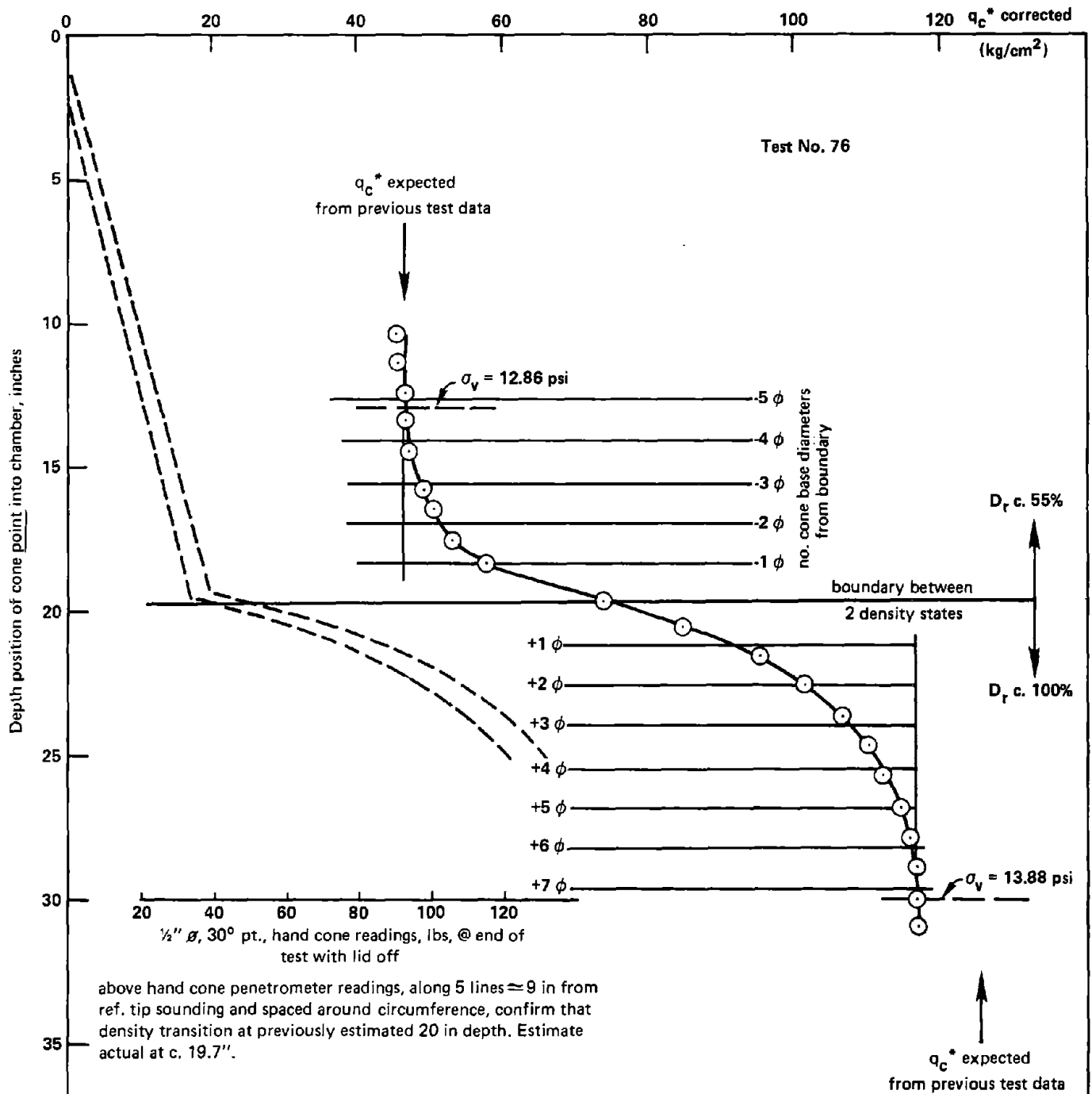
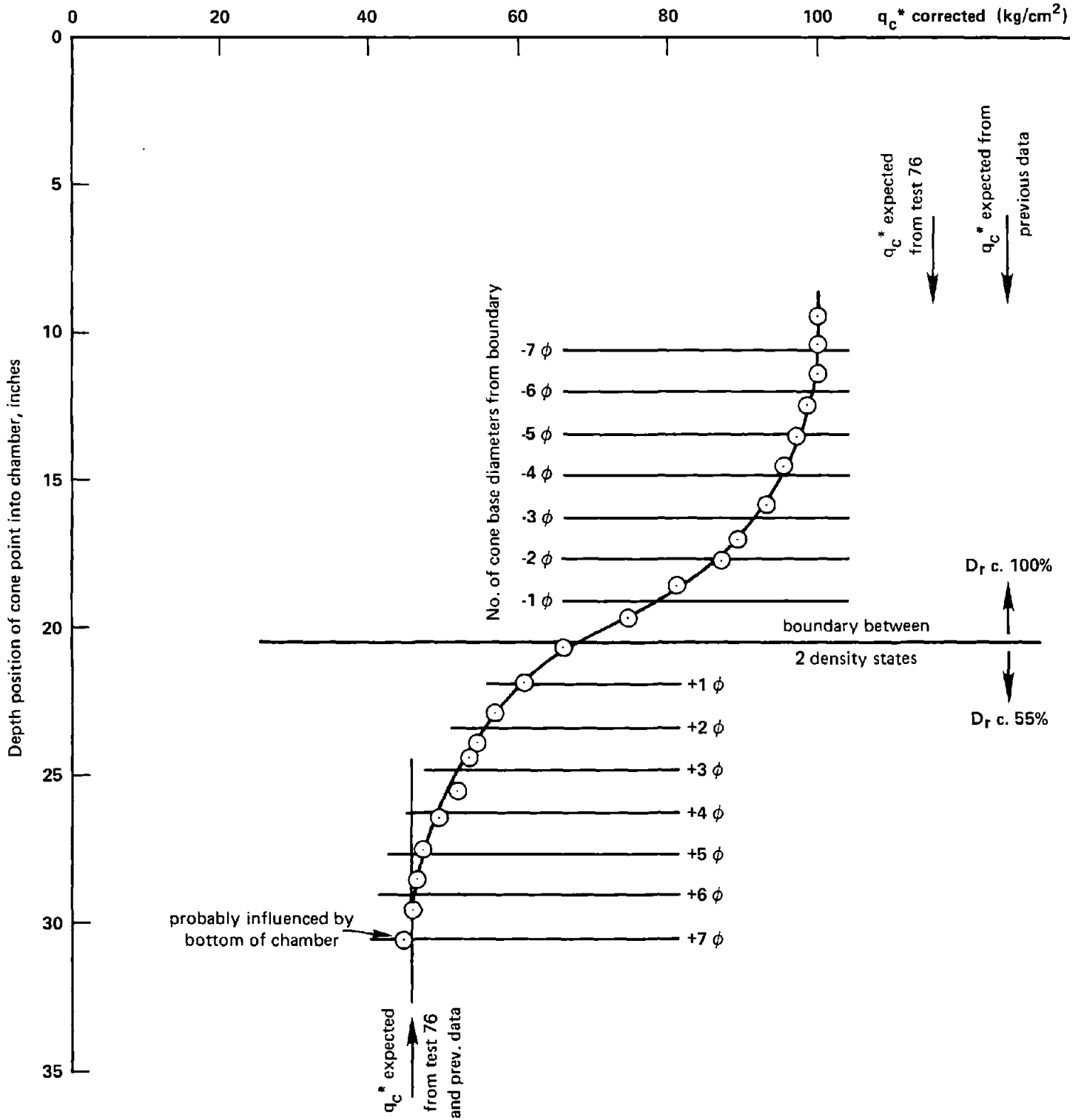


FIGURE I-6 (a) -- PENETRATION OF FIG. 5 FUGRO-TYPE TIP THRU LOOSE-TO-DENSE SAND BOUNDARY ( $q_c$  during cone advance only)

Note: In view of expected reasonableness of the  $q_c^*$  results, separate dry unit wts. not obtained after test. Sand not weighed.

Same conditions as for test No. 76, but layers reversed



Note: layer dry densities not determined

FIGURE I-6 (b) – PENETRATION OF FIG. 5 FUGRO-TYPE TIP THRU DENSE-TO-LOOSE SAND BOUNDARY ( $q_c$  during cone advance only)

APPENDIX II

COPY OF TEXT OF ASTM STANDARD FOR THE CPT  
(Found in Part 19 )

(Reprinted with permission)



## Tentative Method for DEEP, QUASI-STATIC, CONE AND FRICTION-CONE PENETRATION TESTS OF SOIL<sup>1</sup>

This Tentative Method has been approved by the sponsoring committee and accepted by the Society in accordance with established procedures, for use pending adoption as standard. Suggestions for revisions should be addressed to the Society at 1916 Race St., Philadelphia, Pa. 19103.

### 1. Scope

1.1 This method covers the determination of end bearing and side friction, the components of penetration resistance which are developed during the steady slow penetration of a pointed rod into soil. This method supplies data on the engineering properties of soil intended to help with the design and construction of earthworks and foundations for structures. This method is sometimes referred to as the "Dutch Cone Test."

1.2 This method includes the use of both cone and friction-cone penetrometers, of both the mechanical and electric types.

NOTE 1—This method does not include hydraulic penetrometers. Such penetrometers use a hydraulic system to extend the penetrometer tip, or to transmit the penetration resistance(s) from the tip to the recording unit, or both. However, many of the requirements herein could also apply to hydraulic penetrometers.

1.3 Mechanical penetrometers of the type described in this method operate incrementally, using a telescoping penetrometer tip, resulting in no movement of the push rods during the measurement of the resistance components. Design constraints for mechanical penetrometers preclude a complete separation of the end-bearing and side-friction components. Electric penetrometers are advanced continuously and permit separate measurement of both components. Differences in shape and method of advance between cone penetrometer tips may result in significant differences in one or both resistance components.

### 2. Definitions

2.1 *cone penetrometer*—an instrument in

the form of a cylindrical rod with a conical point designed for penetrating soil and soft rock and for measuring the end-bearing component of penetration resistance.

2.2 *friction-cone penetrometer*—a cone penetrometer with the additional capability of measuring the local side friction component of penetration resistance.

2.3 *mechanical penetrometer*—a penetrometer that uses a set of inner rods to operate a telescoping penetrometer tip and to transmit the component(s) of penetration resistance to the surface for measurement.

2.4 *electric penetrometer*—a penetrometer that uses electric-force transducers built into a nontelelescoping penetrometer tip for measuring, within the tip, the component(s) of penetration resistance.

2.5 *penetrometer tip*—the end section of the penetrometer, which comprises the active elements that sense the soil resistance, the cone, and in the case of the friction-cone penetrometer, the friction sleeve.

2.6 *cone*—the cone-shaped point of the penetrometer tip, upon which the end-bearing resistance develops.

2.7 *friction sleeve*—a section of the penetrometer tip upon which the local side-friction resistance develops.

2.8 *push rods*—the thick-walled tubes, or other suitable rods, used for advancing the penetrometer tip to the required test depth.

<sup>1</sup> This method is under the jurisdiction of ASTM Committee D-18 on Soil and Rock for Engineering Purposes, and is the direct responsibility of Subcommittee D18.02 on Sampling and Related Field Testing for Soil Investigations.

Current edition approved Aug. 29, 1975. Published December 1975.

2.9 *inner rods*—rods that slide inside the push rods to extend the tip of a mechanical penetrometer.

2.10 *cone resistance or end-bearing resistance*,  $q_c$ —the resistance to penetration developed by the cone, equal to the vertical force applied to the cone divided by its horizontally projected area.

2.11 *friction resistance*,  $f_s$ —the resistance to penetration developed by the friction sleeve, equal to the vertical force applied to the sleeve divided by its surface area. This resistance consists of the sum of friction and adhesion.

2.12 *friction ratio*,  $R_f$ —the ratio of friction resistance to cone resistance,  $f_s/q_c$ , expressed in percent.

2.13 *cone sounding*—the entire series of penetration tests performed at one location when using a cone penetrometer.

2.14 *friction-cone sounding*—the entire series of penetration tests performed at one location when using a friction-cone penetrometer.

### 3. Apparatus

#### 3.1 General:

3.1.1 *Cone*—The cone shall have a 60-deg ( $\pm 5$ -deg) point angle and a base diameter of  $1.406 \pm 0.016$  in. ( $35.7 \pm 0.4$  mm), resulting in a projected area of  $1.55$  in.<sup>2</sup> ( $10$  cm<sup>2</sup>).

NOTE 2—In soft soils, the total soil-resistance force on the cone may be insufficient to support the accumulated weight of the cone and inner rods of the mechanical penetrometer. In this case, tips with a larger projected area may be used if their geometry remains similar to that for the  $1.55$  in.<sup>2</sup> ( $10$  cm<sup>2</sup>) tip.

3.1.2 *Friction Sleeve*, having the same outside diameter  $+0.024$  to  $-0.000$  in. ( $+0.5$  to  $-0.0$  mm) as the base diameter of the cone (see 3.1.1). No other part of the penetrometer tip shall project outside the sleeve diameter. The surface area of the sleeve shall be  $15.5$  or  $23.2$  in.<sup>2</sup> ( $100$  or  $150$  cm<sup>2</sup>)  $\pm 2$  %.

3.1.3 *Steel*—The cone and friction sleeve shall be made from steel of a type and hardness suitable to resist wear due to abrasion by soil. The friction sleeve shall have and maintain with use a roughness of  $20$   $\mu$ in. ( $0.5$   $\mu$ m) AA,  $\pm 50$  %.

3.1.4 *Push Rods*—Made of suitable steel, these rods must have a section adequate to

sustain, without buckling, the thrust required to advance the penetrometer tip. They must have an outside diameter not greater than the diameter of the base of the cone for a length of at least  $1.3$  ft ( $0.4$  m) above the base, or, in the case of the friction-cone penetrometer, at least  $1.0$  ft ( $0.3$  m) above the top of the friction sleeve. Each push rod must have the same, constant inside diameter. They must screw or attach together to bear against each other and form a rigid-jointed string of rods with a continuous, straight axis.

3.1.5 *Inner Rods*—Mechanical penetrometers require a separate set of steel, or other metal alloy, inner rods within the steel push rods. The inner rods must have a constant outside diameter with a roughness, excluding waviness, less than  $10$   $\mu$ in. ( $0.25$   $\mu$ m) AA. They must have the same length as the push rods ( $\pm 0.004$  in. or  $\pm 0.1$  mm) and a cross section adequate to transmit the cone resistance without buckling or other damage. Clearance between inner rods and push rods shall be between  $0.020$  and  $0.040$  in. ( $0.5$  and  $1.0$  mm). See 5.8.1.

3.1.6 *Measurement Accuracy*—Maintain the thrust-measuring instrumentation to obtain thrust measurements within  $\pm 5$  % of the correct values.

#### 3.2 Mechanical Penetrometers:

3.2.1 The sliding mechanism necessary in a mechanical penetrometer tip must allow a downward movement of the cone in relation to the push rods of at least  $1.2$  in. ( $30.5$  mm).

NOTE 3—At certain combinations of depth and tip resistance(s), the elastic compression of the inner rods may exceed the downward stroke that the thrust machine can apply to the inner rods relative to the push rods. In this case, the tip will not extend and the thrust readings will rise elastically to the end of the machine stroke and then jump abruptly when the thrust machine makes contact with the push rods.

3.2.2 Mechanical penetrometer tip design shall include protection against soil entering the sliding mechanism and affecting the resistance component(s) (see 3.2.3 and Note 4).

3.2.3 *Cone Penetrometer*—Figure 1 shows the design and action of one mechanical cone penetrometer tip. A mantle of reduced diameter is attached above the cone to minimize possible soil contamination of the sliding mechanism.

**NOTE 4**—An unknown amount of side friction may develop along this mantle and be included in the cone resistance.

**3.2.4 Friction-Cone Penetrometer**—Figure 2 shows the design and action of one telescoping mechanical friction-cone penetrometer tip. The lower part of the tip, including a mantle to which the cone attaches, advances first until the flange engages the friction sleeve and then both advance.

**NOTE 5**—The shoulder at the lower end of the friction sleeve encounters end-bearing resistance. In sands as much as two thirds of the sleeve resistance may consist of bearing on this shoulder. Ignore this effect in soft to medium clays.

**3.2.5 Measuring Equipment**—Measure the penetration resistance(s) at the surface by a suitable device such as a hydraulic or electric load cell or proving ring.

### 3.3 Electric Penetrometers:

**3.3.1 Cone Penetrometer**—Figure 3 shows one design for an electric-cone penetrometer tip. The cone resistance is measured by means of a force transducer attached to the cone. An electric cable or other suitable system transmits the transducer signals to a data recording system. Electric-cone penetrometers shall permit continuous advance and recording over each push rod-length interval.

**3.3.2 Friction-Cone Penetrometer**—The bottom of the friction sleeve shall not be more than 0.4 in. (10 mm) above the base of the cone. The same requirements as 3.3.1 apply. Figure 4 shows one design for an electric friction-cone penetrometer tip.

**3.4 Thrust Machine**—This machine shall provide a continuous stroke, preferably over a distance greater than one push rod length. The machine must advance the penetrometer tip at a constant rate while the magnitude of the thrust required fluctuates (see 4.1.2).

**NOTE 6**—Deep penetration soundings usually require a thrust capability of at least 5 tons (45 kN). Most modern machines use hydraulic pistons with 10 to 20-ton (90 to 180-kN) thrust capability.

**3.5 Reaction Equipment**—The proper performance of the static-thrust machine requires a stable, static reaction.

**NOTE 7**—The type of reaction provided may affect the penetrometer resistance(s) measured, particularly in the surface or near-surface layers.

## 4. Procedure

### 4.1 General:

**4.1.1** Set up the thrust machine for a thrust direction as near vertical as practical.

**4.1.2 Rate of Penetration**—Maintain a rate of depth penetration of 2 to 4 ft/min (10 to 20 mm/s)  $\pm 25\%$  when obtaining resistance data. Other rates of penetration may be used between tests.

**NOTE 8**—The rate of 2 ft/min (10 mm/s) provides the time the operator needs to read properly the resistance values when using the mechanical friction-cone penetrometer. The rate of 4 ft/min (20 mm/s) is suitable for the single resistance reading required when using the mechanical cone penetrometer and provides for the efficient operation of electric penetrometers.

**NOTE 9**—The engineer may wish to test at reduced rates of penetration to study possible pore pressure and other effects on the resistance component(s) obtained using the standard rate.

### 4.2 Mechanical Penetrometers:

**4.2.1 Cone Penetrometer**—(1) Advance penetrometer tip to the required test depth by applying sufficient thrust on the push rods; and (2) Apply sufficient thrust on the inner rods to extend the penetrometer tip (see Fig. 1). Obtain the cone resistance at a specific point (see 4.2.3) during the downward movement of the inner rods relative to the stationary push rods. Repeat step (1). Apply sufficient thrust on the push rods to collapse the extended tip and advance it to a new test depth. By continually repeating this two-step cycle, obtain cone resistance data at increments of depth. This increment shall not ordinarily exceed 8 in. (203 mm).

**4.2.2 Friction-Cone Penetrometer**—Use this penetrometer as described in 4.2.1 but obtain two resistances during the step (2) extension of the tip (see Figs. 2 and 5). First obtain the cone resistance during the initial phase of the extension. When the lower part of the tip engages and pulls down the friction sleeve, obtain a second measurement of the total resistance of the cone plus the sleeve. Subtraction gives the sleeve resistance.

**NOTE 10**—Because of soil layering, the cone resistance may change during the additional downward movement of the tip required to obtain the friction measurement (see Note 14)

**NOTE 11**—The soil friction along the sleeve puts an additional overburden load on the soil above the cone and may increase cone resistance above that measured during the initial phase of the tip extension by an unknown, but probably small amount. Ignore this effect.

**4.2.3 Recording Data**—To obtain repro-



ducible cone-resistance test data, or cone and friction-resistance test data when using a friction-cone tip, record only those thrust readings that occur at a well-defined point during the downward movement of the top of the inner rods in relation to the top of the push rods. Because of the elastic compression of inner rods (see Note 3), this point ordinarily should be at not less than 1.0 in. (25 mm) apparent relative movement of the inner rods. When using the friction-cone penetrometer, this point shall be just before the cone engages the friction sleeve.

NOTE 12—Figure 5 shows one example of how the thrust in the hydraulic load cell can vary during the extension of the friction-cone tip. Note the jump in gage pressure when the cone engages the sleeve.

4.2.3.1 Obtain the cone plus friction-resistance reading as soon as possible after the jump so as to minimize the error described in Fig. 5. Unless using continuous recording as in Fig. 5, the operator should not record a cone plus friction resistance if he suspects the cone resistance is changing abruptly or erratically.

#### 4.3 Electric Penetrometers:

4.3.1 If using continuous electric cable, prethread it through the push rods.

4.3.2 Record the initial reading(s) with the penetrometer tip hanging freely in air or in water, out of direct sunlight, and after an initial, short penetration, test hole so that the tip temperature is at soil temperature.

4.3.3 Record the cone resistance, or cone resistance and friction resistance, continuously with depth or note them at intervals of depth not exceeding 8 in. (203 mm).

4.3.4 At the end of a sounding, obtain a final set of readings as in 4.3.2 and check them against the initial set. Discard the sounding, and repair or replace the tip if this check is not satisfactory for the accuracy desired for the resistance component(s).

### 5. Special Techniques and Precautions

5.1 *Reduction of Friction Along Push Rods*—The purpose of this friction reduction is to increase the penetrometer depth capability, and not to reduce any differences between resistance components determined by mechanical and electric tips as noted in 1.3. To accomplish the friction reduction, intro-

duce a special rod with an enlarged diameter or special projections, called a "friction reducer," into the string of push rods or between the push rods and the tip. Another allowable method to reduce friction is to use push rods with a diameter less than that of the tip.

5.2 *Prevention of Rod Bending Above Surface*—Use a tubular rod guide, at the base of the thrust machine, of sufficient length to prevent significant bending of the push rods between the machine and the ground surface.

NOTE 13—Special situations, such as when working through water, will require a special system of casing support to restrict adequately the buckling of the push rods.

5.3 *Drift of Tip*—For penetration depths exceeding about 40 ft (12 m), the tip will probably drift away from a vertical alignment. Occasionally, serious drifting occurs, even at less depth. Reduce drifting by using push rods that are initially straight and by making sure that the initial cone penetration into soil does not involve unwanted, initial lateral thrust. Passing through or alongside an obstruction such as boulders, soil concretions, thin rock layers, or inclined dense layers may deflect the tip and induce drifting. Note any indications of encountering such obstructions and be alert for possible subsequent improper tip operation as a sign of serious drifting.

NOTE 14—Electric penetrometer tips may also incorporate an inclinometer to monitor drift and provide a warning when it becomes excessive.

5.4 *Wear of Tip*—Penetration into abrasive soils eventually wears down or scours the penetrometer tip. Discard tips, or parts thereof, whose wear changes their geometry or surface roughness so they no longer meet the requirements of 3.1. Permit minor scratches.

5.5 *Distance Between Cone and Friction Sleeve*—The friction resistance of the sleeve applies to the soil at some distance above the soil in which the cone resistance was obtained at the same time. When comparing these resistances for the soil at a specified depth, for example when computing friction ratios or when plotting these data on graphs, take proper account of the vertical distance between the base of the cone and the mid-



height of the friction sleeve.

**5.6 Interruptions**—The engineer may have to interrupt the normal advance of a static penetration test for purposes such as removing the penetrometer and drilling through layers or obstructions too strong to penetrate statically. If the penetrometer is designed to be driven dynamically without damage to its subsequent static performance (those illustrated herein in Figs. 1 to 4 are not so designed), the engineer may drive past such layers or obstructions. Delays of over 10 min due to personnel or equipment problems shall be considered an interruption. Continuing the static penetration test after an interruption is permitted provided this additional testing remains in conformance with this standard. Obtain further resistance component data only after the tip passes through the engineer's estimate of the disturbed zone resulting from the nature and depth of the interruption. As an alternative, readings may be continued without first making the additional tip penetration and the disturbed zone evaluated from these data. Then disregard data within the disturbed zone.

**5.7 Below or Adjacent to Borings**—A cone or friction-cone sounding shall not be performed any closer than 25 boring diameters from an existing, unbackfilled, uncased boring hole. When performed at the bottom of a boring, the engineer should estimate the depth below the boring of the disturbed zone and disregard penetration test data in this zone. This depth shall be at least three boring diameters.

#### **5.8 Mechanical Penetrometers:**

**5.8.1 Inner Rod Friction**—Soil particles and corrosion can increase the friction between inner rods and push rods, possibly resulting in significant errors in the measurement of the resistance component(s). Clean and lubricate the inner rods.

**5.8.2 Weight of Inner Rods**—For improved accuracy at low values of cone resistance, correct the thrust data to include the accumulated weight of the inner rods from the tip to the topmost rod.

**5.8.3 Jamming**—Soil particles between sliding surfaces or bending of the tip may jam the mechanism during the many extensions and collapses of the telescoping mechanical tip. Stop the sounding as soon as uncorrecta-

ble jamming occurs.

#### **5.9 Electric Penetrometers:**

**5.9.1 Water Seal**—Provide adequate waterproofing for the electric transducer. Make periodic checks to assure that no water has passed the seals.

### **6. Report**

**6.1 Graph of Cone Resistance,  $q_c$** —Every report of a cone or friction-cone sounding shall include a graph of the variation of cone resistance (in units of tons/ft<sup>2</sup> or 100 kPa) with depth (in feet or metres). Successive cone-resistance test values from the mechanical cone and friction-cone penetrometers, usually determined at equal increments of depth and plotted at the depth corresponding to the depth of the measurement, may be connected with straight lines as an approximation for a continuous graph.

#### **6.2 Friction-Cone Penetrometer:**

**6.2.1 Graph of Friction Resistance,  $f_1$** —In addition to the graph of cone resistance (6.1) the report may include an adjacent or superposed graph of friction resistance or friction ratio, or both, with depth. Use the same depth scale as in 6.1 (see 5.5).

**6.2.2 Graph of Friction Ratio,  $R_f$** —If the report includes soil descriptions estimated from the friction-cone penetrometer data, include a graph of the variation of friction ratio with depth. Place this graph adjacent to the graph for cone resistance, using the same depth scale (see 5.5).

**6.3 General**—The operator shall record his name, the name and location of the job, date of sounding, sounding number, location coordinates, and soil and water surface elevations (if available). The report shall also include a note as to the type of penetrometer tip used, the type of thrust machine, the method used to provide the reaction force, if a friction reducer was used, the method of tip advancement, the method of recording, the condition of the rods and tip after withdrawal, and any special difficulties or other observations concerning the performance of the equipment.

**6.4 Deviations from Standard**—The report shall state that the test procedures were in accordance with this Method D 3441. Describe completely any deviations from this method.

**7. Precision and Accuracy**

7.1 Because of the many variables involved and the lack of a superior standard, engineers have no direct data to determine the accuracy of this method. Judging from its observed reproducibility in approximately uniform soil deposits, plus the  $q_c$  and  $f_s$  measurement effects of special equipment and op-

erator care, persons familiar with this method estimate its precision as follows:

7.1.1 *Mechanical Tips*—Standard deviation of 10 % in  $q_c$  and 20 % in  $f_s$ .

7.1.2 *Electric Tips*—Standard deviation of 5 % in  $q_c$  and 10 % in  $f_s$ .

NOTE 15—These data may not match similar data from mechanical tips (see 1.3).

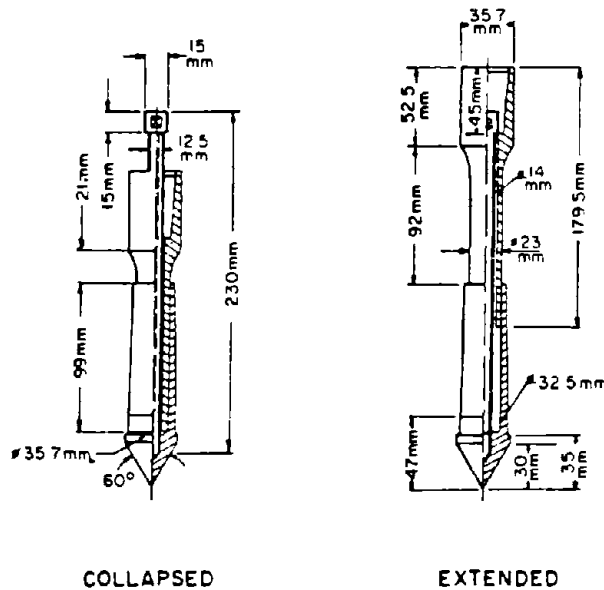


FIG. 1 Example of a Mechanical Cone Penetrometer Tip (Dutch Mantle Cone).

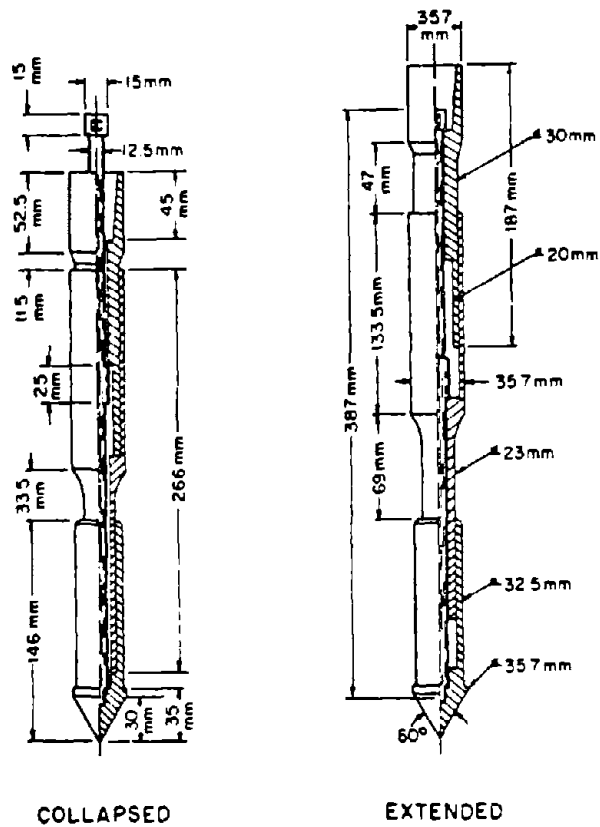
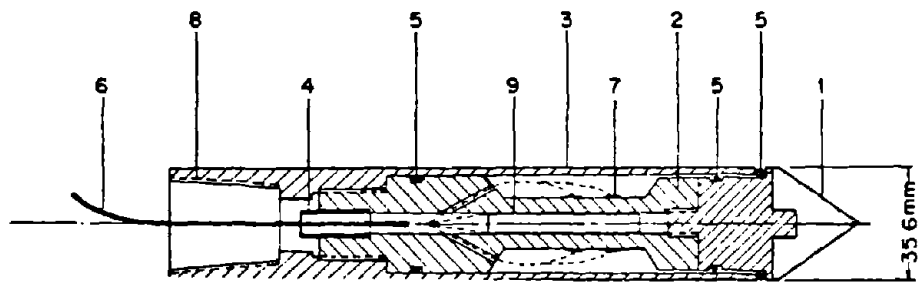
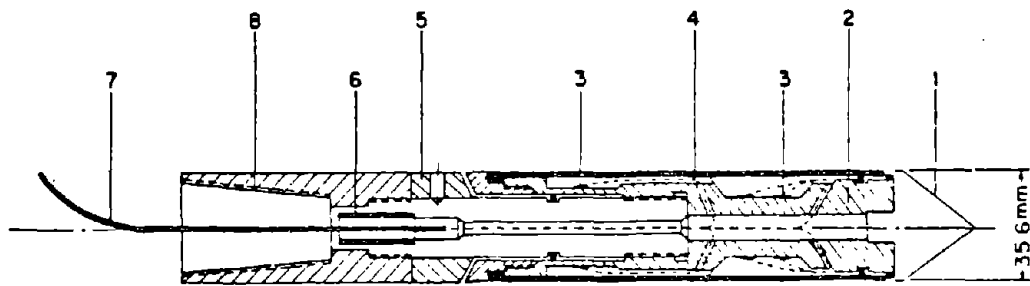


FIG. 2 Example of a Mechanical Friction-Cone Penetrometer Tip (Begemann Friction-Cone).



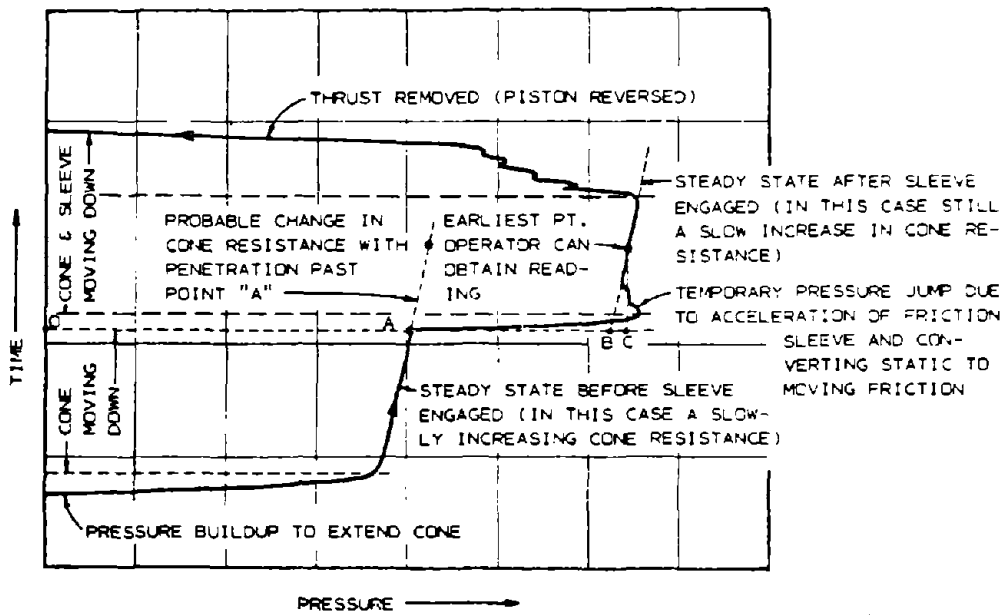
- 1 Conical point (10 cm<sup>2</sup>)
- 2 Load cell
- 3 Protective mantle
- 4 Waterproof bushing
- 5 O-rings
- 6 Cable
- 7 Strain gages
- 8 Connection with rods
- 9 Inclinometer

FIG. 3. Electric-Cone Penetrometer Tip.



- 1 Conical point (10 cm<sup>3</sup>)
- 2 Load cell
- 3 Strain gages
- 4 Friction sleeve (150 cm<sup>3</sup>)
- 5 Adjustment ring
- 6 Waterproof bushing
- 7 Cable
- 8 Connection with rods

FIG. 4 Electric Friction-Cone Penetrometer Tip.



NOTE—"a-a" represents the correct cone resistance reading just before the pressure jump associated with engaging the friction sleeve during the continuing downward extension of the tip. "a-b" is the correct friction resistance if the friction sleeve could be engaged instantaneously and the cone plus friction resistance read instantaneously. However, the operator cannot read a pressure gage dial until it steadies, such as at point "c." By this forced wait, the operator has introduced a friction resistance error of "b-c." The operator must read the gage as soon as possible after the jump to minimize this error. Erratic or abrupt changes in cone resistance may make this error unacceptable.

FIG. 5 Annotated Chart Record of the Pressure Changes in the Hydraulic Load Cell Measuring Thrust on Top of the Inner Rods During an Example Extension of the Mechanical Friction-Cone Penetrometer Tip.

The American Society for Testing and Materials takes no position respecting the validity of any patent rights asserted in connection with any item mentioned in this standard. Users of this standard are expressly advised that determination of the validity of any such patent rights, and the risk of infringement of such rights, is entirely their own responsibility.

APPENDIX III

COPY OF CPT CHAPTER 3 FROM SCHMERTMANN (1975),  
INCLUDING LIST OF REFERENCES

(Reprinted with permission)

## 3. THE CONE PENETRATION TEST (CPT)

3.1 Different Types

The basic idea of the CPT remains a simple one -- to advance a rod into the soil, usually vertically, measure the forces required to produce such advance, and interpret these forces in terms of pile capacity, soil density, shear strength, etc. In response to the variety of problems and soil conditions, engineers have developed a great variety of CPT equipment and methods. For some description of this variety see Sanglerat (1972) and the ESOPT (1974).

Perhaps the simplest way to classify the different methods uses the methods-for and/or rate-of-tip advance. Table 8 offers a broad classification of CPT types. For a more detailed discussion see Holden (1974a). By far the most common are the quasi-static and dynamic methods of penetration. However, one of the key questions which produced more or less consensus at the Stockholm ESOPT was the broad superiority

TABLE 8 - GENERAL TYPES OF CONE PENETRATION TESTS

Type	Tip Advance		Where Used	Notes
	Method	Rate		
1. Static	During increments of constant load	0	Research	Too slow for general field use
2. Quasi-static	Hydraulic or mechanical jacking	1-2 cm/sec	worldwide	Usually 10 cm <sup>2</sup> 60 cone point
3. Dynamic	Impact of drive weight	variable	worldwide	Great variety sizes, weights, etc.
4. Quasi-static & dynamic	Combines 2. and 3., using dynamic when Q-CPT cannot penetrate further		France Switzerland	Uses special penetrometer tips
5. Screw	Rotation of a weighted, helical cone	variable	Sweden Norway	
6. Inertial	Dropped or propelled into soil/rock surface	variable during measured deceleration	Offshore, Military	Useful for near-surface soils in inaccessible area

of the quasi-static over dynamic methods to produce data of quantitative usefulness for design, including insitu shear strength.

No doubt the dynamic CPT has a use, as demonstrated by Schmid's (1975) contribution to this Conference. Many organizations have some type of in-house dynamic CPT they use with in-house correlations. But, the more difficult to understand dynamic nature of the test, as well as some of the relatively poorly controlled variables such as the extent of rod-soil shear contribution to blow count resistance, makes the dynamic CPT a poor choice compared to the quasi-static CPT if the investigator wishes to evaluate insitu shear strength. Hence, this section now focuses exclusively on the quasi-static CPT.

We might consider herein many types of Q-CPT equipment and methods. Sanglerat (1972) describes many. Some are very sophisticated and intended for special applications (see Brons & Broussard, 1965). Others might have a broader usage, see for example Kallstenius (1961), but for one reason or another have not "caught on". In contrast, the Dutch Q-CPT sounding systems and methods have caught on throughout the world, including the USA. This paper refers specifically to the Dutch methods listed in Table 9, although the general aspects of the discussions herein might apply to all Q-CPT methods.

TABLE 9 - TYPES OF Q-CPT EQUIPMENT/METHODS DISCUSSED  
(all developed in The Netherlands, 10 cm<sup>2</sup>, 60° cones)

System	Tip	Measures	By	Soil-friction protection
Mechanical	Delft mantle	$q_c$ ea. 20 cm	Hydraulic load cell pushing alternately on pushrods and inner rods	Reduced diameter above cone (the mantle)
	Begemann friction-cone	$q_c$ and $f_s$ ea. 20 cm		Inner rods between tip and load cell
Electrical	Fugro cylindrical shape	$q_c$ , or $q_c$ and $f_s$ continuously in 1m increments	Strain gage transducers in tip, cable thru pushrods to surface recorder	Measurements at tip below soil friction, no tip sliding parts.
	Delft shape	$q_c$ and $f_s$		Same as above

The invention of the local friction sleeve to measure  $f_s$  (Begenann, 1965) has greatly expanded the value of information obtained from the q-CPT and the use of friction-cone tips has now become routine. But, they are also more expensive and more easily damaged. As discussed in 3.31, the electric tips have many advantages. However, the mechanical tips will probably always have a place because of their relative ruggedness and simplicity.

### 3.2 Current Methods for Estimating Shear Strength

As with the SPT, the CPT does not measure shear strength directly but measures cone bearing capacity,  $q_c$ , and soil-steel friction along the local friction sleeve,  $f_s$ , both of which depend on shear strength. Alternately, the advance of a cone penetrometer opens a cylindrical cavity in the soil and thus suggests the probable usefulness of cavity expansion theory to evaluate soil strength properties from the CPT. Although, when compared to the SPT, there has been much more attempt to use theory and controlled laboratory research, including the use of large triaxial calibration chambers, the current state-of-the-art still depends largely on empirical correlations.

3.21  $\phi'$  in Sands: deBeer developed a conservative method for determining  $\phi'$  that has received extensive use in some countries, notably Belgium. See Sanglerat (1972, p. 121) and ESOPT (1974, p. 24) for details. The method originates from bearing capacity theory. It often produces results too conservative for economical design. A less conservative procedure, with a semi-empirical basis, appears to be in use in the USSR (ESOPT, 1974, p. 151). Figure 8 presents this correlation.

The DEGEBO research in W. Berlin with large-scale model footings on sands, as reported by Muhs and Weiss (1971, p. 27) noted that:

$$q_c \left( \frac{\text{kgf}}{\text{cm}^2} \right) = 0.80 N_Y \quad \dots \text{ (eq. 1)}$$

with  $N_Y$  the ordinary bearing capacity factor from the Terzaghi general shear case. Because this factor depends only on  $\phi'$ , the engineer can estimate  $\phi'$  from this estimate of  $N_Y$ . The results would apply most directly to bearing capacity computations for shallow foundations, as in

IN SITU MEASUREMENT

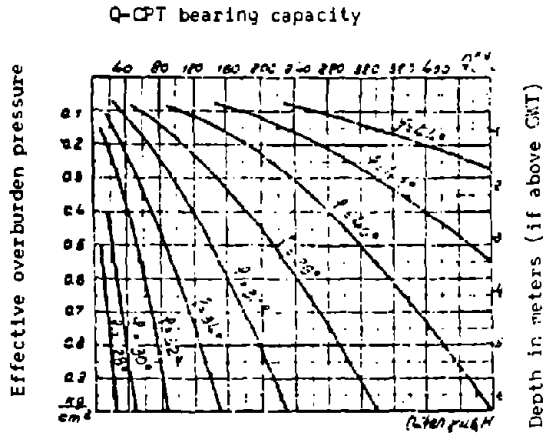
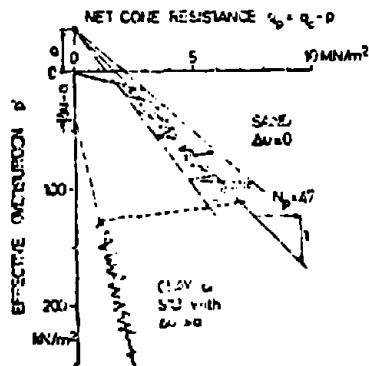


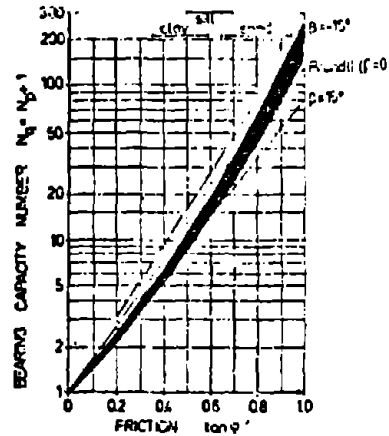
FIGURE 6 - METHOD FOR ESTIMATING  $\phi'$  from  $q_c$  REPORTED IN USE IN USSR (ESOPI, 1974, p. 151)



(a) Example modified  $q_c$ -depth profile

$a = 35 \text{ kN/m}^2$   
 $\tan \phi' = 0.78 \pm 0.04$   
 since  $N_q = 48 \pm 10$

Results from this example



(b) Chart to determine  $\tan \phi'$  from bearing capacity number

FIGURE 9 - JANBU & SENNESSET METHOD FOR DETERMINING  $\phi'$  FROM A Q-CPT SOUNDING LOG

the DEGEBO study. Actually,  $q_c$  depends on many other variables besides most notably compressibility and stress level.

Durgunoglu and Mitchell (1975 ) have presented papers to this Conference explaining in detail the theory and procedures for their method for estimating  $\phi'$  in sands using CPT data. They used a rigid-plastic, wedge-displacement bearing capacity theory, with empirical modifications to take account of the circular shape of the cone. However, almost all observations of soil displacements around an advancing cone in sands show the failure as primarily a compressibility-displacement, concentrated in the zone immediately below the cone point. Only tests in dense sand near the surface sometimes show wedge shaped patterns. It seems likely this theory will prove most useful for purposes such as trafficability and roller compaction control, when evaluating  $\phi'$  over the first meter or two of depth -- a depth interval not usually investigated by other theories.

Janbu & Senneset(1974) have a method for determining  $\phi'$  in sands which also has its basis in bearing capacity theory modified by empirical observation. Their theory applies to situations where the  $q_c$  profile increases approximately linearly with depth in sand deposits assumed to have an approximately constant  $\phi'$  over the linear depth interval. Figure 9 (a) illustrates such a profile, with depth converted to effective overburden pressure,  $p'$ , and  $q_p = q_c - p$ , with  $p$  = total overburden pressure. The investigator then estimates an average linear  $q_c - p'$  profile through this deposit and obtains the slope,  $N_p$ , and intercept  $a$  (usually negative) of this profile. One then enters  $N_q = N_p + 1$  into the shaded tone in Figure 9 (b) and determines a probable value of  $\tan \phi'$  applicable to the insitu overburden pressure range. The figure includes the determination of  $\tan \phi'$  for the sand in 9 (a). This J & S method appears to produce reasonable results for the conditions they studied. They used Fugro-type tips. It has the advantage of taking account of the overburden pressure effects. Their method can also include pore pressure effects by using a supplementary procedure.

Finally, as with the SPT, one can use an indirect method for estimating  $\phi'$  through the relative density parameter. Figure 10 presents a

relative density versus cone bearing correlation in current, but temporary use by the writer. It applies to normally consolidated, medium to fine sands. Its basis lies in part on a series of about 70  $q_c$  determinations in two dry sands at different relative densities in the University of Florida's 4 foot diameter triaxial calibration chamber. See Laier *et al.* (1975) for a description of the chamber and Holden (1971) for some of the testing details. These curves are also based in part on the results from the WES (Shockley and Stroh, 1961) relative density studies of Mississippi River sands below the water table. The data points shown indicate the distribution of the data extracted from the WES reports on these tests. The differences between  $D_r$  predicted from the Figure 10 curves and the  $D_r$  values measured by special undisturbed sampling had a standard deviation of about 7%. After making such an estimate of relative density the engineer enters Figure 3 to estimate  $\phi'$ .

The user of Figure 10 must correct overconsolidated sands to their equivalent normally consolidated  $q_c$  before entering Figure 10. He may use Equations (2) and (3) for this purpose if he can make an independent estimate of the overconsolidation ratio (OCR) or the insitu  $K_o'$  coefficient of the sand.

$$K_o' / K_o_{NC} \approx (OCR)^{0.42} \quad \dots \text{ (eq. 2)}$$

$$q_c / q_{cNC} \approx [1 + 3/4 (K_o' / K_o_{NC} - 1)] \quad \dots \text{ (eq. 3)}$$

Equation (2) comes from the chamber-test experience with sands and is surprisingly similar to what has been observed in the laboratory from tests on clay. Equation (3) expresses the average results from chamber tests as presented by Schmertmann (1974, Fig. 2).

3.22  $s_u$  in Clays: At present engineers use an equation in the form of Equation (4) almost exclusively to evaluate the undrained shear strength  $s_u$ , with  $N_c$  the bearing capacity factor for clay appropriate for a deep, circular foundation. Unfortunately, we can no longer

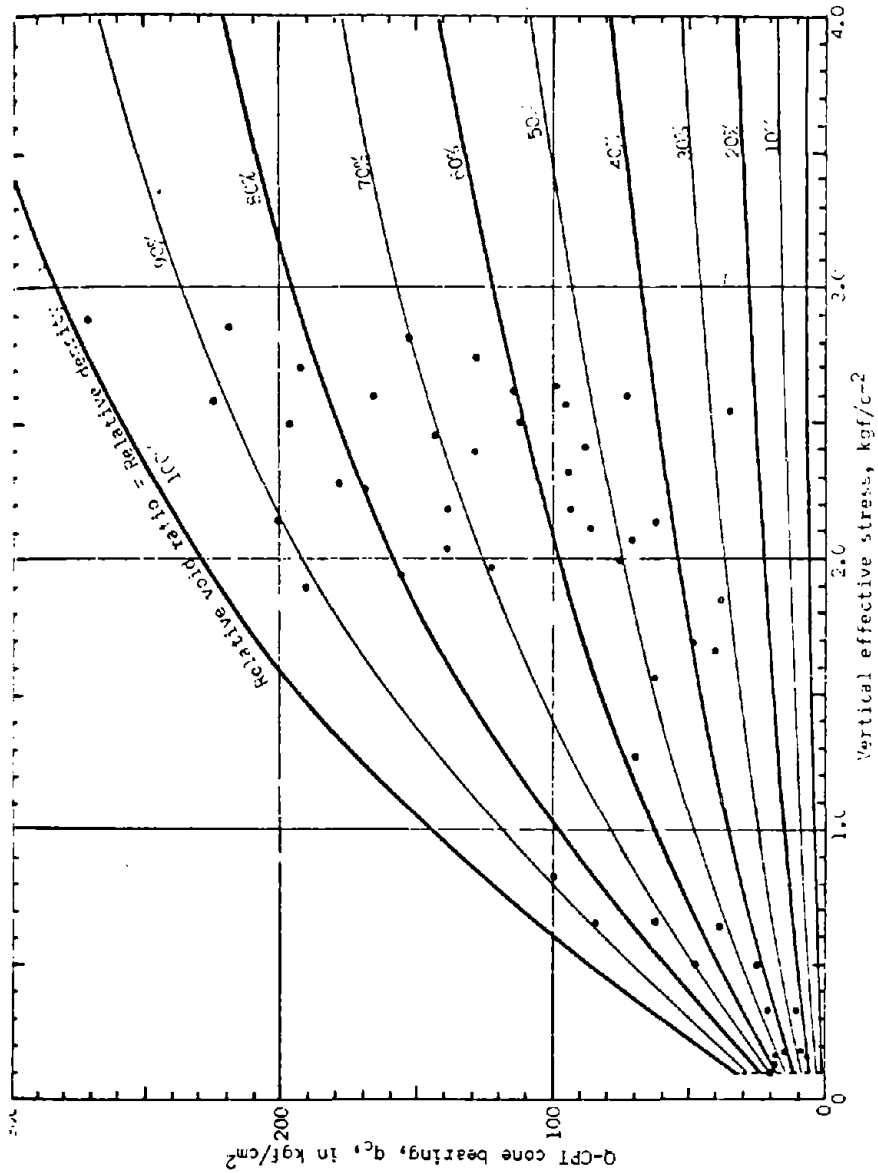


FIGURE 10 - Q-CPT BEARING CAPACITY TO ESTIMATE RELATIVE DENSITY IN NORMALLY CONSOLIDATED, SILTY FINE TO UNIFORM MEDIUM SANDS

imagine  $N_c$  as a simple constant. Today we recognize that  $N_c$  varies with at least the factors indicated in Table 10. One can easily see

$$s_u = \frac{q_c - \gamma z}{N_c} \quad \dots \text{ (eq. 4)}$$

where  $\gamma z$  = total overburden pressure at depths of  $q_c$

TABLE 10 - SOME OF THE VARIABLES THAT INFLUENCE  $N_c$

Variable	Approx. $N_c$ factor potential	Direction	Notes
1. Changing the test method for obtaining reference $s_u$	2 to 3	Better sampling, thinner vanes, use of $s_{uPMT}$ all decrease $N_c$	see Eqn 4.
2. Clay stiffness ratio = $G/s_u$	3	Increases with increasing stiffness	Vesić (1972)
3. Ratio increasing/decreasing modulus ( $E^+/E^-$ ) at peak $s_u$	3	Decreases with decreasing ratio	Ladanyi (1967)
4. effective friction, $\tan \phi'$	2 to 3	Increases with increasing $\phi'$	Janbu (1974)
5. $K_o'$ , or OCR	3	Increases with increasing $K_o'$ or OCR	Janbu (1974)
6. Shape of penetrometer tip	2	Clay adhesion on mantle of mechanical tips increases $N_c$	example in Amar et.al. (1975, Fig. 2)
	1.5	Reduced diameter above cone can decrease $N_c$ in very sensitive clays	Schmertmann (1972b)
7. Rate of penetration	1.2	Increasing rate increases $N_c$	viscous, no pore pressure effects
8. Method of penetration	1.2	Continuous (electrical tips) penetration decreases $N_c$ compared to incremental (mechanical tips) because of higher pore pressures.	

why the  $N_c$  values reported from various empirical correlation studies vary from about 5 to 70 (for example in Amar *et.al.* 1975). Thus, to use a single  $N_c$  value for all soils and all penetrometer tips represents a gross oversimplification which can lead to serious error.

Despite this variation in  $N_c$ , the use of equation (4) represents such a convenience that engineers use "average" values for  $N_c$  which they believe applicable to most "ordinary" clays. If the reference  $s_u$  comes from compression tests on samples obtained from undisturbed sampling using high quality borehole samples, of young, non-fissured clays with  $OCR < 2$  and not highly sensitive, and with  $PI$  at least 10%, many engineers use  $N_c = 10$  with electrical penetrometer tips with cylindrical shafts and  $N_c = 16$  for the Begemann mechanical tip, both at rates of penetration of 1 to 2 centimeters per second. The best procedure is to make your own correlation for  $N_c$  to match your clays, CPT tips, and ref.  $s_u$ . An engineer may also find it useful when using friction-cone tips to compute the adhesion on the local friction sleeve,  $f_s$ , and use this as a lower limit for  $s_u$ .

3.23  $s_u/p'$  Ratio: For some purposes this dimensionless form for undrained strength will prove especially useful, as for example when estimating the  $OCR$  insitu and  $K_o'$  or when using SHANSEP methods (Ladd and Foott, 1974) for compressibility. Until the use of the field vane shear test, the expected linearity of  $s_u$  with overburden depth, and therefore  $p'$ , in NC clays had not been demonstrated clearly insitu. Now CPT  $q_c$  depth profiles in clay as well as sand (see Janbu's method in 3.21) often also clearly show this linearity. Consider the example presented in Figure 11. For another see deRuiter and Fox (1975).

Figure 11 presents data obtained from a young, slightly organic, marine silty clay known to be normally consolidated under the fill placed for LaGuardia Airport in New York City. Using  $N_c = 16$  for the Begemann tip produces  $s_u/p' \approx 0.25$ . Compression tests on 3 inch diameter, fixed piston, undisturbed samples also produced  $s_u/p' \approx 0.3$  for this clay. For this study we used an especially sensitive hydraulic load cell to measure the force applied to the inner rods of the Begemann mechanical friction-cone tip. The computations for  $q_c$  also included the additional pressure due to the accumulated weight of inner rods,

IN SITU MEASUREMENT

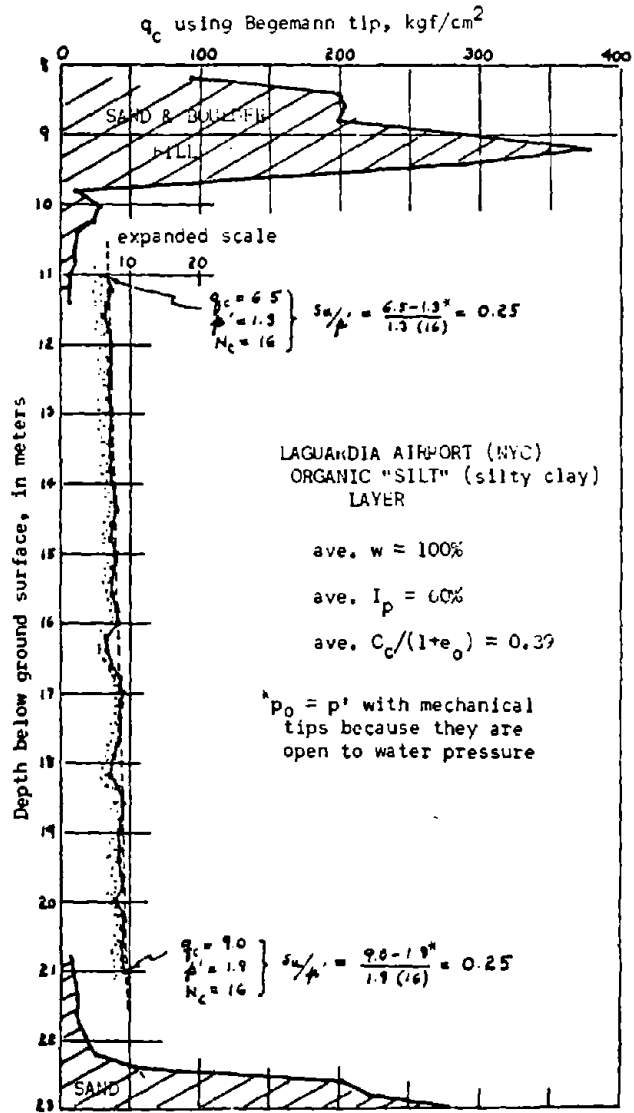


FIGURE 11 - EXAMPLE OF LINEAR INCREASE IN  $q_c$  WITH DEPTH IN NC CLAY, AND OF ESTIMATING THE  $s_u/p'$  RATIO USING EQN. 4

with inner-outer rod friction assumed zero.

Sometimes the weight of the inner rods in the mechanical system prevents a  $q_c$  measurement because the pressure due to this weight alone exceeds the bearing capacity of a soil. In such a very weak soil the engineer can sometimes succeed in obtaining a  $q_c$  measurement by using aluminum inner rods. For extremely weak clays, as for example sometimes found offshore, he must employ electrical, or possibly hydraulic, tips which measure bearing resistance at the tip itself (Hirst, *et. al.* 1972).

3.24 Pile Capacity: One of the earliest and most obvious uses for the CPT considers this test as a model pile test from which to extrapolate the end bearing capacity of real piles. The Dutch have used their well known form of the CPT for many years to predict, usually within  $\pm 50\%$ , the ultimate capacity of displacement piles driven through soft clays to end bearing in medium and fine sands. Note that gravelly soils increase  $q_c$  disproportionately to pile capacity. The reader can find the details of this prediction method for end bearing in the ESOPT paper by Heijnen (1974, p. 81). L. Nottingham (1975) recently completed, but has not yet published, a CPT and model pile study to evaluate, and if possible improve, the CPT prediction methods for pile capacity. His work, together with that of Freed (1973), included a large number of field tests of three and four inch diameter straight-sided and step tapered steel, and four inch square concrete piles, all from 2 to 10 foot length, into both sands and sandy clays. Nottingham obtained the end bearing prediction comparisons summarized in Table 11. He concluded that he could not improve upon the Dutch method and he recommended its continued use. The writer agrees.

The recent addition of a local friction sleeve to the CPT tips now permits the more accurate determination of the side-shear strength contribution, both positive and negative, to the total pile capacity. Nottingham concentrated his efforts on developing a procedure, as simple as possible consistent with accuracy, to use  $f_s$  from both electrical (Fugro) and mechanical (Begemann) friction-cone tips. He found that he could use  $f_s$ , with appropriate modification factors, and predict the

**TABLE 11 - SUMMARY OF NOTTINGHAM'S (1975) MODEL  
PILE END BEARING PREDICTIONS USING  
THE DUTCH (HEIJNEN, 1974) METHOD**

Soil	Pile	Friction-cone tip	No. cases	$(Q_{pred} - Q_{meas.}) / Q_{meas.}$	
				ave	ave
Fine sand above GW	pipe	Fugro	35	+11%	25%
		Begemann	35	+16%	33%
	concrete	Fugro	20	+14%	23%
		Begemann	20	+20%	36%
Sandy clay below GW	both pipe and concrete	Fugro	14	+ 9%	17%
		Begemann*	14	+71%	71%*

\*Not recommended in cohesive soils without a tip correction factor. Factor = 0.6

friction capacities of his model piles, and also of full-scale displacement piles, with about the same accuracy as noted in Table 11 for end bearing. For example, before any pile load tests the writer, using Nottingham's method and assuming the H-pile equivalent to a square concrete pile, predicted the total capacity of 10 HP42 piles, driven to 96.5 foot depth at the site with the uniform soil conditions shown in Figure 7, as 86 tons. Nottingham independently predicted 88 tons. The two piles failed at 80 and 85 tons. These piles were deliberately placed with their tips in a layer with low bearing capacity, and tested for friction capacity 7 days after driving, prior to final driving to rock. Approximately 85% of total capacity of these 96.5 ft. piles consisted of side friction.

Nottingham (1975) also applied the Dutch end bearing and his side friction prediction methods to 17 full-scale piles load tested to failure in Florida and Georgia. He then compared prediction with reality. The comparisons included 10 to 18 inch square concrete, 11 inch pipe, step-taper and timber piles. His prediction error for total ultimate capacity ranged from about -40 to +20%, with an algebraic average error of -11%. He recommended maximum safety factors for design of 2.25 when using Fugro-type friction-cone tips and 3.0 if using the Begemann tip. All Q-CPT data for the full-scale piles came from using the Begemann tip.

Hopefully, Nottingham will soon publish the details of his research. Because of its immediate usefulness he has agreed to let the writer present herein the following summary of his method for estimating drained pile-soil friction capacity. Basically, the method takes the local friction measurements,  $f_s$ , and corrects them for the type penetrometer tip used, the type of soil penetrated, the pile material and taper, and the relative depth of the pile penetration. Equation (5) presents the

$$Q_s = K_{s,c} \left[ \sum_{l=0}^{8B} \left( \frac{l}{8B} \right) f_s A_s' + \sum_{8B}^L f_s A_s' \right] \dots (\text{eq. 5})$$

- where:  $Q_s$  = total ultimate side friction resistance  
 $K_{s,c}$  =  $f_s$  correction factors,  $K_c$  in clay layers,  
 $K_s$  in sand layers (see Fig. 12)  
 $l$  = depth to  $f_s$  value considered  
 $B$  = pile width or diameter  
 $f_s$  = unit local friction sleeve resistance  
 $A_s'$  = pile-soil contact area per  $f_s$  depth interval  
 $L$  = total embedded length of pile

prediction formula for ultimate pile friction with the various terms explained below. Figure 12 presents graphs for the  $f_s$  correction factors in clay and in sand. The first summation term represents a depth-of-embedment correction applied only over the  $8B$  penetration from the ground surface.

With a continuously tapered or step-tapered pile, divide the pile into appropriate increments of constant-diameter length having the same total perimeter area and use the same procedure as for straight-sided piles. However, determine  $K_{s,c}$  applicable to each constant-diameter length by using the  $L/B$  at the bottom of each such length. At each real (for step-tapered piles), or imagined (for continuously tapered) step assume an additional "side friction" equal to the average  $q_c$  at the depth of the step times the horizontal area of the step times a factor "S" given in Table 12.

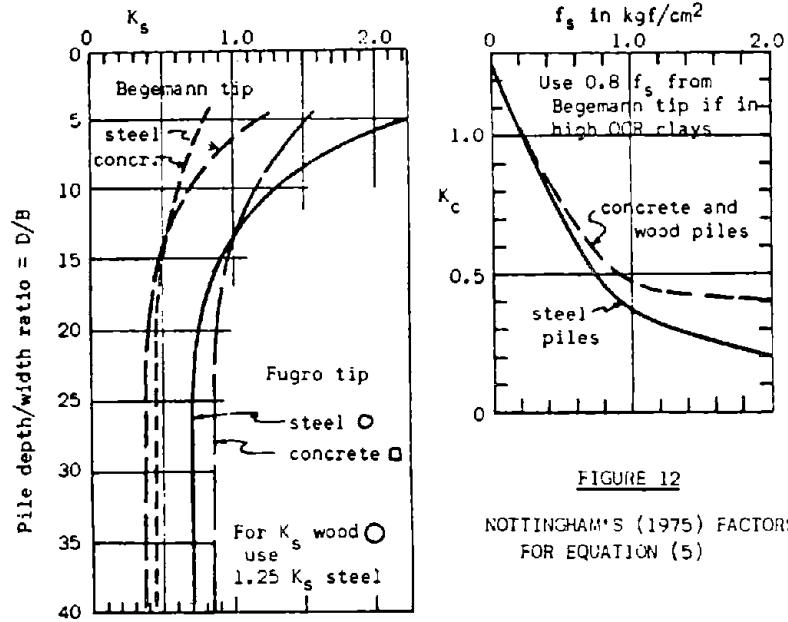


FIGURE 12  
NOTTINGHAM'S (1975) FACTORS  
FOR EQUATION (5)

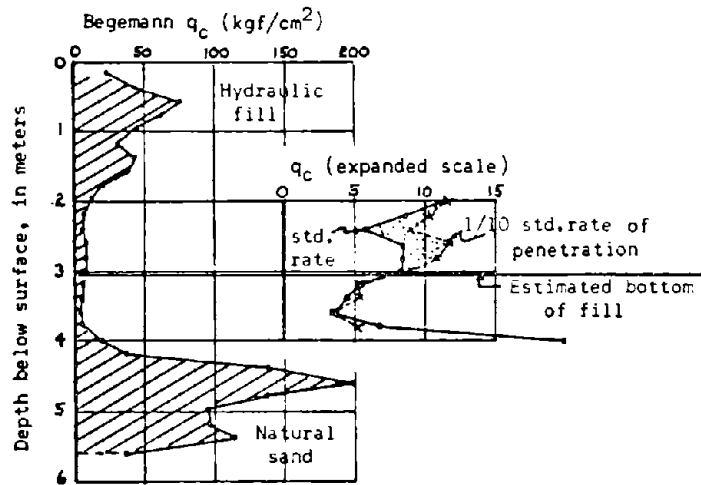


FIGURE 13 - EXAMPLE OF USING PORE PRESSURE EFFECTS TO  
DETERMINE SOIL LAYER BOUNDARY

TABLE 12 - NOTTINGHAM'S CORRECTION  
FACTOR "S" FOR ADDITIONAL  
FRICTION ALONG TAPERED  
AND STEP-TAPERED PILES

Type friction- cone penetrometer	Soil	S
Fugro	sand	1.6
	clay	1.0
Begenann	sand	1.6
	clay	0.6

The capacity prediction accuracy obtainable when using these CPT end bearing and friction methods represents an important improvement in the state-of-the-art, at least in the USA, for this type insitu strength problem. For example, consider a recent "contest" between different prediction methods made before the pile load tests, including SPT, static computation from undisturbed sampling and lab testing strengths, wave equation predictions from driving records, wave equation predictions from special pile-energy input measurements, as well as the CPT. The investigation involved about 20 piles of different types carried to failure in the vicinity of Jacksonville under the supervision of Law Engineering Testing Company. The CPT predictions proved most accurate (7 of 11 within  $\pm 25\%$ ).

The CPT method also has the advantage of permitting predictions and design decisions before any actual driving. Of course, it also has several disadvantages. One of these is that CPT penetration must extend four pile diameters past the pile tip, which is often not possible for high capacity, end bearing piles when using present penetrometer equipment.

Although Nottingham, as well as others, recognized the theoretical advantage of analyzing the capacity of piles in clay using drained (effective stress) methods, these have not yet developed to the point of practical usefulness. The recently proposed  $\lambda$ -method (Vijayvergiya and Focht, 1972) and the  $\beta$ -method (Burland, 1973) involve a partial introduction of effective stress concepts, but they still require estimates of  $s_u$ . Vesic (1975) suggests a method that does not require  $s_u$ .

### 3.3 Other Recent Technical Developments

3.31 Increased Use of Electrical Tips: Because of the many advantages offered by the use of electric tips, they are gradually taking over CPT work as organizations obtain the instrumentation and maintenance facilities required to operate with such tips. These advantages include continuous (usually in one meter rod length increments) logging of tip resistances, the more accurate separation of the  $q_c$  and  $f_s$  components of resistance, greater overall sounding speed because of avoiding the stopping and starting necessary for each measurement as required with the telescoping mechanical penetrometers, the elimination of soil-pushrod, inner-outer rod, and hydraulic load cell friction effects by taking the readings directly at the tip, the ability to test very weak soils by appropriate adjustment of transducer sensitivity, and the ability to relatively easily incorporate instruments such as inclinometers and pore pressure devices. But, one must consider the added costs of the tips and the support facilities needed to use and maintain them. Mechanical tips will continue to have a usefulness because of cost and simplicity.

In the offshore testing environment the use of electric tips has become almost essential. CPT work from fixed offshore platforms becomes difficult after about 30 meters water depth and almost impossible after about 60 meters depth because of the support casing requirements. Operating offshore usually requires equipment that operates remotely on the seabed or on a wireline at the bottom of a cased boring -- both controlled by electric cables from the surface ship. The thrust capability of CPT platforms lowered to the seabed has now reached 20 metric tons! For references on offshore CPT work see deRuiter (1971) and Hirst *et. al.* (1972).

The cylindrical electrical tips also have the advantage of providing a better model of the shape of most displacement piles. Nottingham used both the Fugro electric and Begemann mechanical friction-cone tips for the research discussed in 3.24. As shown in Table 11 for end bearing, and in his safety factor recommendation, he found that on the average he could consistently predict either pile end bearing or pile friction more accurately when using the electric tip. The

difference in accuracy did not result from chart recording vs. Bourdon gage reading because he also had a transducer and chart recording system to replace the manual gage reading ordinarily used with the mechanical tip.

3.32 Shape of Electric Tip: An important technical argument developed in Europe concerning the best tip shape to use for the electrical tips. The design of the mechanical tips has the constraints imposed by the need for telescoping operation and a reduced diameter mantle above the cone, both to keep the sliding parts as free from soil contamination as possible. These, and other constraints do not exist for the electrical tips and designers can choose almost any shape they wish. Fugro (deRuiter, 1971) chose the simplest shape, a conventional  $60^\circ$  cone point with a constant diameter cylindrical shaft, including the local friction sleeve, above that point. The Delft Soil Mechanics Laboratory chose a shape which they believed best reproduced the results achieved from their widely used mechanical tips (Heijnen, 1973). The Delft tip design has a section of reduced diameter above the cone point so as to produce  $q_c$  data supposedly better matching that obtained with the Delft mechanical tips. Part of the argument also concerns the best location for the local friction sleeve. The Fugro tip has the sleeve immediately above the cone and the Delft tip a considerable distance above the cone and above their reduced diameter section. This review will not discuss all the pro and con arguments for these two tips. Holden (1974b) discusses this in some detail and recommends the Fugro shape. At this point the writer has no doubt that the consensus of world opinion, expressed in the form of the actual construction of electrical tips, favors the Fugro cylindrical shape. The current proposed ASTM standard for quasi-static cone penetration tests also requires electrical tips have the cylindrical shape.

3.33 Calibration Work in Large Triaxial Chambers: Largely as a result of the efforts of J. C. Holden, several universities and other organizations have now constructed large CPT triaxial calibration chambers. These have the purpose of assisting with the evaluation of various CPT tip designs and calibrating CPT results in sands placed at controlled, uniform densities and subject to known boundary stresses

and stress histories. Holden built the first such chamber at the Country Roads Board research facility in Melbourne, Australia, and the second, somewhat larger, at the University of Florida. See Laier *et al.* (1975) for a description of the University of Florida chamber. There is now at least one still larger but similar chamber in Australia (Chapman, 1974) and one under construction at the Norwegian Geotechnical Institute. WES in Vicksburg, Mississippi, and Duke University at Durham, North Carolina, have built chambers of different design. Still other organizations have plans for constructing such chambers. The use of these chambers has already helped to better understand and calibrate the performance of the CPT, the PMT, and even the SPT.

A very important reason to justify the use of these large chambers is that they permit separating the similar effects of increased effective stress level and increased density, whereas field calibration rarely permits such separation.

3.34 Pore Pressure Effects: As discussed in 2.32, pore pressures change the ambient effective stress conditions surrounding an advancing penetrometer and therefore modify its resistance to penetration. Such pore pressures effect the CPT as well as the SPT. In fact, it has been the CPT research using tips also carrying quick-response, electric piezometers that has demonstrated the significant magnitude of these pore pressures and their now obvious importance to any interpretation of  $q_c$  and  $f_g$ . For examples of significant pore pressures, both positive and negative in the area around the point of the cone, see the contribution to this Conference by Wissa *et al.* (1975). For other discussion of the importance of pore pressures see Schmertmann (1974a, b) and Seneset (1974, p. 91).

At present the best method for evaluating pore pressure effects on  $q_c$  and  $f_g$  consists of observing the effect of changing the rate of penetration. The engineer can decrease rate until he no longer observes a change in  $q_c$ , at which point he may perhaps assume that any pore pressure effects have become negligible and he has the drained case. Conversely, he can increase rate of penetration and estimate the  $q_c$  for which any further rate increase does not change  $q_c$  and assume this the

undrained case. The writer suspects that the factor-of-2 rate of penetration effects noted by Amar *et.al.* (1975, Fig. 3) in sands and silts result from greater positive or negative pore pressure dissipation at the slower rates. Bembem and Myers (1974) showed the effect of rate on  $q_c$  in a varved clay.

The engineer might also use pore pressure effects as a tool to help distinguish different soil types. For example, consider the CPT log in Figure 13 obtained using mechanical equipment. Somewhere in the low- $q_c$  layer exists transition between an overlying non-plastic, saturated, easily liquefied, loose fill and a highly plastic, organic, fibrous natural clay. The  $q_c$  and FR data did not clearly define this boundary. However, reducing the penetration rate to about 1/10 the ordinary rate noticeably increased  $q_c$  in the fill, probably because a slower penetration rate allowed pore pressure dissipation, while this reduction had no effect in the organic clay. The writer could thus use the difference in pore pressure behavior to determine the boundary between fill and natural soil.

One might also reasonably expect that the magnitude of excess pore pressure generated by a cone penetrometer, and its rate of dissipation after stopping the cone advance, would involve primarily the soil's insitu compressibility and permeability -- two pieces of data and two unknowns. This looks like an area for useful research.

3.35 Testing Soil Compaction: The CPT tip insertion by hydraulic or mechanical methods at a controlled, standard rate of penetration, and the automatic recording (electrical tips) or simple reading of Bourdon gages (mechanical tips with load cell at surface) minimizes the human factors when obtaining CPT data. The resultant high level of CPT reproducibility, and the continuous or almost-continuous  $q_c$ -depth profile, makes the CPT test an ideal tool to evaluate site stratigraphy, search for any remnants of unexcavated weak layers, and to evaluate the depths, uniformity and degree of compaction.

After appropriate calibration, the insitu bearing strength,  $q_c$ , makes a convenient indicator for evaluating compaction effort. Woodward-Clyde & Associates made very extensive use of the CPT to help control the large compacted fill embankments at the Luddington pumped

storage project (Leary and Swan, 1971). Before and after compaction studies via  $q_c$  profiles are particularly effective because of the high reproducibility of the CPT. Webb and Hall (1969) illustrated this use for the CPT on a project involving sand densification by the Vibrofloatation process. Schmertmann (1970) showed its effectiveness in defining the limits of surface roller compaction. Figure 14 presents another example where the writer helped to evaluate the effects of the Terraprobe densification method under a large oil tank. At this site the Terraprobos had been inserted at 6 foot centers, to a depth of 50 feet, but only under the tank. The "before" condition was obtained by CPTs around the tank and outside the Terraprobe influence. These  $q_c$  profiles, obtained using the Begemann tip, illustrate their reproducibility and permit some relatively sophisticated conclusions. For example, each successively deeper sand layer was less improved, probably due to the vibratory screening action of the intermediate cohesive layers. The surface layer greatly increased  $q_c$ . The middle sand layer  $q_c$  increased measurably and consistently but only a relatively small amount. The deepest sand layer did not increase  $q_c$ . Note that the various compaction methods do not always produce the increases in  $q_c$  shown in the above example and references.

3.36 Theories of CPT Behavior: As mentioned in 3.21, the theoretical developments with respect to the CPT continue along two separate directions. One direction, as exemplified by the recent work of Janbu (1974) continues to use bearing capacity theory. The other direction involves the use of cavity expansion theory, as exemplified by the work of Ladanyi (1967, 1972), Vesić (1972) and Al-Awkati (1975). Although Janbu continues to demonstrate the usefulness of the traditional, with modifications, bearing capacity approach the writer believes that ultimately the cavity expansion related theories will dominate. They should provide a better opportunity for including the very important compressibility and pore pressure effects.

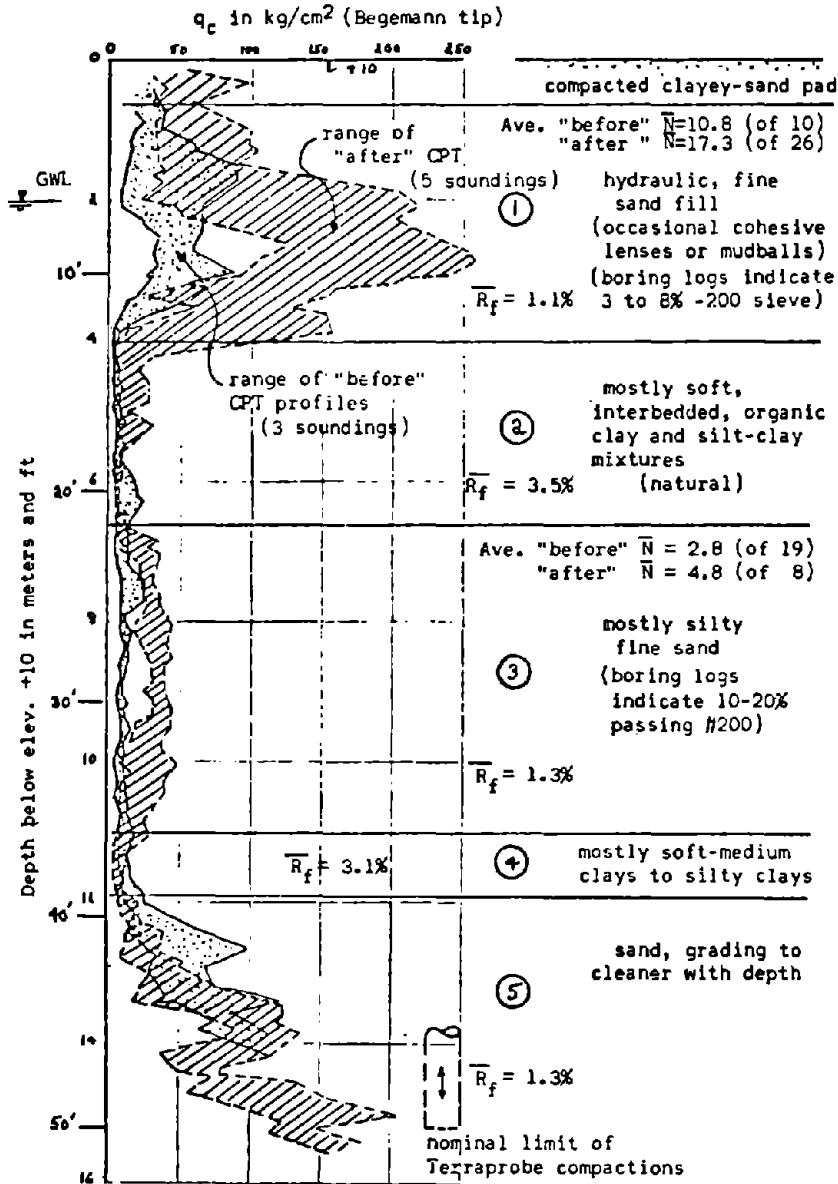


FIGURE 14 - EXAMPLE OF COMPARING Q-CPT SOUNDING DATA BEFORE AND AFTER ATTEMPT AT DEEP COMPACTION (some N data included)

## J. LIST OF REFERENCES

Abbreviations used herein:

- J-SMFD = Journal of the Soil Mechanics and Foundations Division  
 J-GEED = Journal of the Geotechnical Engineering Division  
 ICSMFE = International Conference of Soil Mechanics and Foundation Engineering  
 PanAm = Pan American  
 SC-IMSPE = Specialty Conference on Insitu Measurement of Soil Properties  
 SC-PEESS = Specialty Conference on the Performance of Earth and Earth-Supported Structures  
 SQA = State-of-the-art  
 STP = Special Technical Publication
- Aas, G., 1967, "Vane Tests for Investigation of Anisotropy of Undrained Shear Strength of Clays," Proc. of the Geotechnical Conference, Oslo, Vol. 1, pp. 3-8. See also Proc. 6th ICSMFE, Vol. 1, pp. 141-145.
- Adam, J., 1971, Discussion of deMello (1971), 4th PanAm Conf. on SMFE, Puerto Rico, Vol. III, pp. 82-84.
- Al-Awkati, Z., 1969, "A Study of the Cone Penetration Test in Insensitive Cohesive Soils," Master's thesis to the Department of Civil Engineering, University of Florida, 103 pp.
- Al-Awkati, Z., 1975, "On Problems of Soil bearing Capacity at Depth," Ph.D. dissertation to the Department of Civil Engineering, Duke University, 204 pp.
- Amar, S., F. Baguelin, J. F. Jezequel and A. Le Mehaute, 1975, "In situ Shear Resistance of Clays," ASCE, SC-IMSPE, Vol. 1, pp. 22-45.
- Arman, A., J. K. Poplin and J. Ahmad, 1975, "Study of the Vane Shear," ASCE, SC-IMSPE, Vol. 1, pp. 93-120.
- Baguelin, F., J. F. Jezequel, E. L. Yee and A. Le Mehaute, 1972, "Expansion of Cylindrical Probes in Cohesive Soils," ASCE, J-SMFD, Vol. 98, SM-11, pp. 1129-1142.
- Barthélemy, H. C., 1974, "An Investigation of Relationships Between the SPT and the Cone Penetrometer Resistance in Sands, Project Report, Department of Civil Engineering, Duke University.
- Bazaraa, A., 1967, "Use of the Standard Penetration Test for Estimating Settlements of Shallow Foundations on Sand," Ph.D. Dissertation, University of Illinois, Civil Engineering, 379 pp.
- Begemann, H. K., 1965, "The Friction Jacket Cone as an Aid in Determining the Soil Profile," Proc. 6th ICSMFE, Vol. 1, pp. 17-20.
- Begemann, H. K., 1974, "Penetration Testing in Central and Western Europe", ESOPF, Stockholm, General Report 3, Vol. 2.1, p. 33.

- Bemben, S. M. and D. A. Myers, 1974, "The Influence of the Rate of Penetration on Static Cone Resistance Values in Connecticut River Valley Varved Clay", ESOPT, Stockholm, Vol. 2.2, p. 34.
- Bjerrum, L., and N. Flodin, 1960, "The Development of Soil Mechanics in Sweden 1900-1925," Geotechnique, Vol. 10, No. 1, pp. 1-18.
- Bjerrum, L., and T. C. Kenney, 1967, "Effect of Structure on the Shear Behavior of Normally Consolidated Quick Clays," Proc. of the Geotechnical Conference, Oslo, Vol. II, pp. 19-27.
- Bjerrum, L., 1972, "Embankments on Soft Ground," ASCE, SC-PEESS, Lafayette, Proc., Vol. II, pp. 1-54.
- Bjerrum, L., 1973, "Problems of Soil Mechanics and Construction on Soft Clays," State-of-the-Art Report to Session IV, 8th ICSM&FE, Moscow, Vol. 3, p. 111.
- Brons, B. B., and D. E. Broussard, 1965, "Self-recording Soil Penetrometers," J-SMFD, ASCE, Vol. 91, No. SM1, January, pp. 53-62.
- Burland, J., 1973, "Shaft Friction of Piles in Clay: A Simple Fundamental Approach," Ground Engineering, Vol. 6, No. 3, May, pp. 30-42.
- Cadling, L., and S. Odenstad, 1950, "The Vane Borer," Royal Swedish Geotechnical Institute, Proc. No. 2.
- Casagrande, A., and N. Carrillo, 1944, "Shear Failure of Anisotropic Materials," Journal of the Boston Soc. of Civil Engineers, Vol. 31, No. 4, April (also in Contributions to Soil Mechanics, BSCE, 1941-53).
- Casagrande, L., 1966, "Subsoils and Foundation Design in Richmond," ASCE, J-SMFD, Vol. 92, SM-5, Sept., pp. 109-126.
- Chapman, G. A., 1974, "A Calibration Chamber for Field Test Equipment," ESOPT, Stockholm, Vol. 2.2, pp. 59-66.
- deMello, V., 1971, "The Standard Penetration Test -- A State-of-the-Art Report," 4th PanAm Conf. on SM&FE, Puerto Rico, Vol. 1, pp. 1-86.
- deRuiter, J., 1971, "Electric Penetrometer for Site Investigations," ASCE, J-SMFD, Vol. 97, SM-2, Feb., pp. 457-72.
- deRuiter, J., and D. A. Fox, 1975, "Site Investigations for North Sea Forties Field," paper OTC 2246, Offshore Technology Conference, Houston, Fig. 6.
- DM-7, 1962, Design Manual for Soil Mechanics, Foundations and Earth Structures, U. S. Navy, bureau of Yards & Docks.
- Duncan, J. M., and H. B. Seed, 1966, "Anisotropy and Stress Reorientation in Clay," ASCE, J-SMFD, Vol. 92, SM-5, Sept., pp. 21-50.
- Durgunoglu, H. and J. K. Mitchell, 1975, "Static Penetration Resistance of Soils: I - Analysis, II - Evaluation of Theory and Implications for Practice," ASCE, SC-IMS, Vol. 1, pp. 172-189.
- ESOPT, 1974, European Symposium on Penetration Testing, Stockholm, June, Vol. 1, State-of-the-Art Reports.

- Fletcher, G., 1965, "Standard Penetration Test: Its Uses and Abuses," ASCE, J-SMFD, Vol. 91, SM-4, July, p. 67.
- Freed, D. L., 1973, "Prediction of Pile Side Resistance of Smooth and Rough 4 Inch Square Concrete Model Piles Driven in Sand Using Static Cone Penetrometer Data," Master's thesis to Department of Civil Engineering, University of Florida, December, 207 pp.
- Frydman, S., 1970, Discussion of Ireland, et.al., 1970, Géotechnique, Vol. 20, No. 4, p. 454.
- Gibbs, H. J. and W. H. Holtz, 1957, "Research on Determining the Density of Sands by Spoon Penetration Testing," 4th ICSMFE, London, Vol. 1, p. 35.
- Gibson, R. E. and W. F. Anderson, 1961, "In-situ Measurement of Soil Properties with the Pressuremeter," Civil Engineering and Public Works Review, Vol. 56, pp. 615-18.
- Hartman, J. P., and J. H. Schmertmann, 1975, "FEM Study of Elastic Phase of Pressuremeter Test," ASCE, SC-IMSP, Vol. 1, pp. 190-207.
- Heijnen, W. J., 1973, "The Dutch Cone Test; Study of the Shape of the Electrical Cone," Proc. 8th ICSMFE, Vol. 1.1, pp. 181-184.
- Heijnen, W. J., 1974, "Penetration Testing in Netherlands," ESOPT, Stockholm, SOA Report, Vol. 1, pp. 79-83.
- Hirst, T. J., A. F. Richards, and A. L. Inderbitzen, "A Static Cone Penetrometer for Ocean Sediments," ASTM, STP 501, pp. 69-80.
- Holden, J. C., 1971, "Laboratory Research on Static Cone Penetrometers," Univ. of Florida, Dept. of Civil Engineering, Internal Report CE-SM-71-1. Also, final report, Churchill Fellowship 1970, Country Roads Board of Victoria, Australia (1971).
- Holden, J. C., 1974a, Discussion to ESOPT, "Towards Standardization of Terminology, Symbols and Abbreviations in Penetration Testing," Vol. 2.1, pp. 102-107.
- Holden, J. C., 1974b, Discussion to ESOPT, "The Shape of the Electrical Penetrometer Tip," Vol. 2.1, pp. 100-102.
- Holtz, W. G. and H. J. Gibbs, 1969, Discussion in ASCE J-SMFD, Vol. 95, SM-3, May, pp. 900-905.
- Houston, W. N., 1960, "Correlation of Field Penetration and Vane Shear Tests for Saturated Cohesive Soils," (A progress report), Bureau of Reclamation, Earth Lab Report No. EM-586, Sept. 30, Figure 6.
- Ireland, H. O., O. Moretto and M. Vargas, 1970, "The Dynamic Penetration Test: A Standard That is Not Standardized," Géotechnique, Vol. 20, No. 2, p. 185.
- Janbu, N., (1974), Discussion to ESOPT, "Penetrations in Clay at Undrained Conditions", Vol. 2.1, pp. 129-132.
- Janbu, N., and K. Senneset, 1974, "Effective Stress Interpretation of In-situ Static Penetration Tests," ESOPT, Stockholm, Vol. 2.2, pp. 181-194.

- Kallstenius, T., 1961, "Development of Two Modern Continuous Sounding Methods," Proc. 5th ICSMFE, Vol. 1, pp. 475-480.
- Kenney, T. C. and G. H. Watson, 1961, "Multiple-stage Triaxial Test for Determining  $c'$  and  $\phi'$  of Saturated Soils," Proc. 5th ICSMFE, Paris, Vol. 1, pp. 191-196.
- Kenney, T. C., 1968, "A Review of Recent Research on Strength and Consolidation of Soft Sensitive Clays," Canadian Geotechnical Journal, Volume V, No. 2, May, pp. 97-119.
- Ladanyi, B., 1960, "Etude des Relations entre les contraintes et des Déformations lors du cisaillement des soils Pulverulents," Annales des Travaux Publics de Belgique, No. 3, pp. 1-30.
- Ladanyi, B., 1963, "Evaluation of Pressuremeter Tests in Granular Soils," Proc. 2nd PanAm Conf. S&MFE, Sao Paulo, Vol. 1, pp. 3-20.
- Ladanyi, B., 1967, "Deep Punching of Sensitive Clays," Proc. 3rd PanAm Conf. S&MFE, Caracas, Vol. 1, pp. 533-46.
- Ladanyi, B., 1972, "In situ Determination of Undrained Stress-Strain Behavior of Sensitive Clays with the Pressuremeter," Technical Note, Canadian Geotechnical Journal, Vol. 9, No. 3, pp. 313-19
- Ladd, C. C., 1973, Invited Discussion of Bjerrum (1973), Presented at 8th ICSMFE, Moscow.
- Ladd, C. C., and R. Foot, 1974, "New Design Procedure for Stability of Soft Clays," ASCE, J-GeD, Vol. 100, GT-7, p. 76-786.
- Laier, J. E., 1973, "Effects of Pressuremeter Probe Length/Diameter Ratio and Borehole Disturbance on Pressuremeter Test Results in Dry Sand," Ph.D. dissertation to Department of Civil Engineering, University of Florida, 202 pp.
- Laier, J. E., J. H. Schmertmann and J. H. Schaub, 1975, "Effect of Finite Pressuremeter Length in Dry Sand," ASCE, SC-IMSP, Vol. 1, pp. 241-259.
- LaRochelle, P. and G. Lefebvre, 1971, "Sampling Disturbance in Champlain Clays," ASTM, STP 483, pp. 143-163.
- LaRochelle, P., M. Roy and F. Tavenas, 1973, "Field Measurements of Cohesion in Champlain Clays," Proc. 8th ICSMFE, Moscow, Vol. 1.1, pp. 229-236.
- LaRochelle, P., B. Trak, F. Tavenas and M. Roy, 1974, "Failure of a Test Embankment on a Sensitive Champlain Clay Deposit," Canadian Geotechnical Journal, Vol. 11, No. 1, pp. 142-162.
- Leary, D., and C. Swan, 1971, "Earthwork Quality Control of Ludington Pumped Storage Reservoir," Woodward-Clyde Co. reprint of paper presented at Internat. Conf. on Pumped Storage Development and its Environmental Effects, Milwaukee, 19-24 September.
- Lenasson, H., 1974, "Une nouvelle methode pour la mesure de l'anisotropie des argiles", Rapport Laboratoire Regional de Saint-Brieuc. (discussion in Anar, et.al. (1975))

- Lo, K. Y., 1965, "Stability of Slopes in Anisotropic Soils," ASCE, J-SMFD, Vol. 91, SM-4, July, pp. 85-106.
- McLean, F. G., A. G. Franklin and T. K. Dahlstrand, 1975, "Influence of Mechanical Variables on the SPT," ASCE, SC-IMSP, Vol. 1, pp. 287-318.
- Ménard, L., 1956, "An Apparatus for Measuring the Strength of Soils in Place," Master's thesis to the Department of Civil Engineering, University of Illinois.
- Ménard, L., 1965, "Rules for the Calculation of Bearing Capacity and Foundation Settlement Based on Pressuremeter Tests," Proc. 6th ICSMFE, Montreal, Vol. II, pp. 295-99 (in French).
- Meyerhof, G. G., 1965, "Shallow Foundations," ASCE, J-SMFD, Vol. 91, SM-2, March, pp. 21-31.
- Mohr, H. A., 1966, Discussion to Fletcher (1965), ASCE, J-SMFD, Vol. 92, No. SM-1, January, p. 196.
- Muhs, H. and K. Weiss, 1971, "Untersuchung von Grenztragfähigkeit und Setzungsverhalten flachgegründeter Einzelfundamente im Ungleichförmigen nichtbindigen Boden," Degebo Heft 26.
- Nordlund, R. L., 1963, "Bearing Capacity of Piles in Cohesionless Soils," ASCE, J-SMFD, Vol. 89, SM-3, May, pp. 1-36.
- Nottingham, L. C., 1975, "Use of Quasi-Static Friction Cone Penetrometer Data to Predict Load Capacity of Displacement Piles," Ph.D. dissertation to the Department of Civil Engineering, University of Florida, 552 pp.
- Palmer, A. C., 1972, "Undrained Expansion of a Cylindrical Cavity in Clay: A Simple Interpretation of the Pressuremeter Test," Géotechnique, Vol. 22, No. 3, pp. 451-57. See also Discussions in Vol. 23, No. 2, pp. 284-292.
- Pilot, G., 1972, "Study of Five Embankment Failures on Soft Clay," ASCE, SC-PEESS, Lafayette, June, Vol. 1, part 1, p. 81.
- Richards, A. F., V. J. McDonald, P. E. Olsen and G. H. Keller, 1972, "In-place Measurement of Deep Sea Soil Shear Strength," ASTM STP 501, pp. 55-68.
- Richardson, A. M., E. W. Brand and A. Memon, 1975, "In-situ Determination of Anisotropy of a Soft Clay," ASCE, SC-IMSP, Vol. 1., p. 336.
- Rodenhauser, J., 1974, "The Effect of Mean Normal Stress on the Blow-count of the SPT in Dense Chattahoochee Sand," Project Report to the Department of Civil Engineering, Duke University.
- Roy, M., R. Juneau, P. LaRoche, F. Tavenas, 1975, "In-situ Measurement of the Properties of Sensitive Clays by Pressuremeter Tests," ASCE, SC-IMSP, Vol. 1, pp. 350-372.
- Sanglerat, G., 1972, The Penetrometer and Soil Exploration, Elsevier Publishing Co., Amsterdam.
- Schmertmann, J., 1963a, Discussion in ASCE, J-SMFD, Vol. 90, SM-4, p. 187.

- Schmertmann, J., 1963b, "Reconsolidation Study of Manglerud Quick Clay," Norwegian Geotechnical Institute Internal Report F. 234, July, Appendix I.
- Schmertmann, J., 1966, Discussion in ASCE, J-SMFD, Vol. 92, SM-1, p. 206.
- Schmertmann, J., 1967, "Guidelines for use in the Soil Investigation and Design of Foundations for Bridge Structures in the State of Florida," Florida Department of Transportation, Research Bulletin 121, 87 pp + appendices.
- Schmertmann, J., 1970, Discussion in ASCE, J-SMFD, Vol. 96, SM-1, pp. 363-5.
- Schmertmann, J., 1971, Discussion to deMello (1971), 4th PanAm Conf. on SM&FE, Puerto Rico, Vol. III, pp. 90-98.
- Schmertmann, J., 1972a, Discussion in ASCE, J-SMFD, Vol. 98, SM-4, pp. 430-33.
- Schmertmann, J., 1972b, "Static Cone Penetration Tests," Canadian National Research Council, Div. Building Research, Ottawa, Project G-1, Internal Report 1.
- Schmertmann, J., 1972c, "Pressuremeter Tests in Leda Clay," Canadian National Research Council, Div. Building Research, Ottawa, Project G-1, Internal Report 3.
- Schmertmann, J., 1974a, "Penetration Pore Pressure Effects on Quasi-Static Cone Bearing,  $q_c$ ," ESOPT, Stockholm, Vol. 2.2, pp. 345-52.
- Schmertmann, J., 1974b, "Pore Pressures that Produce Nonconservative  $q_c$  Data," ESOPT discussion, Vol. 2.1, pp. 146-50.
- Schmid, W. E., 1975, "Evaluation of Vibratory Compaction Field Tests," ASCE, SC-IMSP, Vol. 1, pp. 373-94.
- Sermeset, K., 1974, "Penetration Testing in Norway," ESOPT, Stockholm, SOA report, Vol. 1, pp. 85-95.
- Serota, S. and G. Lowther, 1973, "SPT Practice Meets Critical Review," Ground Engineering, Vol. 6, No. 1, January, pp. 20-22. See also Géotechnique, Vol. 23, No. 1, pp. 301-03.
- Shockley, W. G., and W. E. Strohm, 1961, "Investigations with Rotary Cone Penetrometer," Proc. 5th ICSMFE, Vol. I, pp. 523-26. For more detailed data see "Rotary Cone Penetrometer Investigations," U. S. Army Corps of Engineers, Waterways Experiment Station, Potamology Investigations, Report 18-1, June, 1962.
- Tavenas, F. A., 1971, Discussion to deMello (1971), 4th PanAm Conf. on SM&FE, Puerto Rico, Vol. III, pp. 64-69.
- Tavenas, F., 1972, Discussion in ASCE, J-SMFD, Vol. 98, SM-4, pp. 433-36.
- Veismanis, A., 1974, "Laboratory Investigations of Electrical Friction-cone Penetrometers in Sands," ESOPT, Stockholm, Vol. 2.2, pp. 407-20.

- Vesić, A. S., 1972, "Expansion of Cavities in Infinite Soil Mass," ASCE, J-SMFD, Vol. 98, SM-3, March, pp. 265-290.
- Vesić, A. S., 1975, "Principles of Pile Foundation Design, Lecture 1," Lecture Series on Deep Foundations, Boston Soc. of Civil Engineers, March-April.
- Vijayvergiya, V., and J. Focht, Jr., 1972, "A New Way to Predict Capacity of Piles in Clay," Offshore Technology Conference, Dallas, paper 1718.
- Webb, D. L., and R. I. Hall, 1969, "Effects of Vibroflotation on Clayey Sands," ASCE, J-SMFD, Vol. 95, SM-6, November, pp. 1365-78.
- Wineland, J. D., 1975, "The Borehole Shear Device," ASCE, AS-IMSP, Vol. 1, pp. 511-522.
- Winter, E. and A. Rodriguez, 1975, "Evaluation of Preconsolidation and Friction Angle in Granular Soils Using the Pressuremeter," ASCE, SC-IMSP, Vol. 1, pp. 523-535.
- Wissa, A., R. T. Martin and J. E. Carlander, 1975, "The Piezometer Probe," ASCE, SC-IMSP, Vol. 1, pp. 536-545.
- Wroth, C. P., and J. M. O. Hughes, 1973, "An Instrument for the In-situ Measurement of the Properties of Soft Clays," Proc. 8th ICSMFE, Vol. 1.2, pp. 487-494.
- Wroth, C. P., and J. M. O. Hughes, 1974, "The Development of a Special Instrument for the In-situ Measurement of the Strength and Stiffness of Soils," paper presented to the 1974 Engineering Foundation Conference, New England College, Henniker, N. H.
- Zolkov, E., and G. Wiseman, 1965, "Engineering Properties of Dune and Beach Sands and the Influence of Stress History," 6th ICSMFE, Montreal, Vol. I, p. 134.
- Zolkov, E., 1971, "The SPT and Foundation Practice in Fine Sands in Israel," preprint submitted to ASTM for possible publication.
- Zolkov, E., 1972, Discussion in ASCE, J-SMFD, Vol. 98, SM-4, p. 436.

## 9. NOTATION

BST	=	abbrev. for borehole shear test
$c'$	=	effective cohesion
$C_c$	=	compression index (consolidation)
CD	=	abbrev. for consolidated-drained
CPT	=	abbrev. for cone penetration test, usually implies Q-CPT
CU	=	abbrev. for consolidated-undrained
$D_r$	=	relative density (relative void ratio)
$e_0$	=	initial void ratio
E	=	energy input into penetration, or Young's modulus
$E_i$	=	initial tangent modulus
$E^+$	=	ave. undrained Young's modulus to failure
$E^-$	=	ave. decreasing Young's modulus after undrained failure
$f_s$	=	unit friction on local friction sleeve in Q-CPT
FR	=	friction ratio, in per cent, = $f_s/q_c$ , now denote as $R_f$
G	=	undrained shear modulus
GWT	=	abbrev. for ground water table
$I_p$	=	Atterberg plasticity Index
$K_o$	=	ratio of insitu horizontal/vertical effective stresses for condition of zero horizontal strain
N	=	standard blowcount from SPT, in accord with ASTM D1586
$N_c$	=	bearing capacity factor for cohesive contribution to bearing, used herein to convert $q_c$ to $s_u$
$N_N, N_A$	=	N-values using N-rods and A-rods, respectively
$N_{FF}$	=	N-values obtained with free fall of hammer
$N_q$	=	bearing capacity factor to account for overburden effects
$N_Y$	=	bearing capacity factor
NC	=	abbrev. for normally consolidated
OC	=	abbrev. for overconsolidated
OCR	=	abbrev. for overconsolidation ratio
$p'$	=	overburden vertical effective stress
$P_L$	=	limit pressure from a PMT
$P_o$	=	insitu total horizontal stress
P.E.	=	potential energy
PMT	=	abbrev. for pressuremeter test
$q_c$	=	unit bearing capacity on cone in a Q-CPT

- $q_u$  = unconfined compressive strength =  $2 s_u$   
 Q-CPT = abbrev. for quasi-static cone penetration test  
 R = total resistance to penetration on SPT sampler (also denoted F)  
 $R_f$  = friction ratio, in per cent  
 $s_u$  = undrained shear strength  
 $S_t$  = sensitivity =  $s_u$  (undisturbed)/ $s_u$  (remolded)  
 SPT = abbreviation for standard penetration test  
 T = torque at failure in a VST  
 UU = abbrev. for unconsolidated-undrained  
 VST = abbrev. for vane shear test  
 $V_o$  = initial volume of pressuremeter when  $p = p_o$   
 $\Delta V$  = change in volume from  $V_o$  during a PMT  
 w = water content  
 WES = Waterways Experiment Station, Vicksburg, Miss.  
 $w_L$  = Atterberg liquid limit  
 $w_p$  = Atterberg plastic limit  
 $w_s$  = shrinkage limit (by slow drying)  
 z = depth from ground surface  
 1-D, 3-D = abbrev. for one dimensional, three dimensional  
 $\gamma$  = total unit weight of soil  
 $\epsilon$  = strain  
 $\lambda$  = an assumed constant of proportionality  
 $\mu$  = reduction factor to apply to  $s_{uv}$  (from Bjerrum)  
 $\nu$  = Poisson's ratio  
 $\sigma_1$  = major principal stress  
 $\sigma_3$  = minor principal stress  
 $\sigma_o'$  = octahedral normal effective stress (= mean effective stress)  
 $\phi'$  = effective stress angle of internal friction  
 $\phi_o'$  =  $\phi'$  when volumetric strain = 0 at maximum strength in sands

Additional subscripts

- e = ends of vane cylinder      v = vane test, or volume  
 p = vane penetration  
 PMT = pressuremeter test  
 ps = plane strain  
 R = vane rotation  
 s = side of vane cylinder

Superscripts

- $\bar{\quad}$  denotes average  
 ' denotes effective stress

## APPENDIX IV

### EXAMPLES OF PILE CAPACITY CALCULATIONS (Taken from Nottingham and Schmertmann, 1975)

#### Notes to readers of Appendix IV

1. Sections 6.1 through 6.3 are attached for easy reference to Chapter 7. The material in these sections has already been presented elsewhere in the text.
2. Figure 6.1 appears as Figure 11 in the main text. Figures 6.2 and 6.5 appear as Figure 12 in Appendix III. Equations 6.1, 6.2, and 6.3 appear as equation 5 of Appendix III.
3. Notation shown in this text may differ from the main text.

## CHAPTER 6

### RECOMMENDED CPT PILE CAPACITY DESIGN PROCEDURES

#### 6.1 Introduction

This chapter presents the author's recommendations for using quasi-static cone penetration data to estimate the load capacity of driven displacement piles. The recommendations are based on an evaluation of the model and full-scale pile studies described in the preceding chapters and are applicable to the types of piles, penetrometers, and soils considered in this study. The limitations of the recommended methods are further discussed in Section 6.6.

#### 6.2 Tip Bearing Capacity

Use the Begemann procedure illustrated in Fig 6.1 to estimate the ultimate unit tip bearing capacity in both sands and clays. If the mechanical penetrometer is used in clays, the computed  $q_c$  value should be multiplied by 0.60 to account for the possible increase in  $q_c$  resulting from friction on the tip mantle. If the design is to be based on yield capacity criteria, multiply the computed tip resistance by 0.73.

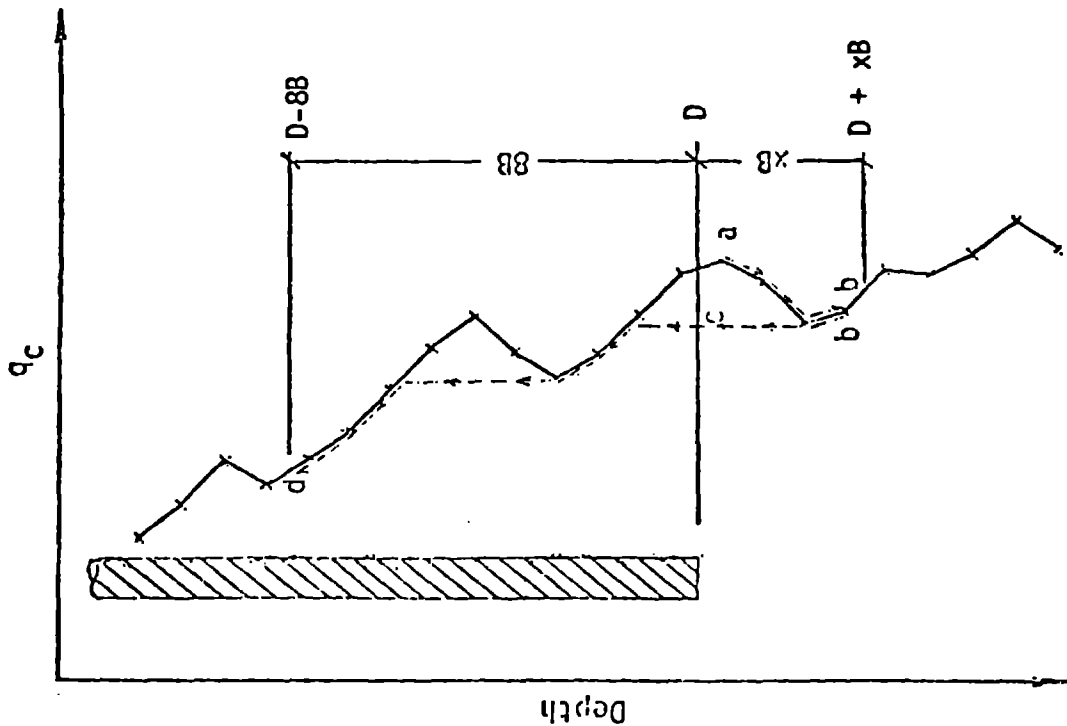
Pile capacities computed using this procedure are greatly affected by isolated very low  $q_c$  values which may not be representative of actual soil conditions. Therefore, single  $q_c$  values which are very low in relation to the surrounding values should be ignored unless there is reason to believe that the values are representative of actual weak soil layers, i.e., similar data from an adjacent sounding or soil samples which indicate thin layers of weak soil.

It is customary in The Netherlands to place an upper limit on allowable unit tip bearing capacity when CPT data are used for design. This limit, usually between 50 and 150 tsf, is intended to protect against grain crushing, long-term, high-pressure creep, and other unknown factors affecting the behavior of soils subjected to extremely high-pressure loading. Schmertmann (1974c) has recommended using a maximum allowable tip bearing capacity of 100 tsf for onshore design. This recommendation should be followed unless data are available to show that higher contact pressures are permissible. It should be noted that this limitation applies to allowable unit bearing capacity and will seldom be a serious limitation since piles usually are not driven to such a high resistance.

#### 6.3 Side Friction on Constant Section Piles

##### 6.3.1 Granular Soils

Compute the ultimate side friction on constant section piles using Eq 6.1 and the design curves in Fig 6.2.



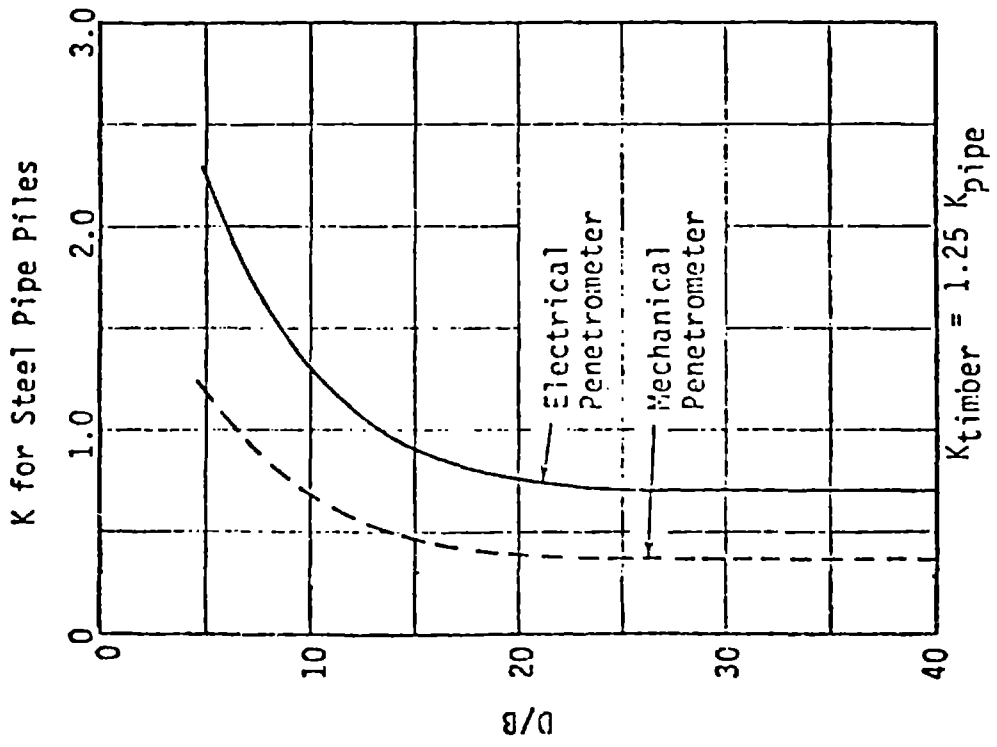
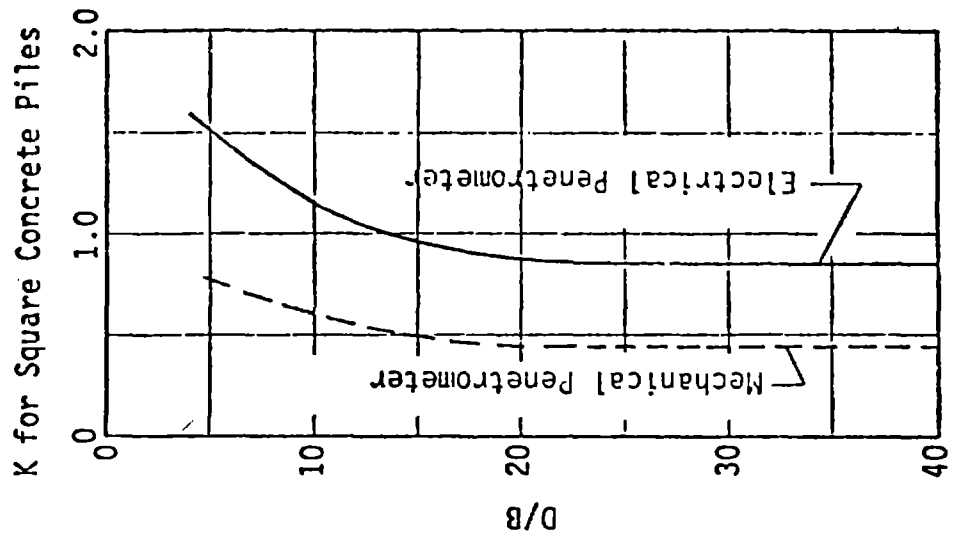
$$q_p = \frac{q_{c1} + q_{c2}}{2}$$

$q_{c1}$  = Average  $q_c$  over a distance of  $xB$  below the pile tip (path a-b-c). Sum  $q_c$  values in both the downward (path a-b) and upward (path b-c) directions. Use actual  $q_c$  values along path a-b and the minimum path rule along path b-c. Compute  $q_{c1}$  for  $x$ -values from 0.7 to 3.75 and use the minimum  $q_{c1}$  value obtained.

$q_{c2}$  = Average  $q_c$  over a distance of  $8B$  above the pile tip (path c-d). Use the minimum path rule as for path b-c in the  $q_{c1}$  computations.

BEGEMANN PROCEDURE FOR PREDICTING PILE TIP CAPACITY

FIGURE 6.1



PENETROMETER DESIGN CURVES FOR PILE SIDE FRICTION IN SAND

FIGURE 6.2

$$F_s = K \sum_{d=0}^{-8B} \frac{d}{8B} f_s A'_s + \sum_{d=8B}^L f_s A'_s \quad (6.1)$$

where

- $F_s$  = total ultimate side friction resistance
- $K^s$  = ratio of unit pile friction to unit sleeve friction from Fig 6.2
- $d$  = depth to the  $f_s$  value being considered
- $B$  = pile width or diameter
- $f_s$  = unit sleeve friction resistance
- $A'_s$  = pile-soil contact area per  $f_s$  depth interval

The design curves in Fig 6.2 are the curves developed from the model pile side friction analysis detailed in Section 4.3 and are the same as the curves presented in Figs 4.6 and 4.7. The K factor is the ratio between unit sleeve friction and unit pile friction. As pointed out in Section 4.3, the K factor should be determined by computing  $L/B$  using the total embedded pile length. A separate K factor should not be used for each  $f_s$  value.

Side friction calculations can be greatly simplified if sleeve friction resistance does not vary significantly with depth. For this case, Eq 6.1 can be simplified to Eq 6.2, provided the pile length is equal to or greater than  $8B$ .

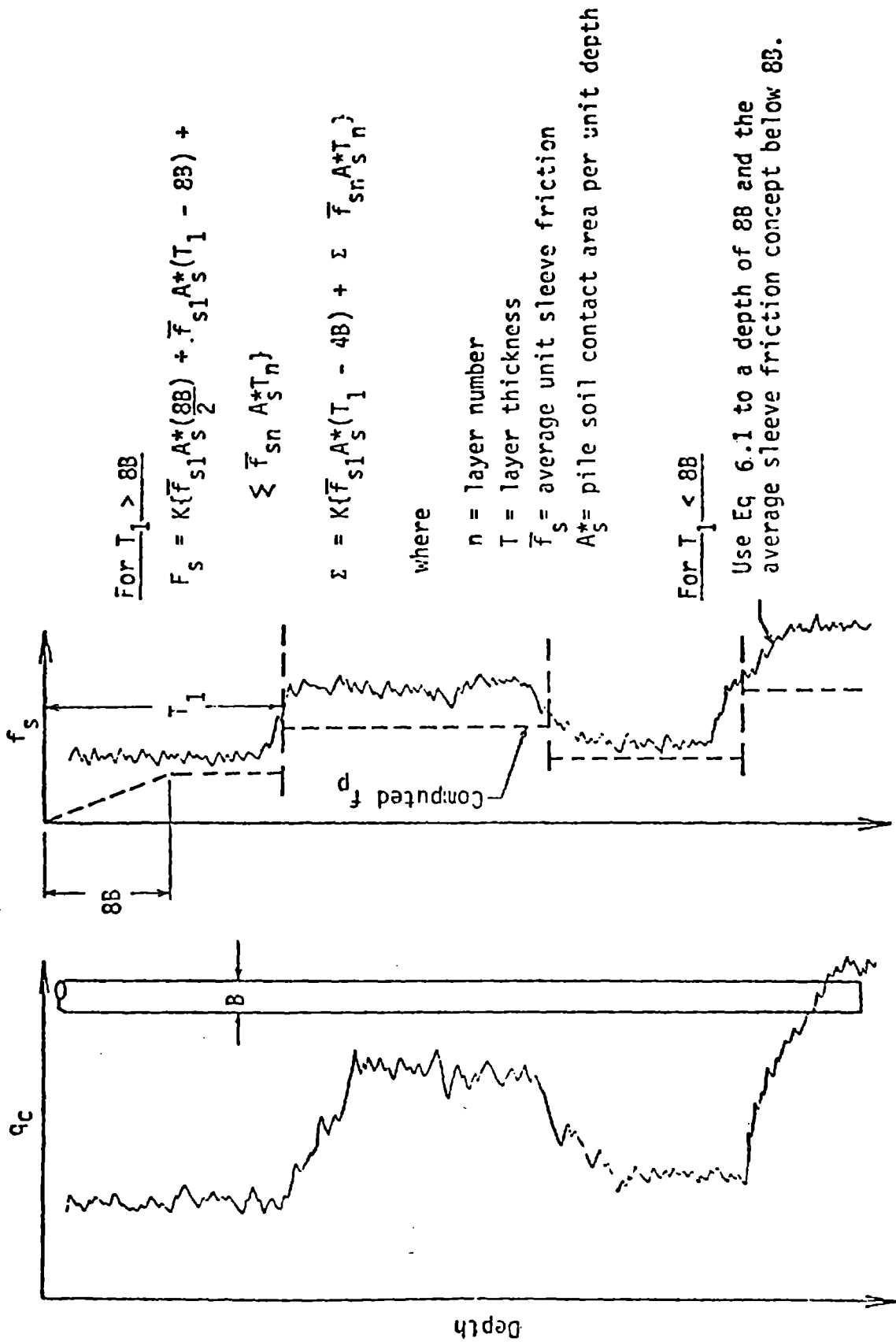
$$F_s = K \left[ \frac{1}{2} (\bar{f}_s A''_s)_{0-8B} + (\bar{f}_s A''_s)_{8B-L} \right] \quad (6.2)$$

where

- $\bar{f}_s$  = average unit sleeve resistance over the depth interval indicated by the subscript
- $A''_s$  = pile-soil contact area over the above  $\bar{f}_s$  depth interval

If two or more sand layers are involved, Eq 6.2 can be used by considering each layer individually as shown in Fig 6.3. The K value used for a multi-layered system should be determined using the total pile length and will, therefore, be the same for each layer.

Note that Eqs 6.1 and 6.2 only incorporate a depth of embedment correction at the ground surface. Schmertmann (1967) and Freed (1972) recommended that a correction be made each time the pile enters a stronger soil layer. Their recommendations were based on the assumption that the CPT friction ratio remains constant near layer interfaces and unit friction varies in proportion to unit tip resistance, as shown in Fig 6.4. Some CPT results are available, e.g., Schmertmann (1969), which tend to substantiate this assumption; however, it is difficult to draw any definite conclusions from these kinds of data, since the normally used 20-cm cone sounding interval is approximately equal to the 5 to 10B interval over which  $f_s$  would be expected to vary.



For  $T_1 > 8B$

$$F_s = K \left\{ \bar{f}_{s1} A_s^* (8B) + \bar{f}_{s1} A_s^* (T_1 - 8B) \right\} + \sum \bar{f}_{sn} A_s^* T_n$$

$$\Sigma = K \left\{ \bar{f}_{s1} A_s^* (T_1 - 4B) \right\} + \Sigma \bar{f}_{sn} A_s^* T_n$$

where

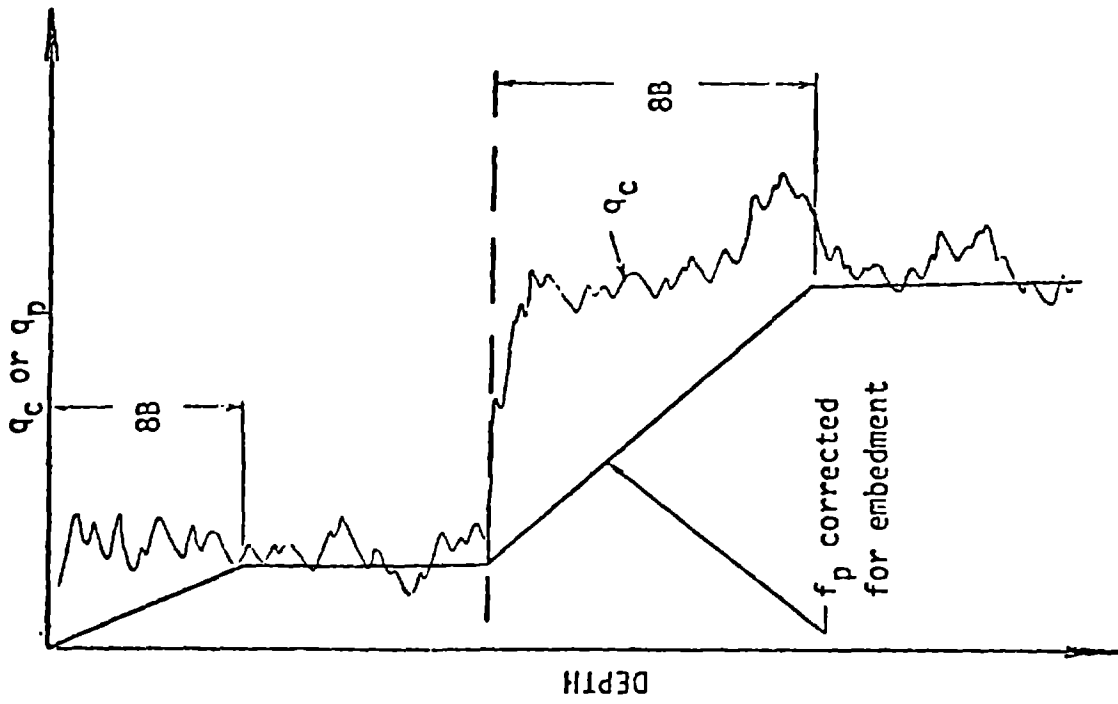
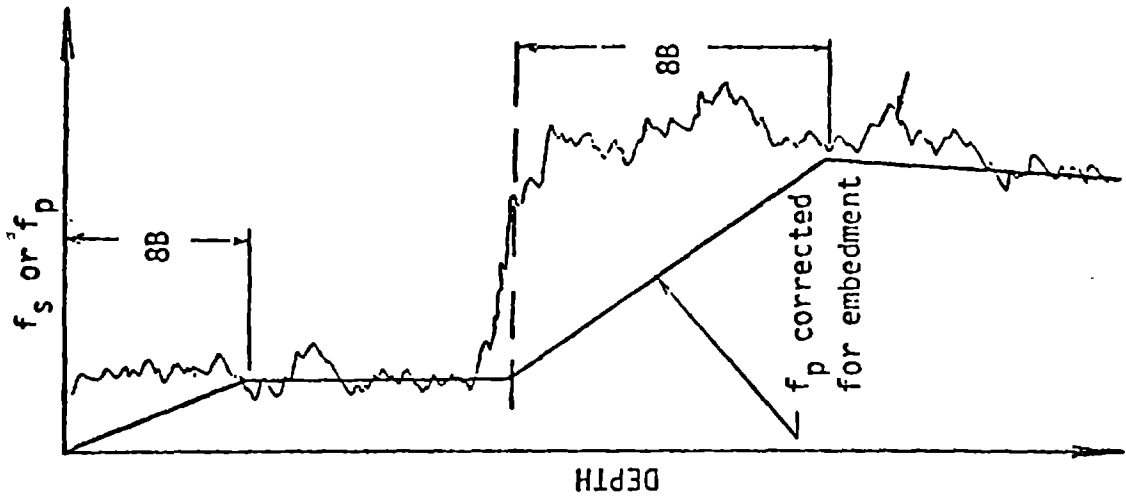
- $n$  = layer number
- $T$  = layer thickness
- $\bar{f}_s$  = average unit sleeve friction
- $A_s^*$  = pile soil contact area per unit depth

For  $T_1 < 8B$

Use Eq 6.1 to a depth of  $8B$  and the average sleeve friction concept below  $8B$ .

SIDE FRICTION COMPUTATION METHOD FOR LAYERED SOILS

FIGURE 6.3



SCHMERTMANN & FREED METHOD FOR PILE FRICTION EMBEDMENT CORRECTION  
 FIGURE 6.4

The recommendation that depth of embedment corrections not be made at layer interfaces when computing pile side friction is based on the following:

1. A lack of conclusive data to indicate such a correction should be made.
2. The fact that not making this correction did not result in any apparent large errors in the full-scale pile capacity predictions presented in Chapter 5.
3. The possibility that unit pile friction just below a layer interface may increase in the same manner as near the ground surface. The increase which occurs near the ground surface is reflected in the shape of the K curves in Fig 6.2.
4. Smear effects resulting from soil being carried down with the pile will mask layer boundary friction changes.
5. The desire to keep the prediction method simple and easy to apply. The existence of a distinct, significant interface is often difficult to decide and, in many cases, different engineers would disagree as to whether or not an interface actually exists. Eliminating the correction at layer interfaces eliminates these problems.

Pile friction predictions in sands can be based on  $q_c$  data when sleeve friction resistance information is not available. The calculations should be made by replacing  $f_s$  terms in Eq 6.1 (or 6.2) with  $0.007 q_c$  and using the electrical penetrometer design curves in Fig 6.2. This is equivalent to assuming an average electrical penetrometer friction ratio of 0.70 percent, which is a slightly conservative typical value for the sands in this study and in most other areas of Florida. The 0.70 percent FR value should be increased or decreased to better match experience in other areas.

### 6.3.2 Cohesive Soils

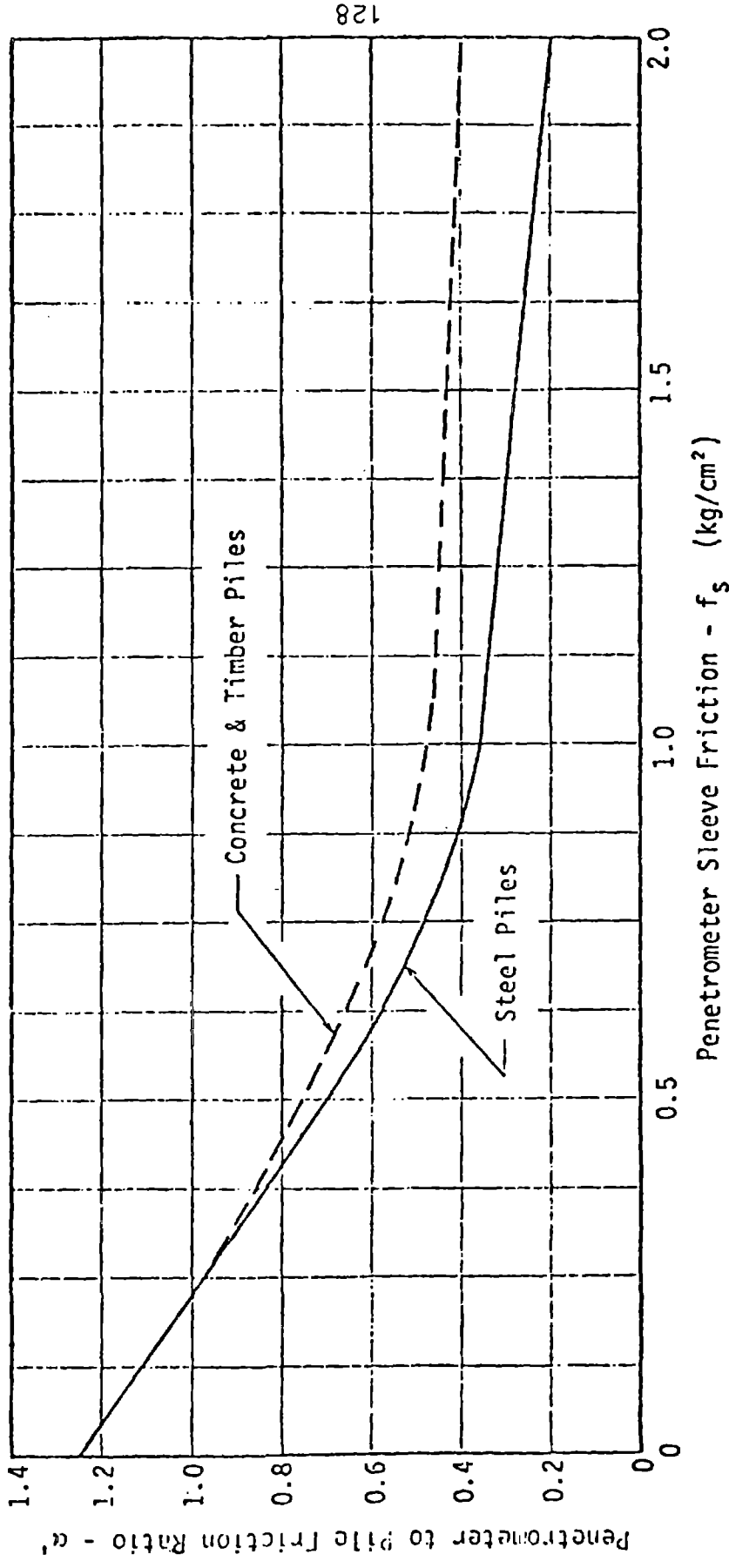
Total ultimate side friction in cohesive soils should be estimated using Eq 6.3 and the design curve in Fig 6.5.

$$F_s = \alpha' \bar{f}_s A_s \quad (6.3)$$

where

- $\alpha'$  = ratio of pile to penetrometer sleeve friction in clay
- $\bar{f}_s$  = average undrained sleeve friction
- $A_s$  = total soil-pile contact area

This recommendation is based primarily on the model pile studies which showed that, of the currently available clay-pile friction theories, Tomlinson's  $\alpha$ -method provided the best predictions.



PENETROMETER DESIGN CURVES FOR PILE SIDE FRICTION IN CLAY

FIGURE . 6.5

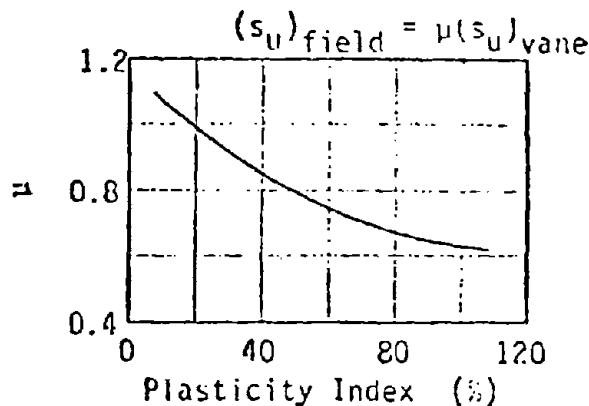
The  $\alpha'$  curves shown in Fig 6.5 are identical to Tomlinson's  $\alpha$  curves as presented in tabular form in NAVDOCKS DM-7, except that the  $\alpha'$  curves are plotted as a function of  $f_s$ .

Additional full-scale pile capacity correlation studies may show that the  $\lambda$  (or  $\lambda'$ ) method described in Chapter 4 provides better predictions; however, this method is not recommended at this time because of the poor correlation obtained during the model pile studies. Ultimately, a drained friction approach to the clay-pile friction problem should be adopted, but it appears that at this time it is impossible to make sufficiently accurate predictions of the radial effective stress acting on a pile driven in clay. Schmertmann's (1973) suggested procedure for estimating radial effective stress, coupled with additional CPT and pressuremeter research, may provide the basis for an eventual solution to this problem.

Eq 6.3 is based on a limited amount of data which indicate that  $f_s$  values obtained using either the electrical or mechanical penetrometer are a good approximation of undrained shear strength of clays. Since the relationship has not been proven for a wide variety of clays, undisturbed sampling and strength testing should be performed whenever possible to check the  $f_s$ - $s_u$  ratio. This method should not be used for highly sensitive clays. Also, mechanical penetrometer  $f_s$  data should be reduced approximately 20 percent in hard clays to account for possible end bearing on the friction sleeve.

Eqs 6.4 or 6.5, applicable to electrical and mechanical penetrometer data, respectively, can be used to estimate pile friction in clays when  $f_s$  data are unavailable. The  $\mu$  term in these equations is Bjerrum's (1972) field vane shear strength correction factor, as shown in Fig 6.6.

$$F_s = 0.10 \mu \bar{q}_c A_s \tag{6.4}$$



BJERRUM'S FIELD VANE SHEAR STRENGTH CORRECTION CURVE  
FIGURE 6.6

$$F_s = 0.067 \mu \bar{q}_c A_s \quad (6.5)$$

Whenever possible, pile friction should be estimated using both Eqs 6.3 and 6.4 or 6.5 to determine a range of possible friction resistance. If the predictions provided by each equation do not compare reasonably well, the undrained shear strength of the soil should be evaluated by other means.

#### 6.4 Tapered Pile Shaft Resistance

##### 6.4.1 Step-Taper Piles

Compute total ultimate shaft resistance as the sum of two independently determined components, friction on the constant diameter sections and end bearing at the diameter steps. The side friction component should be estimated using the procedures recommended for constant section piles in Section 6.3, with the following exception. In sands, the K term for each constant diameter section should be determined using the depth to which that diameter section extends. This point is illustrated by the example problem in Fig 6.7.

Use Eq 6.6 to estimate the end bearing component at the diameter steps.

$$Q_{\text{steps}} = \sum_{\text{steps}} S q_c^* A_{\text{step}} \quad (6.6)$$

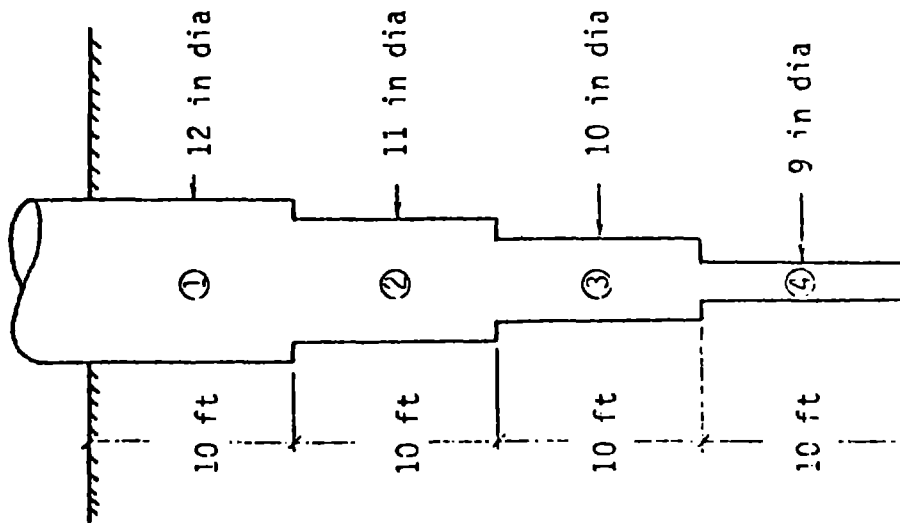
where

- $Q_{\text{step}}$  = total end bearing component of shaft resistance over the entire tapered pile length
- $S$  = ratio of  $q_c$  to unit step bearing resistance
- $A_{\text{step}}$  = bearing area at the diameter step
- $q_c^*$  = average  $q_c$  value in the vicinity of the diameter step

The values of  $S$  which should be used in Eq 6.6 are contained in Table 6.1. The mechanical penetrometer  $S$  value for clays incorporates the 0.60 correction factor recommended in Section 6.2 to account for tip mantle friction. The two  $q_c$  values occurring immediately above and below the step depth should be used to compute  $q_c^*$ ; however, unusually high or unusually low  $q_c$  values should be ignored.

TABLE 6.1  
S VALUES FOR ESTIMATING TAPERED PILE SHAFT RESISTANCE

Penetrometer	Soil Type	S
Electrical	Sand	1.6
	Clay	1.0
Mechanical	Sand	1.6
	Clay	0.6



SOIL: Uniform Sand -  $f_{se} = 0.50$  tsf

SECTION 1

$$L/B = 10.0/1.0 = 10 \quad K_{se} = 1.30$$

$$Q_{s1} = 1.30\{\frac{1}{2}(0.5)(\pi)(8) + 0.5\pi(2)\} = 12.25 \text{ tons}$$

SECTION 2

$$L/B = 20/(11/12) = 21.8 \quad K = 0.73$$

$$Q_{s2} = \{0.73 \cdot 0.50(11/12)(\pi)(10)\} = 9.16 \text{ tons}$$

SECTION 3

$$L/B = 30/(10/12) = 36 \quad K = 0.70$$

$$Q_{s3} = 0.70(0.5)(10/12)(\pi)(10) = 9.16 \text{ tons}$$

SECTION 4

$$L/B = 40/(9/12) = 53.3 \quad K = 0.70$$

$$Q_{s4} = 0.70(0.5)(9/12)(\pi)(10) = 8.24 \text{ tons}$$

$$\underline{\underline{\Sigma Q_s = 40.2 \text{ tons}}}$$

NOTE: This calculation is for the side friction component only. Step-bearing must be computed and added to the side friction component to determine total shaft resistance.

EXAMPLE OF STEP-TAPER PILE FRICTION COMPUTATION

FIGURE 6.7

### 6.4.2 Continuously Tapered Piles

The shaft resistance of piles with continuously tapered sections, such as timber or monotube piles, can be estimated by considering 'equivalent' step-taper piles and using the procedures in Section 6.4.1. In estimating the side friction components, diameter steps of the equivalent pile should be placed at layer interfaces as illustrated by the example problem in Fig 6.8.

Experimental K curves for timber piles could not be developed since model timber piles were not tested. The recommendation for timber pile K values presented in Fig 6.2 was developed using the friction test data presented by Nottingham (1975). The pipe pile K curve was used as a base for the timber pile because both types of piles have the same cross section shape. The results of tests by Potyondy (1961) and Lingo (1962) indicated that the friction coefficient between timber and soil is approximately the same as for smooth concrete. Freed's (1973) data showed that the smooth concrete friction coefficient was 29 percent higher than that for the model pile steel. Combining Freed, Potyondy, and Lingo's results indicates that the timber friction coefficient should be approximately 1.3 times that for normal pile steel. The recommended ratio of 1.25 was chosen to be slightly conservative, since test data were not available to confirm the ratio inferred from the shear test data.

The step bearing component should be estimated by considering an 'equivalent' pile diameter step at each cone sounding depth. This procedure can be simplified by constructing a graph of pile step area per sounding interval ( $A_{s/si}$ ), noting the soil layering as indicated by the CPT data, and using the following equation:

$$Q_{\text{step}} = \sum_n S \bar{q}_{cn} \bar{A}_{s/si} \quad (6.7)$$

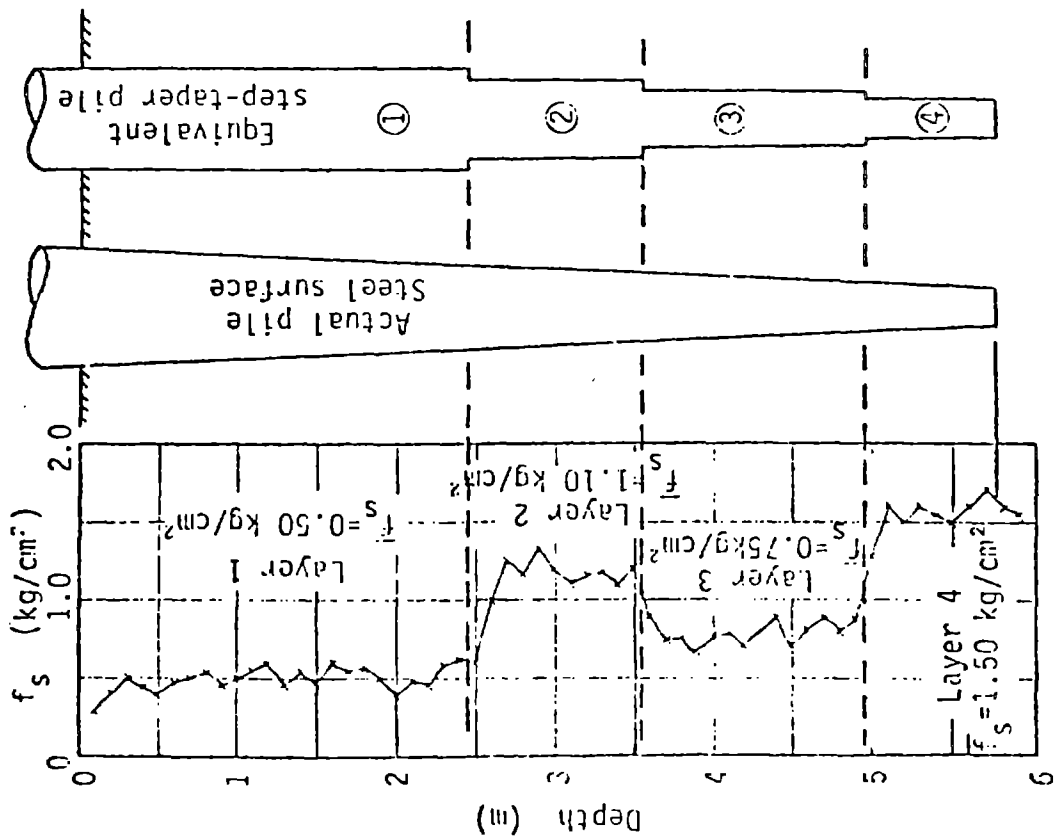
where

- n = soil layer number
- S = ratio of  $q_c$  to unit step bearing
- $\bar{q}_{cn}$  = average  $q_c$  for layer n
- $\bar{A}_{s/si}$  = average step area per sounding interval for layer n

The step bearing component for the example problem in Fig 6.8 is completed in Fig 6.9 to illustrate this procedure.

### 6.5 Safety Factors

It is impossible to establish fixed safety factor criteria for pile capacity design since the degree of safety appropriate for each design depends on a large number of factors.



Actual Pile

Diameter @ ground surface = 30 cm  
 Tip diameter = 20 cm

Equivalent Step-taper Pile

- $B_1 = 30 - (1.27/5.8)(10) = 27.81$  cm
- $B_2 = 30 - (3.04/5.8)(10) = 24.75$  cm
- $B_3 = 30 - (4.24/5.8)(10) = 22.68$  cm
- $B_4 = 30 - (3.37/5.8)(10) = 20.74$  cm

Side Friction Computations

Section 1 -  $D/B = 2.54/0.278 = 9.1, K = 1.40$   
 $F_{s1} = 1.4\{0.5\}(27.8\pi)(222.5) + 0.5(27.8\pi)(31.5)\}$   
 $F_{s1} = 2727$  kg

Section 2 -  $D/B = 3.54/0.2475 = 14.3, K = 0.94$   
 $F_{s2} = 0.94(1.10)(24.75\pi)(100) = 8040$  kg

Section 3 -  $D/B = 4.94/0.2268 = 21.8, K = 0.73$   
 $F_{s3} = 0.73(0.75)(22.68\pi)(140) = 5461$  kg

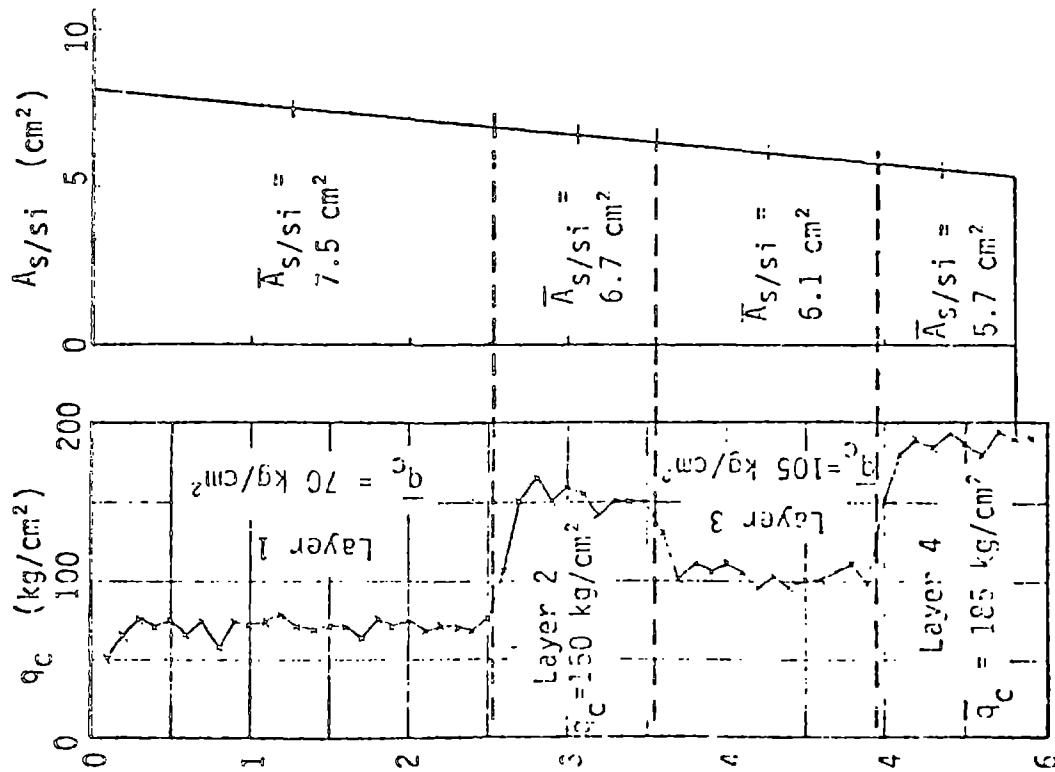
Section 4 -  $D/B = 5.8/0.2074 = 28, K = 0.70$   
 $F_{s4} = 0.70(1.5)(20.74\pi)(86) = 5884$  kg

$\Sigma F_s = 28,100$  kg = 28 metric tons

NOTE: This computation is for the side friction component only. The step-bearing component must be calculated and added to  $F_s$  to determine total shaft resistance. See Fig .9.

EXAMPLE COMPUTATION FOR CONTINUOUSLY TAPERED PILE SIDE FRICTION

FIGURE 6.8



From Fig 6.8, the pile taper is 0.01724 cm per cm of depth. The step-area curve was computed using this value.

Shaft Bearing Computation

Layer 1

$$Q_{s1} = S\bar{q}_c\bar{A}_s/si$$

$$= 1.6(70)(25.4)(7.5) = 21,340 \text{ kg}$$

Layer 2

$$Q_{s2} = 1.6(150)(10.0)(6.7) = 16,080 \text{ kg}$$

Layer 3

$$Q_{s3} = 1.6(105)(14.0)(6.1) = 14,510 \text{ kg}$$

Layer 4

$$Q_{s4} = 1.6(185)(8.6)(5.7) = 14,510 \text{ kg}$$

$$\Sigma Q_s = 65.9 \text{ metric tons}$$

$$Q_{\text{shaft}} = \Sigma F_s + \Sigma Q_s = 23.1 + 55.9$$

$$Q_{\text{shaft}} = 94 \text{ metric tons}$$

EXAMPLE STEP BEARING COMPUTATION FOR A CONTINUOUSLY TAPERED PILE

FIGURE 6.9

## CHAPTER 7

### EXAMPLE DESIGN PROCEDURE APPLICATIONS

This chapter presents three example problems to illustrate use of the recommended CPT pile capacity design procedure. Fictitious CPT profiles were developed and used for Example Nos 1 and 2 to show application of the different aspects of the recommended procedures, while Example No 3 shows capacity calculations for Pile No 2 at the Jefferson County site. All three examples use mechanical friction sleeve penetrometer data to estimate capacities of 18-in square precast concrete piles to correspond to the typical DOT application.

The different aspects of the design procedure illustrated by Example Nos 1 and 2 are:

1. The soil profile for Example No 1 includes a sand layer at the ground surface. This necessitates making a depth of embedment correction when computing side friction resistance.
2. The Example No 2 soil profile includes clay at the ground surface; thus, no depth of embedment correction for side friction is necessary.
3. In Example No 1, the pile tip is embedded in sand while in Example No 2, the tip is founded in clay. In computing tip bearing capacity for Example No 2, it is necessary to reduce the  $q_c$  values to account for possible penetrometer tip mantle friction.
4. Layered soil profiles are used in both examples to show side friction calculations for both granular and cohesive soils.

The following sections present the pile capacity calculations for each example and explain the details of the computational procedure.

#### 7.1 Example No 1

Fig 7.1 presents the CPT profile for this example and pile capacity calculations are shown in Fig 7.2. End bearing calculations were made using the procedure shown in Fig 6.1. Calculations for  $q_{c1}$  are shown for a number of  $x$ -values ranging from 0.70 to 3.75 and the averaging path that produced the minimum  $q_c$  value is shown in Fig 7.1. Note that the  $q_c$  value at the bottom point of the averaging path (Point B) is included twice in the  $q_{c1}$  computation and that the first  $q_c$  value used in the  $q_{c2}$  averaging procedure cannot be greater than the last  $q_c$  value in the  $(q_{c1})_{\min}$  calculation. In this example, and all following examples, units of  $\text{kg}/\text{cm}^2$  and  $\text{tsf}$  are used interchangeably. This simplifies the problem of maintaining consistent units without introducing appreciable errors.

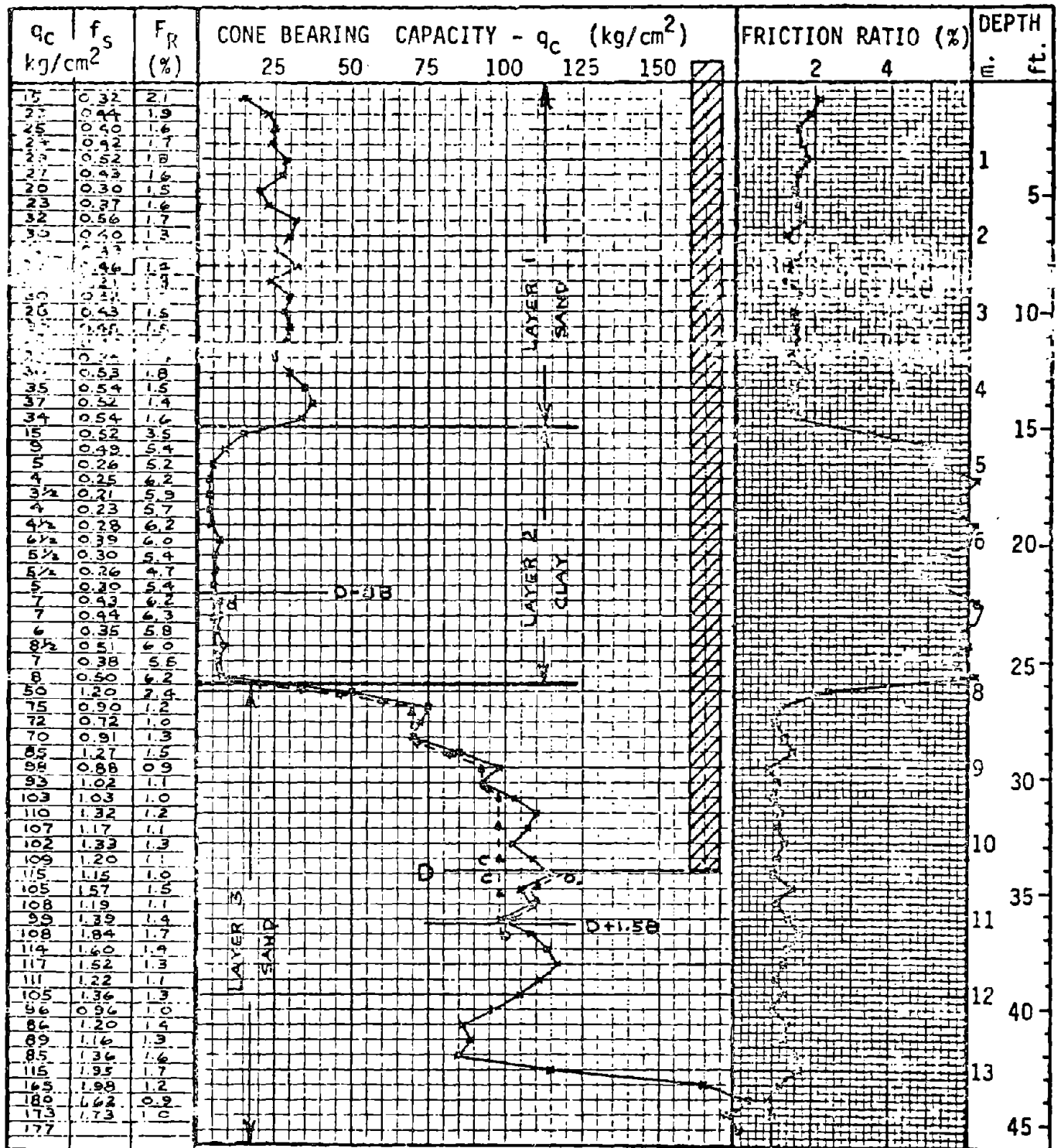


FIGURE 7.1  
EXAMPLE NO 1 CPT LOG

PILE TYPE: Prestressed concrete  
 PILE LENGTH: 34 ft (10.36 m)  
 PILE X-SECTION: 18 in (45.7 cm) square

END BEARING CALCULATIONS

x	xB (m)	D+xB (m)	q <sub>c1</sub> calculation	q <sub>c1</sub> (kg/cm <sup>2</sup> )
0.7	0.32	10.68	$\frac{1}{4}[115 + 3(105)]$	107.5
1.0	0.46	10.82	$\frac{1}{6}[115 + 105 + 2(108) + 2(105)]$	107.7
1.5	0.69	11.05	$\frac{1}{8}[115 + 105 + 108 + 5(99)]$	102.9 ←
2.0	0.91	11.27	$\frac{1}{10}[115 + 105 + 108 + 99 + 2(108) + 4(99)]$	103.9
2.5	1.14	11.50	$\frac{1}{12}[115 + 105 + 108 + 99 + 108 + 2(114) + 108 + 4(99)]$	105.6
3.0	1.37	11.73	$\frac{1}{4}[115 + 105 + 108 + 99 + 108 + 114 + 2(117) + 114 + 108 + 4(99)]$	107.2
3.5	1.60	11.96	$\frac{1}{6}[115 + 105 + 108 + 99 + 108 + 114 + 117 + 4(111) + 108 + 4(99)]$	107.1
3.75	1.71	12.07	$\frac{1}{8}[115 + 105 + 108 + 99 + 108 + 114 + 117 + 111 + 6(105) + 4(99)]$	105.7

$(q_{c1})_{min} = 102.9 \text{ kg/cm}^2 \text{ (or tsf)}$

D - 8B = 10.36 - 8(18)(2.54/100) = 6.70 m = upper limit of q<sub>c2</sub> averaging

$q_{c2} = 1/18 \{ 5(99) + 2(93) + 85 + 3(70) + 50 + 0.6 \overset{\text{mantle friction factor } c_2}{[8 + 2(7) + 3(6)]} \} = 58.3 \text{ kg/cm}^2$

$q_p = \frac{1}{2}(102.9 + 58.3) = 80.6 \text{ kg/cm}^2 \text{ (or tsf)}$

$\underline{Q_t} = A_t q_p = (1.5)^2 (80.6) = \underline{181 \text{ tons}}$

SIDE FRICTION CALCULATIONS

LAYER 1:  $F_s = K \left[ \frac{1}{2} (\bar{f}_s A_s'')_{0-8B} + (\bar{f}_s A_s'')_{8B-L} \right]$  --- Eq 6.3<sup>2</sup>

$(\bar{f}_s)_{0-8B} = 0.42 \text{ kg/cm}^2$  -----  $(\bar{f}_s)_{8B-L} = 0.53 \text{ kg/cm}^2$  -- 8B = 3.66 m

D/B = 34/1.5 = 22.7 ----- from Fig 6.2, K = 0.44

$\underline{F_{s1}} = 0.44 \left[ \frac{1}{2} (0.42)(3.66 \text{ m})(3.28 \text{ ft/m})(6 \text{ ft}^2/\text{ft}) + 0.53(4.50 - 3.66)(3.28)(6) \right] = 10.5 \text{ tons}$

LAYER 2:  $F_s = \alpha' \bar{f}_s A_s$  ---  $\bar{f}_s = 0.36 \text{ kg/cm}^2$  --  $\alpha' = 0.85$  from Fig 6.5

$\underline{F_{s2}} = 0.85(0.36)(7.9 - 4.5)(3.28)(6) = 20.5 \text{ tons}$

LAYER 3:  $F_s = K \bar{f}_s A_s''$  (Eq 6.3<sup>2</sup>) -----  $\bar{f}_s = 1.08 \text{ kg/cm}^2$  (or tsf)

$\underline{F_{s3}} = 0.44(1.08)(10.36 - 7.9)(3.28)(6) = 23.0 \text{ tons}$

TOTAL SIDE FRICTION ( $F_s$ ) = 10.5 + 20.5 + 23.0 = 54 tons

TOTAL PILE CAPACITY ( $P_{ult}$ ) = 181 + 54 = 235 tons

FIGURE 7.2

EXAMPLE NO 1 PILE CAPACITY CALCULATIONS

Side friction resistance in Layer 1 was calculated using the simplified procedure represented by Eq 6.2. For comparison, Layer 1 friction is computed using Eq 6.1 in Fig 7.3. The difference in friction computed from these two equations is not significant because sleeve friction variations are not large between the ground surface and a depth of 8B. If the sleeve friction profile is erratic within this depth range, Eq 6.1 should be used. Both Eqs 6.1 and 6.2 will produce the same results below a depth of 8B, thus Eq 6.2 was used for Layer 3 calculations. This equation is easier to use for hand calculations while Eq 6.1 is better suited to computer calculations. As indicated in Fig 7.2, Layer 2 friction was computed using Eq 6.3 and Fig 6.5.

### 7.2 Example No 2

The CPT log for this example is shown in Fig 7.4. The soil profile consists of three main layers: an upper layer of soft clay, a middle layer of sand, and a lower layer of stiff clay. End bearing and side friction calculations are presented in Fig 7.5. Note that in computing end bearing, the  $q_c$  data in the stiff clay layer have been reduced by 0.6 to account for possible tip mantle friction as recommended in Chapter 6. The reduced  $q_c$  values are shown on Fig 7.4. Except for this  $q_c$  reduction, the end bearing calculation procedure is identical to that used for Example No 1.

End bearing calculations were again made for several  $x$ -values between 0.70 and 3.75 to fully illustrate the design procedure. After developing an understanding of the end bearing computation method, it is usually possible to preselect the averaging depth which will result in the minimum  $q_{c1}$  value and eliminate the calculations for other  $x$ -values.

In computing side friction, the upper clay layer (Layer 1) has been subdivided into two layers (1a and 1b) because of the large difference in  $f_s$  values above and below a depth of 1.5 m. Also, no depth of embedment correction was made since the soil between the ground surface and a depth of 8B consists of clay. The computed friction in Layer 4 has been reduced by 20 percent (by multiplying by 0.80) to account for possible friction sleeve end bearing as recommended in Chapter 6. All other side friction calculations were made in the same manner as for Example No 1.

### 7.3 Example No 3

The CPT log for Pile No 2 at the Jefferson County site is shown in Fig 7.6 and the pile capacity calculations are presented in Fig 7.7. When computing end bearing, the  $q_{c1}$  averaging depth interval that would produce the minimum  $q_{c1}$  value was determined by inspecting the portion of the  $q_c$  profile between 0.70 and 3.75B below the pile tip. The reader can verify that the  $q_{c1}$  value computed is actually the minimum value by performing calculations for other  $x$ -values.

COMPUTE LAYER 1 SIDE FRICTION USING EQ 6.2

$$(F_s)_{\text{layer 1}} = K \sum_0^{8B} (d/8B)(f_s A'_s) + K \sum_{8B}^L f_s A'_s \quad (\text{Eq 6.2})$$

8B = 3.6 m ----- L = 4.50 m

D/B = 34/1.5 = 22.7 ----- from Fig 6.2, K = 0.44

d (m)	d/8B	f <sub>s</sub> kg/cm <sup>2</sup>	A' <sub>s</sub> (cm <sup>2</sup> )	d/8B(f <sub>s</sub> A' <sub>s</sub> )
0.20	0.05	0.32	5486*	90
0.40	0.11	0.44	3658**	180
0.60	0.16	0.40		230
0.80	0.22	0.42		340
1.00	0.27	0.52		510
1.20	0.33	0.43		520
1.40	0.38	0.30		420
1.60	0.44	0.37		600
1.80	0.49	0.56		1000
2.00	0.55	0.40		800
2.20	0.60	0.43		940
2.40	0.66	0.46		1110
2.60	0.71	0.31		810
2.80	0.77	0.52		1460
3.00	0.82	0.43		1290
3.20	0.87	0.45		1430
3.40	0.93	0.45		1530
3.60	0.98	0.34	2926***	970
3.80	-	0.53	3658	1940
4.00	-	0.54		1980
4.20	-	0.52		1900
4.40	-	0.54		1980

$\sum_{0}^{8B} = 14,230$   
 $\sum_{8B}^L = 7800$

- \* = 0-30 cm depth interval
- \*\* = 20 cm depth intervals
- \*\*\* = 3.50-3.66 m depth interval

F<sub>s1</sub> = 0.44(14,230 + 7800) = 9690 kg (2.2/2000 ton/kg)  
 = 10.7 tons

FIGURE 7.3  
 EXAMPLE NO 1 SIDE FRICTION CALCULATIONS



The computed friction in Layer 1 was reduced by 20 percent for the reasons explained in Section 7.2. The  $\alpha'$  value of 0.25 used in the Layer 1 calculations was chosen as a reasonable minimum value of  $\alpha'$  since the curve in Fig 6.5 does not extend to very high  $f_s$  values. It was necessary to make a depth of embedment correction when computing Layer 2 friction because the top portion of this layer falls within a depth of  $8B$  from the ground surface. This was accomplished by computing an average  $d/8B$  correction factor for the top portion of this layer and using a modified form of Eq 6.3. Friction in this portion of the layer could also have been calculated using the approach illustrated in Fig 7.3. Friction in Layer 3 was computed in the same manner as Layer 1 friction.

The computed total pile capacity is slightly different from the value reported in Table 5.1 because some of the design factors included in the final design procedure recommendations were generalized from the values developed from the model pile study. The revised factors, primarily  $\alpha'$  and the percent reduction to account for tip mantle friction, are only slightly different from the factors used in the previously reported model and full-scale capacity analyses and their effect on computed pile capacity is small.

PILE TYPE: Precast concrete  
 PILE LENGTH: 36 ft (10.97 m)  
 PILE X-SECTION: 18 in (45.7 cm) square

END BEARING CALCULATIONS

x	xB (m)	D+xB (m)	q <sub>c1</sub> Calculation	q <sub>c1</sub> (kg/cm <sup>2</sup> )
0.7	0.32	11.29	$\frac{1}{4} [32+34+34+32]$	33.0
1.0	0.46	11.43	$\frac{1}{6} [32+34+4(28)]$	29.7
1.5	0.69	11.66	$\frac{1}{8} [32+34+28+5(25)]$	27.4
2.0	0.91	11.88	$\frac{1}{10} [32+34+28+25+6(23)]$	25.7 ←
2.5	1.14	12.11	$\frac{1}{12} [32+34+28+25+23+2(26)+5(23)]$	25.8
3.0	1.37	12.34	$\frac{1}{14} [32+34+28+25+23+26+2(28)+26+5(23)]$	26.1
3.5	1.60	12.57	$\frac{1}{16} [32+34+28+25+23+26+4(28)+26+5(23)]$	26.3
3.75	1.71	12.68	$\frac{1}{18} [32+34+28+25+23+26+2(28)+2(34)+2(28)+26+5(23)]$	27.2

$(q_{c1})_{min} = 25.7 \text{ kg/cm}^2 \text{ (or tsf)}$

$D - 8B = 10.97 - 8(18)(2.54/100) = 7.31 \text{ m} = \text{Upper limit of } q_{c2} \text{ averaging}$

$q_{c2} = 1/18 [12(23) + 4(22) + 2(18)] = 22.2 \text{ tsf}$

$q_p = (25.7 + 22.2)/2 = 24.0 \text{ tsf}$        $Q_t = (1.5)^2(24.0) = \underline{\underline{54.0 \text{ tons}}}$

SIDE FRICTION CALCULATIONS

LAYER 1:  $F_s = \alpha' \bar{f}_s A_s$  (Eq 6.3) --  $\bar{f}_s = 0.57 \text{ kg/cm}^2$  --  $\alpha' = 0.70$ , from Fig 6.5  
 $F_{s1} = 0.70(0.57)(1.5 \text{ m})(3.28 \text{ ft/m})(4)(1.5) = \underline{11.8 \text{ tons}}$

LAYER 2:  $\bar{f}_s = 0.17 \text{ kg/cm}^2$  --  $\alpha' = 1.07$  (Embedded length = 4.9 - 1.5) = 3.4 m  
 $F_{s2} = 1.07(0.17)(3.4 \text{ m})(3.28 \text{ ft/m})(4)(1.5) = \underline{12.2 \text{ tons}}$

LAYER 3:  $F_s = K \bar{f}_s A_s'$  (Eq 6.2) --  $\bar{f}_s = 0.39 \text{ kg/cm}^2$   
 $D/B = 36/1.5 = 24$  --  $K = 0.44$  from Fig 6.2  
 $F_{s3} = 0.44(0.39)(9.3 - 4.9 \text{ m})(3.28 \text{ ft/m})(4)(1.5) = \underline{14.9 \text{ tons}}$

LAYER 4:  $\bar{f}_s = 2.35 \text{ kg/cm}^2$  --  $\alpha' = 0.38$       ↙ 20% reduction  
 $F_{s4} = 0.38(2.35)(10.97 - 9.30 \text{ m})(3.28 \text{ ft/m})(4)(1.5)(0.80) = \underline{23.5 \text{ tons}}$

TOTAL SIDE FRICTION ( $F_s$ ) = 11.8 + 12.2 + 14.9 + 23.5 = 62.4 tons

TOTAL PILE CAPACITY ( $P_{ult}$ ) = 54.0 + 62.4 = 116.4 tons

FIGURE 7.5

EXAMPLE NO 2 PILE CAPACITY CALCULATIONS

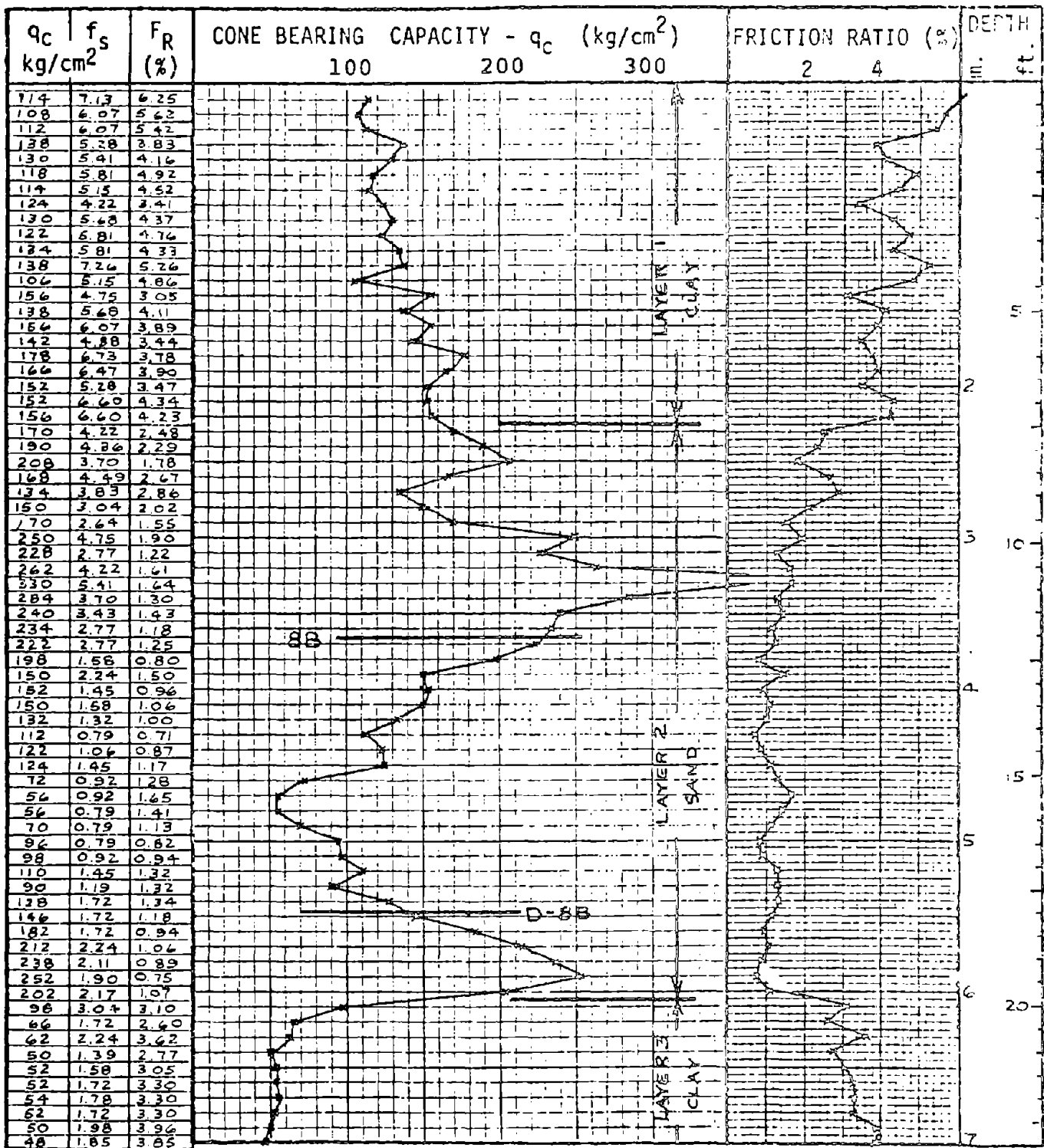
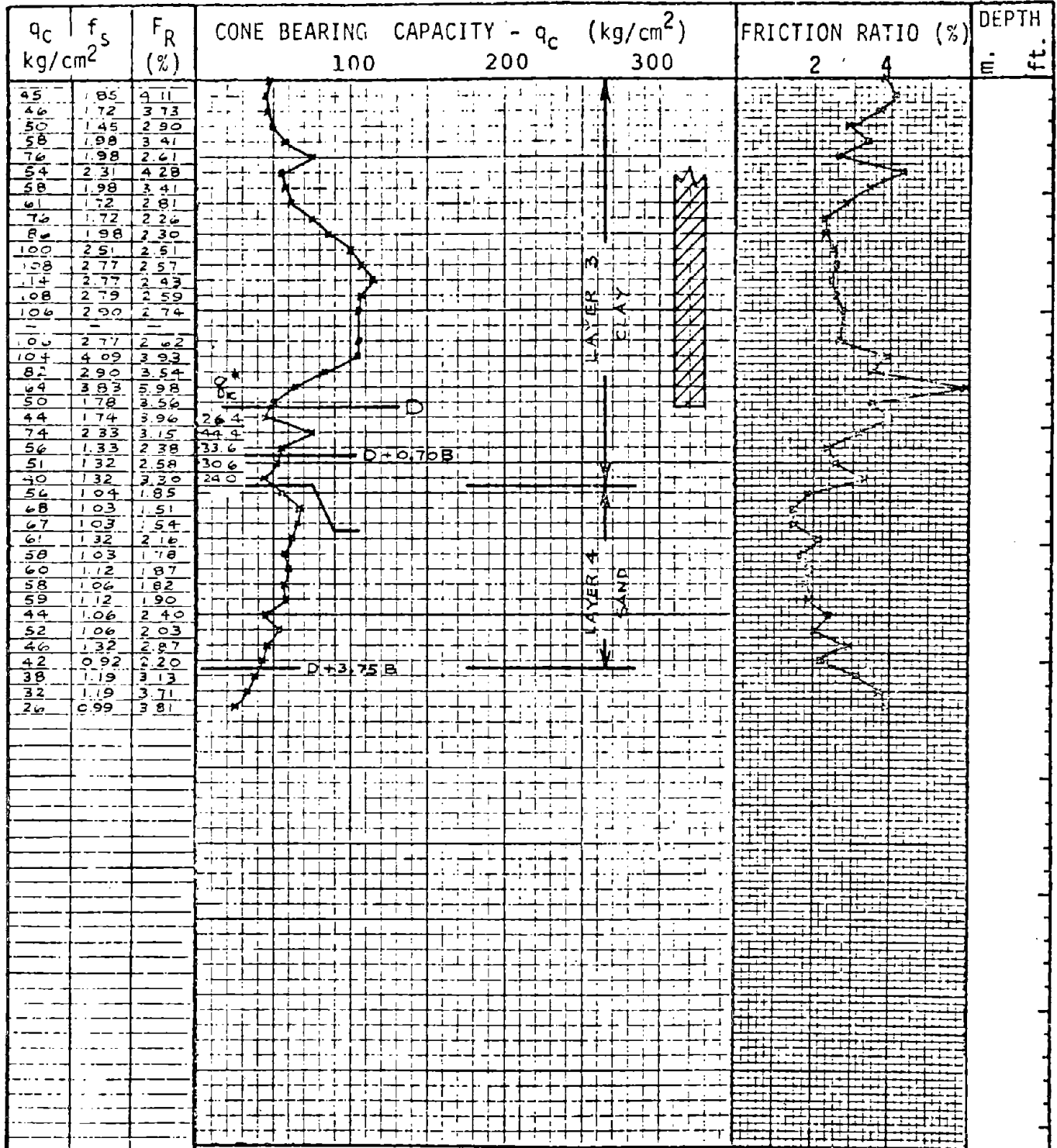


FIGURE 7.6  
EXAMPLE NO 3 CPT LOG



NOTE:  $q_c^* = 0.60q_c$

FIGURE 7.6 (continued)

EXAMPLE NO 3 CPT LOG

### END BEARING CALCULATIONS

From examination of the  $q_c$  log,  $(q_{c1})_{\min}$  will occur when averaging  $q_c$  between the tip depth and 11.65 m (approximately  $D + 1.0B$ )

$$q_{c1} = 1/10 [26.4 + 44.4 + 33.6 + 30.6 + 6(24.0)] = 27.9 \text{ kg/cm}^2$$

$$q_{c2} = 24.0 \text{ kg/cm}^2 \text{ since no } q_c \text{ value for } 8B \text{ above the tip is less than the last value used in computing } q_{c1}$$

$$q_p = \frac{1}{2}(27.9 + 24.0) = 26.0 \text{ kg/cm}^2 \text{ (or tsf)}$$

$$\underline{Q_t} = A_t q_p = (1.5)^2 (26.0) = \underline{58.5 \text{ tons}}$$

### SIDE FRICTION CALCULATIONS:

$$\text{LAYER 1: } F_s = \alpha' \bar{f}_s A_s \text{ ---- } \bar{f}_s = 5.81 \text{ kg/cm}^2 \text{ --- } \alpha' = 0.25$$

$$\underline{F_{s1}} = 0.25(5.81)(2.25 \text{ m})(3.28 \text{ ft/m})(6 \text{ ft}^2/\text{ft})(0.80) = \underline{51.4 \text{ tons}}$$

LAYER 2: A depth of embedment correction must be made between the top of this layer (2.25 m) and a depth of 8B (3.66 m). This correction will be made by computing an average depth of embedment correction factor for this depth interval.

$$(d/8B)_{2.25 \text{ m}} = 2.25/3.66 = 0.61$$

$$(d/8B)_{3.66 \text{ m}} = 1.00$$

$$(d/8B)_{\text{avg}} = \frac{1}{2}(0.61 + 1.00) = 0.80$$

$$D/B = 30/1.5 = 20 \text{ ----- } K = 0.44 \text{ ---- } \bar{f}_s = 3.80 \text{ kg/cm}^2$$

$$\underline{F_{s2a}} = 0.44(0.80)(3.80)(3.66 - 2.25)(3.28)(6) = \underline{37.1 \text{ tons}}$$

$$\text{From } 3.66 \text{ to } 6.05 \text{ m, } \bar{f}_s = 1.48 \text{ kg/cm}^2$$

$$\underline{F_{s2b}} = K \bar{f}_s A_s'' = 0.44(1.48)(6.05 - 3.66)(3.28)(6) = \underline{30.6 \text{ tons}}$$

LAYER 3: (6.05 - 9.14 m)

$$F_s = \alpha' \bar{f}_s A_s$$

$$\bar{f}_s = 2.23 \text{ kg/cm}^2 \text{ ----- } \alpha' = 0.38$$

$$\underline{F_{s3}} = 0.38(2.23)(9.14 - 6.05)(3.28)(6)(0.80) = \underline{41.2 \text{ tons}}$$

$$\underline{\text{TOTAL SIDE FRICTION } (F_s)} = \underline{160.3 \text{ tons}}$$

$$\underline{\text{TOTAL PILE CAPACITY } (P_{ult})} = \underline{218.8 \text{ tons}}$$

FIGURE 7.7

EXAMPLE NO 3 PILE CAPACITY CALCULATIONS

